A Study of Partially Liganded Sickle Hemoglobin Polymerization Kinetics

A Thesis

Submitted to the Faculty

of

Drexel University

by

Donna Anne Yosmanovich

in partial fulfillment of the

requirements for the degree

of

Doctor of Philosophy

March 2012

Dedications

This thesis is dedicated to my family and especially my husband,

whose patience and unwavering support made this all possible

Acknowledgements

I would like to express my deepest gratitude to my thesis advisor, Dr. Frank Ferrone, whose mentorship has been invaluable throughout my time at Drexel. His great passion for his work was inspiring from our first meeting. Working with Dr. Ferrone has taught me many things, the foremost of which is how to be a thorough scientist and a critical thinker. I would also like to thank Dr. Alexey Aprelev whose ingenious problem solving has been both a great help as well as an inspiration. I have been extremely lucky to have him as a resource during my time at Drexel. Many thanks also to Dr. Maria Rotter, who was the first female scientist I had the honor of working with, and who taught and then demonstrated to me the true value of extensive experimental notes and good organization. Our time working together was too short, but the lessons you taught me are with me always.

My colleagues, Dr. Weijun Weng, Dr. Mikhail Zakharov, Dr. Zenghui Liu, and Dr. Yihua Wang have been a great resource as well; from helping me in the lab to engaging in long conversations on hemoglobin. Thanks also to the other physics graduate students and the rest of physics department for encouragement, advice and friendship.

Thanks to my thesis committee as well, Dr. Brigita Urbanc, Dr. Charles Lane, Dr. Alisa Clyne; and a special thanks to Dr. Micheal Vogeley, and Dr. Gouliang Yang as well, all of whom have given me great advice and comments on my thesis work.

Finally, I would like to thank my family, especially my parents Anna and Richard, my husband Robin Islam, and my daughter Leah, for their unwavering support during these years and making this journey an absolute delight.

Table of Contents

List of Tables

List of Figures

Abstract

A Study of Partially Liganded Sickle Hemoglobin Polymerization Kinetics
Donna Yosmanovich
Frank Ferrone Ph.D.

Sickle cell anemia is a debilitating disease that results from the polymerization of mutated hemoglobin (HbS) inside the red blood cells (RBCs). Polymerization kinetics, including nucleation rates, have been well studied for pure HbS, as well as in the presence of nonpolymerizing molecules, such as HbF, or co-polymerizing molecules such as HbA. For polymerization of HbS in the presence of O_2, CO and NO gases there is only one study, using CO, but that work did not resolve nucleation rates. Since polymerization occurs in the presence of these gases ins RBCs in the body, this is a significant gap in understanding. It has already been established that there is a relatively small amount of HbS with O_2 or CO ligands in gelled polymers. How the presence of these ligands affect the rates of formation of homogeneous and heterogeneous nuclei is the focus of this work. Through the use of a photolysis light scattering technique, nucleation rates were measured for HbS solutions partially saturated with CO and then O_2. The heterogeneous nucleation rates were found by fitting an exponential function to the scattered light growth curves; and the homogeneous nucleation rates were found by analysis of the stochastic variation of delay times. The amount of CO saturation was measured through a single wavelength optical density measurement, and the O_2 saturation was measured through a laser photolyzed spectrum. This experiment obtained the nucleation rates of partially saturated CO HbS from 0% to 60% and partially saturated oxygen HbS from 0% to 44%. It was found that the equilibrium model presented by Sunshine et al (J Mol Biol. 1982 158:251-73) is a reasonable approximation for modeling the behavior of nucleation and that O_2 and CO can be modeled as affecting nucleation rates similarly. The preceding analysis required that the Hb allosteric model be incorporated into nucleation theory, which is also described. The knowledge obtained in this study can help describe polymerization of HbS in vivo, which can lead to improved models for describing the time at which RBC sickling occurs during vasculature transit.

Chapter 1: Hemoglobin Background

1.1.1 Blood and circulation

Every living cell inside an animal body requires energy to sustain itself. For humans, it is the circulatory system consisting of blood and blood vessels that provide the sustenance and means of transportation for the blood to sustain cell life. Human blood is composed primarily of two components, plasma and red blood cells. Plasma, which is 55% of the total volume, is a semitransparent straw colored fluid, which contains dissolved metabolites (vitamins, amino acids), wastes, ions and proteins, all necessary for normal cellular function. Red blood cells (RBCs), which are about 45% of the volume (this percent is also known as the hematocrit, and varies from person to person), aid in oxygen delivery to cells and CO_2 removal. The other components are leukocytes or white blood cells and platelets which together make up less than 1% of the cells in blood. Leukocytes aid in immunological defenses while platelets help clot blood. Together these are the components of human blood.[1]

Blood is continuously pumped through the human circulatory system by the heart. The heart is a muscular organ which has four main chambers, two on each side which are divided by a thick wall of muscle called the septum. The left and right sides both have an upper chamber called the left and right atria and two lower chambers called the left and right ventricles. The right side of the heart pumps the same amount of blood into the lungs

---

[1] Ross, M. H. (2003). *Histology:* A Text and Atlas: With Cell and Molecular Biology. (4, Ed.) Lippincott Williams & Wilkins.

that the left side pumps into the rest of the body. The left ventricle of the heart pumps blood first into the arteries, which have strong vascular walls that can handle the high blood pressure and velocity of the blood flow coming from the heart. From there, the arteries divide into smaller branches, the smallest of which are called arterioles. They have a strong muscular wall that allows them to control the flow of blood into the capillaries by contracting completely shut or dilating several times their normal size. Capillaries have the smallest diameter of all the components of circulation. They can have a diameter smaller than that of a single RBC, which means a RBC must squeeze in order to pass through. Capillary walls are thin and have minute pores that are permeable to water and small molecular substances. This is necessary for the exchange of fluid, nutrients, electrolytes, hormones, etc. between the blood and cells of the body.

The capillaries are where the blood exchanges nutrients and sustains life for the human body. From the capillaries, blood is collected together into larger and larger vesicles, finishing with veins which lead to the right ventricle of the heart. From there the blood is pumped into the lungs, where the RBCs exchange CO_2 for O_2. After sufficient exchange has taken place, the blood recollects and is pumped again by the left side of the heart to the rest of the body, repeating the circulatory cycle.[2]

1.1.2 Red blood cells

In a cubic millimeter of blood, there are about 5 $x10^6$ red blood cells (RBC's), also known as erythrocytes. In a human being, there are about 25 $x10^{12}$ RBCs; the most

[2] Guyton, A. C. (2005). Textbook of Medical Physiology: Guyton Physiology. (11 ed.). Saunders.

abundant of any single type of cell in the body. The percentage of RBCs in the blood is called the hematocrit. For men it can be around 42% and for women, 38%. However, the amount can vary greatly depending on the health and activity of the person.

Healthy RBCs develop in the bone marrow and will circulate for 100-120 days before being recycled by the body. In comparison persons with Sickle Cell disease have RBCs that only live for 8-29 days, if the patient is not exercising or under undue stress.[3] A RBC will spend about 20 seconds in circulation if it goes through the typical cycle of circulation (as opposed to storage in the spleen).[4] RBC's are biconcave – donut shaped, with a depression in the center that does not reach all the way through. They are 6-8um in diameter and 2um thick. Their main functionality is to be carriers of the globular protein hemoglobin. A typical human RBC contains about 80- 100 femtoliters of 32 to 36 grams per deciliter of hemoglobin.[5] It is from the iron in the heme group of hemoglobin that RBCs get their distinctive red color.

1.2 Hemoglobin

1.2.1 Hemoglobin – Historical context

As early as 1799, Sir Humphrey Davy showed that blood contained more oxygen and carbon dioxide than could be dissolved in a solution of pure liquid.[6] This led to an increased

---

[3] McCurdy, P. R., and A. S. Sherman. 1978. Irreversibly sickled cells and red cell survival in sickle cell anemia: a study with both DF32P and 51Cr. *Am. J. Med.* 64:253-258.
[4] Hogg, J. C. Et. al. (1994) Erthrocyte and polymorphonuclear cell transit time and concentration in the human pulmonary capillaries. J. Appl. Physiol. 1795-1800.
[5] http://www.nlm.nih.gov/medlineplus/ency/article/003648.htm. Accessed March 2011.
[6] Bunn, H. F. et al. (1986). Hemoglobin Molecular, Genetic and Clinical Aspects. John Dyson. Saunders Co. Chap. 1 p. 2.

interest in studying the relationship between blood and its oxygen content. Fifty three years later in 1862, Felix Hoppe (aka Hoppe-Seyler) studied the relationship between the red pigmentation of blood and the binding of oxygen. He was the first to use the term "hemoglobin" and to observe the optical absorption of oxyhemoglobin.[7] Felix Hoppe's work would lead George G. Stokes to study spectral changes of hemoglobin by removing the oxygen through a chemical reduction with ferrous sulfate.[8] This caused the solution to develop a purplish color that could be reversed back to red when re-exposed to oxygen. This was the first experiment that showed reversible binding of oxygen to hemoglobin. It was also around this time that chemists were able to separate the heme component of hemoglobin from the globin. From this, they demonstrated that the heme could be formed into crystals that contained iron and could predict a minimum molecular weight for hemoglobin of 16,600 Daltons (very close to today's accepted value of 16,125 Daltons per subunit). In the 1920's, Gilbert Adair determined the molecular weight of hemoglobin using an osmotic pressure technique, and found it to be around 67,000 daltons.[9] This meant that hemoglobin was a molecule made up of 4 heme sub groups.

In 1936, Linus Pauling would publish a paper predicting that oxygen binds to the iron in each heme group of the hemoglobin.[10] Each hemoglobin molecule can bind up to four oxygen ligands. In the 1960's, Perutz studied the deoxyhemoglobin and oxyhemoglobin crystalline structures and demonstrated exactly how oxygen binding changes the molecules'

---

[7] Hoppe, F. (1862). Über das Verhalten des Blutfarbstoffes im Spectrum des Sonnenlichtes. *Virchows Arch. Path. Anat. Physiol. 23*:446.
[8] Stokes, G. G. (1864). On the reduction and oxidation of the colouring matter of the blood. *Proc. R. Soc. Lond.* 13:355.
[9] Ada ir, G. S. (1925). A critical study of the direct method of measuring the osmotic pressure of hemoglobin. *Proc. R Soc*. 108A:627.
[10] Pauling, L. and C.D. Corynell. (1936). The oxygen equilibrium of hemoglobin and its structural interpretation. *Proc. Natl. Acad. Sci.* 22:210.

structure. The solution of the three dimensional structure of hemoglobin would earn him the Nobel Prize in 1962.[11]

1.2.2 Hemoglobin –as a protein

A protein is macromolecule that is constructed of different combinations of the 20 possible amino acid residues. It has a "backbone" made of mostly Carbon, Nitrogen and Hydrogen atoms that are linked together in a linear fashion (figure [1.1]). The amino acids are side chains that project from the main chain and are bound to the backbone Carbons. The order of the amino acid residues in a protein is referred to as the primary structure. The primary structure's sequence of amino acids is usually stabilized by hydrogen bonds[12] into another more complex structure, such as an alpha helix or beta sheet which is then connected by short non-helical segments referred to as random coils or turns (secondary structure, figure [1.2]). Alpha helices are represented by helical ribbons, beta sheets by arrows, and random coils by a thickened line. Alpha helices are stabilized by hydrogen bonds between the C=O and fourth down H-N groups of the protein backbone.[13] The tertiary structure is the arrangement of the secondary structure pieces into the overall shape of the protein molecule (figure [1.2] middle). This is the folded protein and can be stabilized by non-local interactions such as a hydrophobic core and a hydrophilic exposed surface (as is the case in hemoglobin). Quaternary structure is several separate tertiary protein molecules put together. They then behave or function as a single protein complex

---

[11] http://nobelprize.org/nobel_prizes/chemistry/laureates/1962/perutz-bio.html. Accessed April 2011.
[12] IUPAC-IUB Commission on Biochemical Nomenclature (1970). Abbreviations and symbols for the description of the conformation of polypeptide chains. *Journal of Biological Chemistry* 245: 6489–6497.
[13] Finelstein. A. V. and O. B. Ptitsyn. (2002). Protein physics: A course of Lectures. *Academic Press*.75-76

and are stabilized by: hydrophobic interactions, salt bridges, hydrogen bonds and disulfide bonds (figure [1.2] right).

Normal adult Hemoglobin (HbA) is a symmetrical quaternary molecule made up of four subunit tertiary protein molecules. The subunits are designated α_1, β_1, α_2 and β_2. These names are not to be confused with the secondary protein structure names of α helix and β sheet. The subunits, $\alpha_{1,2}$ and $\beta_{1,2}$ are very similar in their secondary structure. They are each made up of α helices and random coils which connect the helices, as well as a heme group. However, their slight differences start at the primary structure level, where α subunits have linear sequence of 141 amino acids; β has 146.

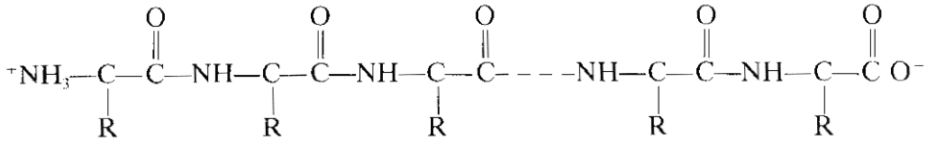

Figure [1.1]: Protein backbone. "R" is where amino acid residues would be.[14]

[14] Bunn, H. F. et al. (1986). Hemoglobin Molecular, Genetic and Clinical Aspects. John Dyson. Saunders Co. p. 13.

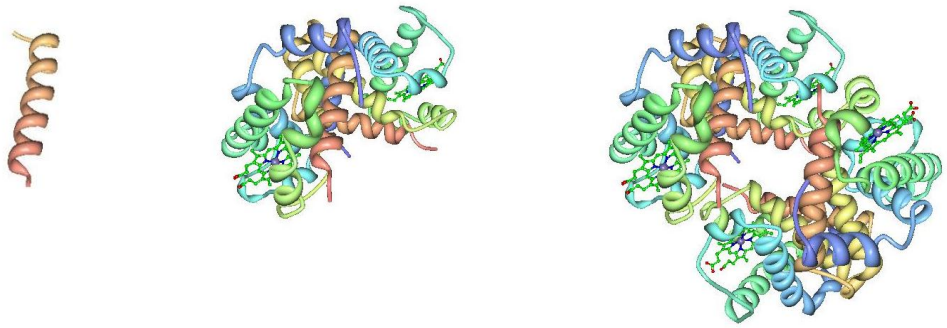

Figure [1.2]: From PDB (Protein DataBase). Left: hemoglobin alpha helix (the secondary structure). Middle: alpha 1 subunit (tertiary). Right: hemoglobin quaternary structure.

Each subunit of Hb, $\alpha_{1,2}$ and $\beta_{1,2}$, has designations given to their multiple alpha helices in order from A to H. The additional amino acid residues in $\beta_{1,2}$ are found mostly in an extra D helix which is not present in $\alpha_{1,2}$. The heme group found in each subunit is ferroprotoporphyrin IX; the molecular structure is shown in figure [3]. The Heme is inserted in a gap between the E and F alpha helices of each subunit. The iron is covalently bonded to the Nitrogen of the proximal F8 Histidine, which is the eight amino acid on the F helix. The heme is stabilized by a large number of interatomic contacts, about 35 between various residues in the F helix and roughly 28 in the E helix. When the iron atom does not have oxygen bound, it has unpaired electron, as well as a stressed bond and the proximal Histidine of the F-Helix. In oxygenated Hb, the iron atom is able to pair its electrons, thereby having a lower spin state and decreased magnetic moment.

It is important to note that a ligand is by definition an ion or a molecule that binds to a central metal atom and donates or shares one or more of its electron pairs. Here the

Nitric Oxide (NO), Carbon Monoxide (CO) and Oxygen (O_2) will be commonly referred to as ligands which bind to the iron atom in the heme in hemoglobin.

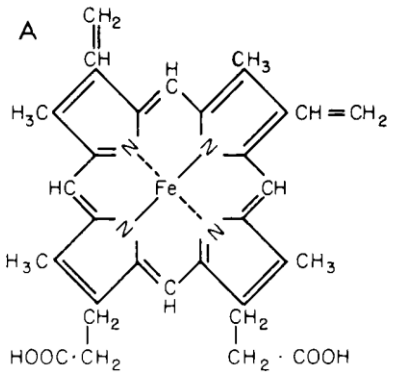

Figure [1.3]: The molecular structure of the Hb heme group, ferroprotoporphyrin IX[15]

The hemoglobin quaternary structure can separate into two "dimers" or two halves each with the subunits of: $\alpha_1\beta_1$ or $\alpha_2\beta_2$. The four subunits of hemoglobin interact via weak non-covalent bonds and hydrogen bonds. The contacts within each dimer are the same for oxygenation and deoxygenation. However, the $\alpha_1\beta_2$ contact loses 18 molecular contacts and 7 hydrogen bonds when Hb enters the oxygenated, or relaxed state. The reduction in contacts allows oxyhemoglobin to dissociate reversible into $\alpha_1\beta_1$ dimers, at a rate of 10^6

[15] Bunn, H. F. et al. (1986). Hemoglobin Molecular, Genetic and Clinical Aspects. John Dyson. Saunders Co. p. 29.

more than in deoxyhemoglobin.[16] This dimerization happens to an even greater extent when Hb is in dilute solutions.

1.2.3 Hemoglobin –the allosteric model

Liganded Hb has a different quaternary structure from unliganded Hb. Unliganded Hb favors a structural configuration called a Tense or T-state. When Hb is in this state it binds oxygen at a lower rate, in comparison to its other configuration, the Relaxed or R-state. The Hb molecule undergoes changes in both the quaternary and tertiary structure when switching between the R and T states. In the quaternary structure, the R-state will cause the two αβ dimers to rotate 15° in relation to each other. Also, the two β subunits will separate by 7.5° as shown in figure [1.5] below.[17] The tertiary structure will have changes in the area of the heme group. When deoxygenated, the iron atom will displace slightly out of the porphyrin ring, causing the decreased oxygen affinity of the T-state. When Hb is in the R-state the iron atom will lie in the plane of the porphyrin ring allowing for a better contact with the proximal histidine as well as allowing stronger binding between the iron atoms and ligands such as oxygen.[18]

The R and T-states are quaternary states. This means that the affinity for a ligand depends on the quaternary structure, not the number of ligands already bound. Therefore,

---

[16] Bunn, H. F. et al. (1986). Hemoglobin Molecular, Genetic and Clinical Aspects. John Dyson. Saunders Co. p. 25.

[17] Bunn, H. F. et al. (1986). Hemoglobin Molecular, Genetic and Clinical Aspects. John Dyson. Saunders Co. p. 22.

[18] Bunn, H. F. et al. (1986). Hemoglobin Molecular, Genetic and Clinical Aspects. John Dyson. Saunders Co. p. 33-34.

one of the four subunits of the Hb molecule cannot be in the R-state while the others are in T. This is a well tested theory[19] whose model is described by Monod, Wyman and Changeux in 1965 (the MWC model). Pictorially, the model is shown in figure [1.4]. This model allows hemoglobin binding to be described by just three variables, L, k_R and c. L is the ratio of the initial population of T-state Hb to R-state Hb:

$$L = [T]/[R] \tag{1.1}$$

And c is the ratio of heme ligand affinities for the two states:

$$c = K_R/K_T \tag{1.2}$$

Where K is the dissociation equilibrium constant:

$$HbO_2 \underset{K}{\rightarrow} Hb + O_2 \tag{1.3}$$

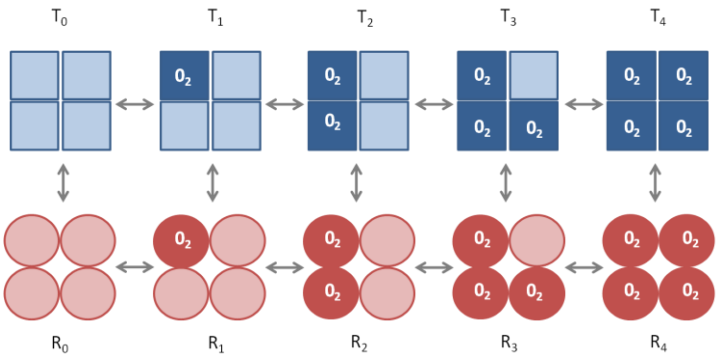

Figure [1.4]: The MWC model.

[19] Shulman, R.G., J. J. Hopfield. S. Ogawa. (1975). Allosteric Interpretation of Hemoglobin Properties. *Quarterly Review of Biophysics*. 8:325-420.

Hemoglobin is often described as having a "switch over point." This is the point at which it is energetically favorable to be in the R-state over the T-state. This occurs at around the binding of the third ligand, or rather, 2.7 ligands. See figure [1.5] for the energy level diagram. The figure shows that the energy level of T_0, the unliganded T-state Hb molecule, has a lower energy than R_0. Therefore Hb, without ligands will prefer the lower energy state and will most likely be found in T_0. At around 3 ligands, the energy levels are almost the same, and Hb can now "switch" in the R-state conformation. This is the switch point, which allows the molecule to remain in the lower energy configuration while still binding ligands[20]. This model uses the parameters of L_0, K_R, and K_T. However, here L_0 is the ratio of T_0 to R_0 (the initial populations of each unliganded state) and defines the R enery levels in respect to the T ones. K_R and K_T are the separation between the energy levels in the R and T-states respectively. Here the parameter c is defined as above, but now we also have the relation below for each population ratio L_i:

$$L_i = \frac{T_i}{R_i} = L_0 c^i \tag{1.4}$$

[20] Shulman, R.G., J. J. Hopfield. S. Ogawa. (1975). Allosteric Interpretation of Hemoglobin Properties. *Quarterly Review of Biophysics*. 8:325-420, p. 5.

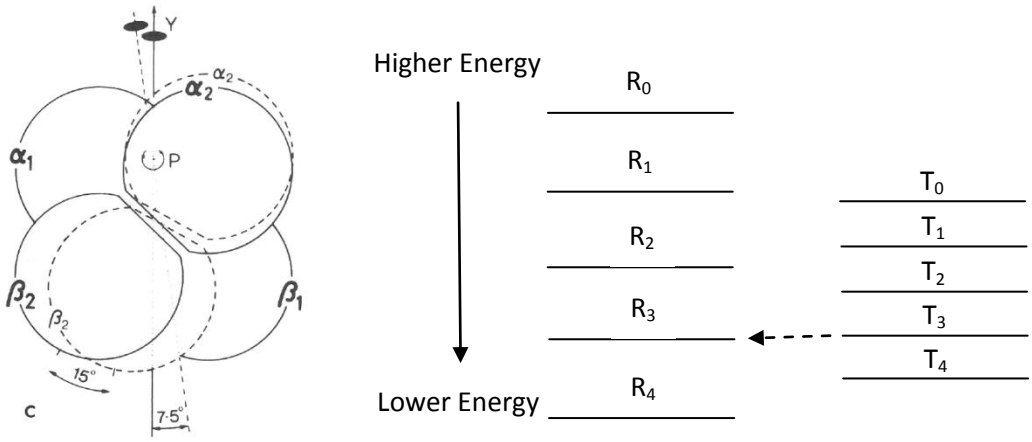

Figure [1.5]: Left: The R and T state quaternary structure.[21] Right: Energy level diagram.

When the fractional saturation of Hb is plotted versus oxygen pressure, a curve with a sigmodial shape will be obtained (figure [1.5] below). The sigmodial shape indicates that Hb binding is a cooperative process, i.e. as Hb switches to the R-state it binds ligands at a faster rate than in the T-state. The fractional saturation of Hb is defined as:

$$Y = \frac{[Hb(O_2)_n]}{[Hb]+[Hb(O_2)_n]} \tag{1.5}$$

This is the ratio of Hb with Oxygen bound to the total amount of hemoglobin (both liganded and unliganded). The Hill coefficient is a way to characterize the cooperatively of a molecule. Below is the Hill equation, with n being the Hill coefficient. If the slope for n is 1, then the system binds ligands only at a single rate. Hb has a Hill coefficient between 2.8 and 3.0 which means it has positively cooperative binding. The equation for n is given below:

[21] Bunn, H. F. et al. (1986). Hemoglobin Molecular, Genetic and Clinical Aspects. John Dyson. Saunders Co. p. 69.

$$log\frac{Y}{1-Y} = n\ log\left(\frac{PO_2}{P_{50}}\right) \quad (1.6)$$

Where P_{50} is the pressure at which the Hb solution is 50% saturated with ligands. In figure [1.6] below the Hill coefficient for Hb has a slope of 1 near the beginning and end of the binding curve, with a maximum slope of 3 in the middle. That is due to most of the Hb molecules being in the T-state in the beginning of the process, and in the R-state in the end of the process.

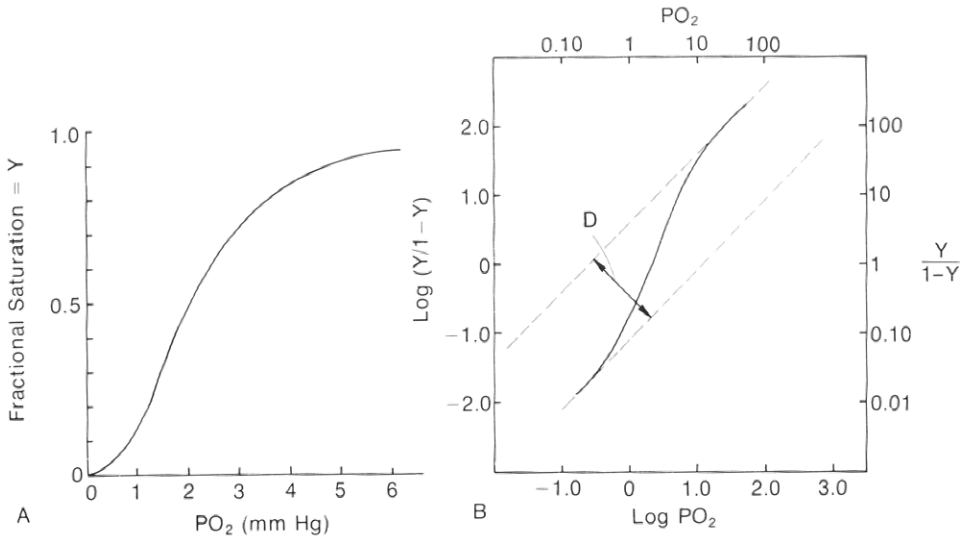

Figure [1.6]: Left: The oxygen binding curve. Right: The Hill coefficient plotted.

1.2.4 Other types of Human Hemoglobin – Fetal Hemoglobin

Until now, when Hb has been mentioned, it was assumed that the species of Hb was HbA: normal adult hemoglobin. There are however, many species of Hb, some naturally

occurring in humans, as well as some abnormal variants. The Hb species most pertinent to this thesis are: HbA (Normal Adult Hemoglobin), HbF (Fetal Hemoglobin) and HbS (Sickle Hemoglobin). Hb will now refer to Hemoglobin in general and not any one particular type.

Fetal Hemoglobin is just one example of a naturally occurring variant of Hb. It is the main mechanism of oxygen transport in the last seven months of human fetal development. HbF has a higher oxygen affinity in comparison to HbA. Whereas HbA has a p50 at an O_2 pressure of 26.8 mmHg, HbF is half saturated at just 19 mmHg. This higher affinity allows the fetus to recover oxygen from the mother's blood stream in order to sustain itself. After birth the amount of HbF rapidly decreases from around 80 ±10 % to less than 10% after 6-12 months due to the increased synthesis of HbA. Normal adults have varying amounts of HbF in their RBC's but the amount is usually less than 2%. HbF levels can be elevated in adults in circumstances of pregnancy and congenital disorders such as hereditary persistence of HbF.

The structural difference between HbA and HbF is in the β subunits of the quaternary molecule. HbF differs in 39 of the 146 amino acid residues, enough of a difference to allow this subunit to be named γ in HbF. Four substitutions which occur at the $\alpha_1\gamma_1$ interface are believed to cause the molecule to be more stable and decrease its dissociation into monomers in comparison to HbA. HbF also interacts less with allosteric effectors, small molecules that change the "switch over point" of Hb. One common allosteric effector, 2,3-DPG binds to the deoxy form of HbA in the cavity made by the four subunits in the middle dyad axis. By binding to the deoxy structure, it stabilizes the T-structure, and therefore makes the switch into R-state more difficult. However, once the R-state is achieved, 2,3-DPG is ejected due to loss of contacts. 2,3-DPG shifts the oxygen binding curve to the right, thereby requiring a higher oxygen pressure to achieve the same

number of ligands bound in a Hb system. In HbF one of the contacts for the 2,3-DPG binding site is mutated; β 143 Histidine becomes γ 143 Serine thereby dimishing the effectiveness of 2,3-DPG.[22] HbF like HbA can dimerize and reform into quaternary structures. If HbF is mixed with HbA, the dimers can reform into a mixed species; HbAF with subunits of: $\alpha_1\beta_1\alpha_2\gamma_2$.

1.3 Sickle Hemoglobin

1.3.1 Sickle Hemoglobin – Historical Background

Sickle Hemoglobin (HbS) is another variant of Hb which is caused by inheriting two homozygous sickle genes. It is so named from the sickle shaped RBCs found in those with Sickle Cell Anemia (see figure [1.7]). In humans, there are two genes needed in order to make each of the subunit types of Hb, i.e. two genes for α, β, γ, etc. Children inherit one gene for each type from each parent. Since these genes are co-dominant, both will be expressed. For example, if a person had inherited one normal and one sickle gene, they would express both sickle and normal β groups in their Hb; a condition called "sickle trait." They also would have a 50/50 chance of passing on the sickle gene to each of their children. See figure [1.7] below.

---

[22] Bunn, H. F. et al. (1986). Hemoglobin Molecular, Genetic and Clinical Aspects. John Dyson. Saunders Co. p. 70.

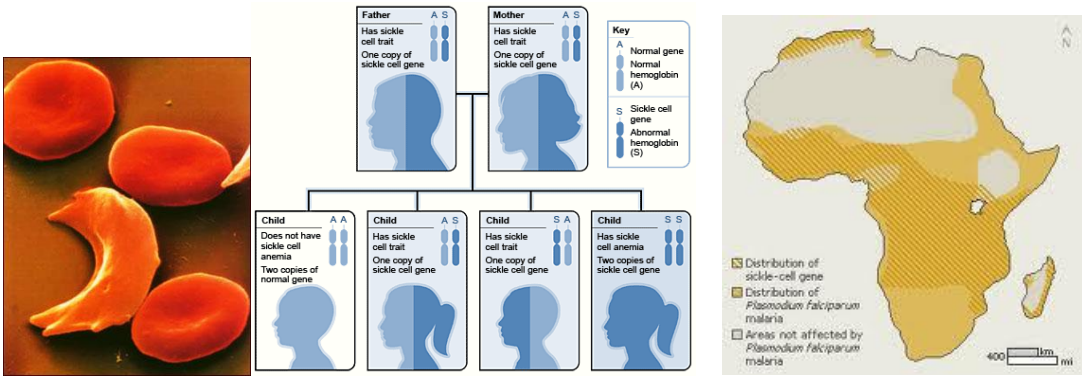

Figures [1.7]: Left: Sickle shaped red blood cell. Middle: Inheritance of sickle and normal genes from parents with sickle trait. Right: Prevalence of Malaria and the sickle-cell gene in Africa.

The Sickle mutation was found generally in African populations where there was a historical prevalence of malaria (see figure [1.7]). It has been found that HbS has some protection against Plasmodium falciparum, the most severe form of malaria. P. falciparum is also the most common type of malaria, causing 80% of infections and 90% of malaria associated deaths.[23] However, studies have shown that the protection offered by sickle cell trait is mostly beneficial to infants and those less than 60 weeks old.[2425] Surviving older children and adults without HbS have usually developed immunity to malaria, so there is no observable difference in their susceptibility later in life in comparison to those with the sickle trait. The malarial infection begins in the liver, where it multiples. Following the rupture of its host cells, malaria will then spread to the blood and infect RBCs. Circulating infected RBCs will be destroyed by the spleen. However malaria circumvents the spleen by

---

[23] Mendis K. B. et. al. (2001). The neglected burden of Plasmodium vivax malaria. *Am. J. Trop. Med. Hyg.* 64:97–106.
[24] Bodmer, W.F. et. al. (1976). Genetics, Evolution and Man. San Francisco, W. H. Freeman, p. 307.
[25] Power, H. W. (1975). A model of how the sickle cell gene produces malaria resistance. *J. Theor. Biol.* 50:121.

displaying adhesive proteins on the surface of infected RBCs which will cause the cell to become lodged in small blood vessels. This allows the parasite to be sequestered from circulation to the spleen as well as causing hemorrhagic complications.[26] The exact mechanism of how HbAS protects against malaria infection has not been well established. One theory is that the malaria infected RBCs with HbAS will deform and sickle when the virus consumes oxygen and will therefore be removed from circulation before the cell becomes adherent and can multiply elsewhere.[27] Another theory is that the virus crowds the cell as well as lowering the pH, thereby enhancing sickling of the cells.

Malaria has been a major cause of death of children worldwide and is also the strongest force for selective evolutionary science worldwide.[28] There is growing evidence of many diverse genetic adaptations to malaria, including the sickle gene. The distribution of the Sickle gene globally has mostly been due to emigration. However, through tracking phenotypes of the Sickle gene, it was found that the mutation has risen independently in West Africa from Central and East Africa.

Sickle Cell Anemia was recognized as a disease in Africa for centuries before its clinical manifestation would be recognized by western science.[29] It was already known by local populace that it ran in families and had differing levels of severity. Most cases of homozygous HbS in Africa did not live past infancy due to the combination of malnutrition, prevalent infections and lack of medical care. This led to a mistaken perception that the

---

[26] Chen, Q. et. al. (2000). Molecular aspects of severe malaria. *Clin. Microbiol. Rev.* 13 (3): 439–50.
[27] Luzzato, L. et. al. (1970). Increased sickling of parasitized erythrocytes is mechanism of resistance against malaria in the sickle trait. *Lancet* 1:319.
[28] Kwiatkowski D. P. (2005) How malaria has affected the human genome and what human genetics can teach us about malaria. *Am J Hum Genet.* 77: 171–92.
[29] Konotey_Ahulu, F. I. (1910). The sickle cell diseases: clinical manifestations including the "sickle crises." *Arch. Intern. Med.* 6:517.

disease was relatively uncommon in Africa, but prevalent in countries like the United States. James B. Herrick, an American physician would be the first to describe a case of sickle cell anemia in medical literature in 1910. His patient suffered from breathlessness, palpitations and jaundice. A medical examination also found he had an enlarged heart and anemia. Dr. Herrick would be the first to show a photomicrograph in his report of the thin crescent shaped red blood cells.[30] In 1915, Victor Emmel, an anatomist would show that the sealed blood of a sickle patient between a microscope slide and a cover slip would sickle over time.[31] Likewise, the patient's father's blood would sickle, even though he was asymptomatic. This would be the beginning of understanding the inheritance of the disease as well as sickle trait.

In 1927 a surgeon, Vernon Hahn and an intern, Elizabeth Gillespie, found that they could sickle the RBCs in a suspended drop when the oxygen pressure was below 45 mmHg. They also showed that sickling was reversible by reoxygenation and that cells without Hb would not sickle. In 1940, Irving Sherman, a student at Johns Hopkins would find that at reduced oxygen tensions the RBCs of those with anemic symptoms would sickle quicker than those with asymptomatic sickle trait. He also found that when the deoxygenated sickle cells were viewed under a polarized microscope they exhibited birefringence. This meant that certain molecules of the cell become oriented when they undergo sickling.[32] Hb was identified as the cause of the RBC sickling by Janet Watson, a hematologist from Brooklyn in 1948. She would note that sickling did not become significant until the HbF in an infant was

---

[30] Herrick, J. B. (1910). Peculiar elongated and sickle-shaped red blood corpuscles in a case of severe anemia. *Arch. Intern. Med.* 6:517.

[31] Emmel, V. E. (1917). A study of the erythrocytes in a case of severe anemia with elongated and sickle-shaped red blood cell corpuscles. *Arch. Intern. Med.* 20:586.

[32] Murphy, R. C. et. al. (1944). Sickle cell disease. I. Observations on behavior of erythrocytes in sickle cell disease. *Arch. Intern. Med*. 74:28.

replaced by mostly "adult" hemoglobin. Finally in 1949, Linus Pauling would use boundary electrophoresis to show that the Hb from those with sickle cell anemia had a different mobility than the Hb from a normal individual. Likewise, those with sickle trait had about equal amounts of normal and sickle type Hb. This would be the first identification of a molecular disease and its inheritance.[33]

1.3.2 Sickle hemoglobin – as a protein (from mutation to polymerization)

Sickle hemoglobin is a disease caused by a mutation in the β^s gene. This mutation produces an amino acid substitution in the 6^{th} position of the β subunit of Hb: β 6 Glu → Val. The negatively charged glutamic acid is replaced by hydrophobic valine, see figure 8 below for the amino acids' molecular structure. This single amino acid substitution in the β subunits causes HbS to polymerize when deoxygenated. The polymerization must be a consequence of the substitution, which is an alteration to the surface of the molecule. Aside from the polymerization, HbS functions the same as HbA. For example, if the p50 oxygen binding curve was compared for the two hemoglobins, they would be the same, as long as the HbS was dilute.[34] Otherwise if the concentration of HbS was above solubility, it would start to form polymers when deoxygenated and the binding curve would not be correctly measured. This is because the binding of ligands to HbS in a polymer is weaker than HbS in solution.

---

[33] Pauling, L. et. al. (1949). Sickle cell anemia: A molecular disease. *Science* 110:543.

[34] Gill, S. J. et. al. (1979). Oxygen binding to sickle cell hemoglobin. *J. of Mol. Bio*. 130(2) 175-189.

Hydrophobic bonding and electrostatic interactions are the primary forces behind the formation of the polymers.[35] When a polymer is formed, it contains 14 strands, or rather 7 double strands of monomers with a right handed helical twist (figure [1.8]).[36] This configuration of the sickle fiber was determined by electron micrographs. However, it does not give any information about the orientation of the HbS molecule in the fiber structure. Using other techniques such as x-ray structural information and optical data, researchers were able to constrain the X axis of the molecule to be within 22 degrees of the fiber axis.[37] [38] Although this constrains the molecules position, it does not provide definitive information on the intermolecular contacts between molecules in the fiber.

There is however better information about possible molecular contacts from HbS crystals. Nevertheless, the crystals are packed differently: they are arranged in pairs of parallel double strands, with each strand staggered by a half molecule and rotated by a half turn. There are two contacts that were identified in the crystal structure, axial and lateral. Axial are contacts between a molecule in a strand and the molecule directly vertical above or below it in the strand. Lateral are the contacts between the molecules from side to side. In figure [1.9], lateral contacts are made between the β 6 of one HbS to the β 85 and β 88 of another molecule. Notice how only one subunits' β 6 mutated contact is needed to make this structure. There is also a lateral contact between β 73 and β 4 on the other Hb molecule. As for axial, there are several, one is the β 22 with the α 20 above it. Axial contacts can include both α and β subunits as seen in figure [1.8].

---

[35] Bookchin, R. M., and R. L. Nagel. (1973). Molecular interactions of sickling hemoglobins. In Abramson, H., Bertles, J. F., and Wethers, D. L. (eds.): Sickle Cell Disease. St Louis. *C. V. Mosby Co.,* p. 140.
[36] Hemoglobin, p. 456.
[37] Hofrichter, J. et. al. (1973). Structure of hemoglobin S fibers: Optical determination of the molecular orientation in sickled erythrocytes. *Proc. Natl. Acad. Sci.* 70:3604.
[38] Eaton, W. A., and J. Hofrichter. (1981). Polarized absorption and linear dichroism spectroscopy of hemoglobin. *Methods Enzymol.* 76:175.

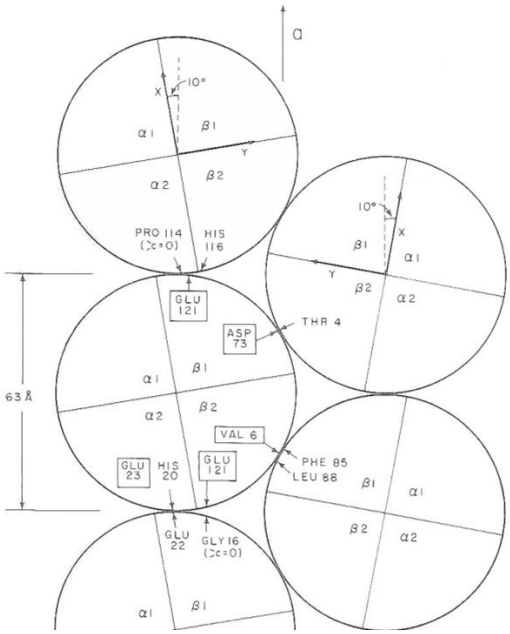

Figure [1.8]: The possible axial and lateral contacts of the Hb crystal

The packing of HbS molecules in the crystal is structurally different than the fiber. The fiber is better described by a group of 7 double strands which are packed and twisted, in comparison to a lattice of parallel and anti-parallel double strands. It is generally accepted that the contacts used to make a crystal can be used in the fiber formation. However, because the fiber structure cannot be studied like a crystal structure, what contacts exist in the fiber cannot be definitively known.

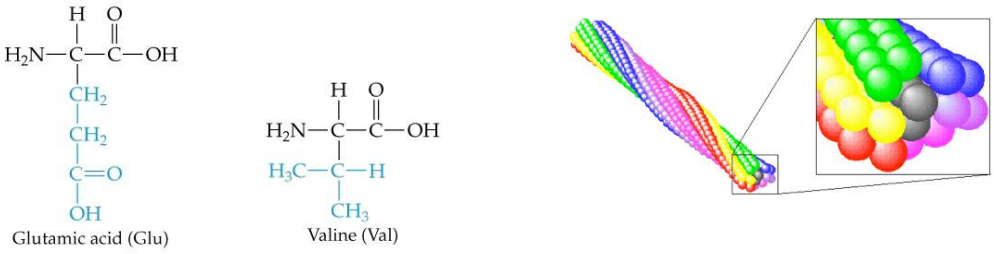

Figure [1.9]: Right: Glu & Val amino acids. Left: 14 strand polymer with twist.

The HbS polymer is formed through a double nucleation pathway. Deoxygenated HbS molecules form nuclei in solution, coming together and separating at random. Eventually, enough molecules will nucleate to overcome the energy barrier, and the growth process will become energetically favorable. The formation of a nucleus is a stochastic event and the critical nucleus is the size of the nucleus at which the addition of a monomer becomes favorable. The nucleus will grow into a polymer. However, HbS can also form new nuclei on preexisting polymers, which will also grow into new polymers. The single nucleation event is called homogeneous nucleation, and is defined by f_0, the homogeneous nucleation rate. The growth of nuclei on existing polymers is called heterogeneous nucleation and is referred to as the heterogeneous nucleation rate, B. See the figure [1.10] below for clarification of the double nucleation model. Due to the two pathways of nucleation, HbS polymer growth is exponential.

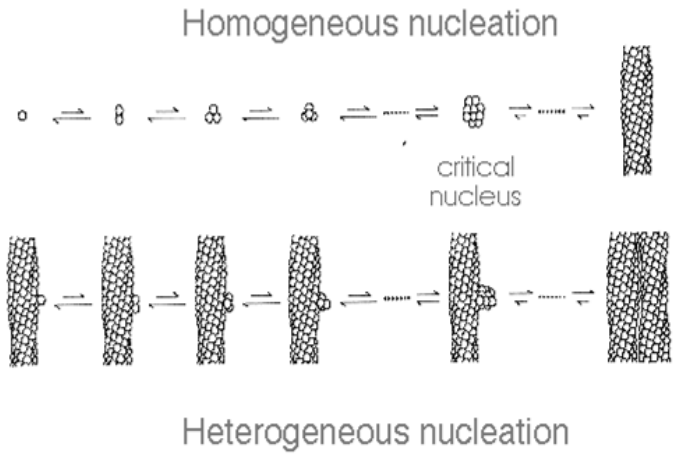

Figure [1.10]: The two pathways of nucleation

1.3.3 Sickle hemoglobin –hybrid and partially liganded molecules

There were many studies done on sickle polymer formation to ascertain the contacts necessary. Most of the early experiments were done using Hb mutants, molecules that have different amino acids at key locations in the α and β subunits. These experiments were often conducted using a gelation and solubility measuring technique. Gelation, or rather minimum concentration required for gelation (MGC) is done by evaporating the HbS solution with a dry gas until it no longer will flow due to fiber formation. Such a technique was used by Singer and Singer to establish that HBSF (fetal and sickle hemoglobin hybrids) will not enter a polymer.[39] Meanwhile, HbS/HbA and HbS/HbC hybrids will enter a polymer. This proved that only one β6 contact was required to form a polymer, and that the HbF molecule was just too different to enter a polymer even as a hybrid. Solubility

[39] Singer, K., and L. Singer. (1953). The gelling phenomenon of sickle cell hemoglobin: Its biological and diagnostic significance. *Blood* 8:1008.

measurements are done by centrifuging a concentrated solution of deoxygenated Hb. The polymers will separate from the solution and the concentration of the supernatant can be measured for the solubility[40]. Aside from providing a more precise measurement than gelation, this technique also gives information on other properties such as solvent conditions and ligand binding.

Other forms of Hb can polymerize, one such example is methemoglobin, the ferrous form (Fe^{+3}) of Hb. At low pH and with organic phosphates it can assume a T-state structure. If concentrated, met-HbS will still polymerize.[41] It is also possible to have Nitric Oxide (NO) bound to HbS in the T-state and still create a polymerized gel.[42] Likewise, an experiment was done that showed oxygenated Hb can be partially converted to a T-state and formed into a gel.[43] Likewise, solubility measurements done by Hofrichter and Eaton showed that polymerized HbS had small amounts of oxygen bound to the monomers in the polymer.[44] [45] Similar results were found using Carbon Monoxide (CO).[46] [47] [48] Although it is known that O2 and CO can enter gelled HbS, it is not known how the presence of these gases effect

---

[40] Bertles, J. F., R. Rabinowitz, and J. Dobler. (1970). Hemoglobin interaction: Modification of solid phase composition in the sickling phenomenon. *Science* 169:375.
[41] Briehl, R. W. and S. Ewert. (1974). Gelation of sickle hemoglobin. II. Methemoglobin. *J Mol. Biol.* 89:759.
[42] Briehl, R. W. and J. M. Salhany. (1975). Gelation of sickle hemoglobin. III. Nitrosyl hemoglobin. *J Mol. Biol.* 96:733.
[43] Gupta, R. K. (1976). Nuclear relaxation and gelation study of the interaction of organophosphates with human normal and sickle oxyhemoglobins. In vitro gelation of sickle oxyhemoglobin in the presence of iosital hexaphosphate. *J Biol. Chem.* 25:6815.
[44] Hofrichter, J. (1979). Ligand binding and the gelation of sickle cell hemoglobin. *J Mol. Biol.* 128: 335.
[45] Sunshine, H. R., J. Hofrichter, F. A. Ferrone, W. A. Eaton. (1982). Oxygen binding by sickle cell hemoglobin polymers. *J Mol. Biol*. 158:251.
[46] Hofrichter, J. (1979). Ligand binding and the gelation of sickle cell hemoglobin. *J Mol. Biol.* 128: 335.
[47] Chung, L. L. and B. Magdoff-Fairchild. (1978). Extent of polymerization in partially liganded sickle hemoglobin. *Arch. Biochem. Biophys*. 189:535.
[48] Christakis, J. et. al. (1977). Mechanism of inhibition of hemoglobin S polymerization by cyanate. *J Lab. Clin. Med*. 89:992.

polymer growth in vivo or in vitro.

1.3.4 Sickle Hemoglobin – as a disease

Sickle cell anemia affects 70,000 to 100,000 African Americans.[49] People who are homozygote for sickle cell disease will have a decreased lifespan of 42 years for men and 48 years for women.[50] Newborns with the disease will begin to exhibit symptoms around the 5th month of new born life. That is when the baby's fetal Hb is mostly replaced with HbS. The first infant symptom of Sickle Cell Anemia is hand-foot syndrome (dactylitis). Sickled cells become stuck in the small blood vessels in the extremities such as the hands and feet, blocking the flow of blood and causing swelling (figure [1.11]). Another ubiquitous complication is chronic hemolytic anemia. Anemia is a condition caused by not having enough healthy RBC's to deliver oxygen to the body. Since the RBC's of Sickle homozygotes only survive for about 15 days rather than the usual 100, they suffer from chronic anemia. Anemia side effects include tiredness, irritability, shortness of breath, slow growth, jaundice and delayed puberty. Hemolytic anemia is a type of anemia associated with the abnormal breakdown of RBCs in the blood vessels or elsewhere in the body leading to free Hb in the plasma. The side effects of this condition are similar to normal anemia, but also include an enlarged spleen which may require a splenectomy. The most substantially painful symptom of sickle cell disease is the sickle cell crisis. It is believed to be caused by sickled cells restricting oxygen delivery to many tissues in the body, and is accompanied by episodes of

---

[49] Solomon O. A. and K. Ohene-Frempong. (2007). Beyond National Borders: A Global Perspective on Advances in Sickle Cell Disease Research and Management, and New Challenges in The Genome Era. [book auth.] B Pace. Renaissance of Sickle Cell Disease Research in the Genome Era. pp. 333-345.

[50] Platt O. S. et. al. (1994). Mortality in sickle cell disease. Life expectancy and risk factors for early death. *N. Engl. J. Med.* 330 (23): 1639–44.

great pain that can last for weeks. There is no effective treatment for a crisis once it happens. Pain medications and the breathing in of oxygen from a mask are the only current therapies available; neither of which address the issue of providing needed oxygen to tissues cut off from the normal blood flow.

Other side effects of sickle cell disease include chronic lung disease, pulmonary hypertension, avascular necrosis, kidney failure, retinopathy, leg ulcers, cerebral infarctions, stroke and morbidity. Chronic lung disease is term that describes the symptoms of difficulty breathing, chest pain and exercise intolerance. It can be caused by sickled cells restricting the oxygen supply to lung tissue and causing it to die. Pulmonary hypertension is caused by the abnormal blood flow in sickle cell patients. They develop high blood pressure in the arteries that supply blood to the lungs which leads to fatigue, dizziness and shortness of breath. Avascular necrosis is the death of bone tissue due to lack of blood supply usually occurring in the hip joint. It can cause extreme pain and flattening or collapsing of the bone, see figure [1.11] for an MRI scan of avascular necrosis. Kidney failure can also occur from chronic sickling and reduced blood supply to the kidneys. Likewise, if the nerve tissue in the retina does not receive enough oxygen it can weaken and the person can become vision impaired or blind, a condition called retinopathy. Leg ulcers are one symptom whose pathology is not yet defined. They occur around 20-50 years of age and begin as small protruding crusting sores on the legs (figure [1.11]). Occurring more often in males than females, they can appear for a short while or persist for years, they can heal and reoccur. The only treatments available are blood transfusions and hyperbolic oxygenation (to try to get oxygen to the local blood vessels near the sore).

Sickle cell disease is the most common cause for stroke in children.[51] Strokes are also more common in children than adults with the average victim being around 6 years old.[52] [53] Around 11% of sickle cell patients will experience a clinical stroke syndrome by age 20.[54] It usually occurs by occluding the middle cerebral and internal carotid arteries.[55] A substantial study conducted on 130 children with sickle cell anemia, STOP, The Stroke Prevention Trial, found that routine blood transfusions that kept the amount of HbS around 30% decreased incidence of stroke by 90%. The trial was so successful it was terminated early. However, cerebral infarctions (a stroke where blood does not reach brain tissue thereby causing it to die, with varying degrees of severity) were still taking place.[56] Another study of 185 patients found that at a mean age of 10 years, 44% of children had an overall prevalence of infarction or related ischemia.[57] Children also suffer from silent infarctions, meaning they do not know they are occurring, but upon detailed examination cognitive impairment and other subtle neurologic affects will be found.[58] Another study of 27 randomly selected children who are not clinically affected by strokes, found 33% with mild retardation levels, which is compared to a normal 1.45% for inner city black children.[59] This demonstrates that even though the patients do not suffer from overt stokes, they still have chronic hypoxia in their brain.

---

[51] Hoppe, C. (2005). Defining stroke risk in children with sickle cell anaemia. *J. of the British Society for Haematology.* 128:751-766.
[52] http://sickle.bwh.harvard.edu/scdmanage.html. Accessed April 2011.
[53] Powars, D. et. al. (1978). The Natural History of Stroke in Sickle Cell Disease. *Am J Med*. 65:461-471.
[54] Powars, D. et. al. (1978). The Natural History of Stroke in Sickle Cell Disease. *Am J Med*. 65:461-471.
[55] Balkaran, B. et. al. (1992). Stroke in a Cohort of Pateints with Homozygous Sickle Cell Disease. *J. of Pediatrics*. 120:360-366.
[56] Adams R. J. et. al. (1998). Stroke Prevention in Sickle Cell Anemia. *Control Clin. Trials.* 19:110-129.
[57] Steen, R. G. et. al. (2003). Brain Imaging in Pediatric Patients with Sickle Cell Disease. *Radiology.* 228:216-225.
[58] Dowling, M. M. et. al. (2010). Brief report acute silent cerebral infarction in children with sickle cell anemia. *Pediatric Blood & Cancer*. 54:461-464.
[59] Steen R. G. et. al. (1999). Subtlebrain abnormalities in children with sickle cell disease: relationship to blood hematocrit. *Ann. Neurol*. 45:279-286.

Figure [1.11]: Right: swollen hands from Sickle Cell Dactylitis. Middle: vascular necrosis of the hip joint. Right: leg ulcer.

1.3.5 Sickle hemoglobin – therapies

The only known cure for sickle cell anemia is a bone marrow transplant. However with the risk of death (5-10%) and the unlikelihood of finding a matching donor, this is an option available to very few with the disease. Human leukocyte-associated antigens, or HLA is a type of bone marrow transplant used to cure those with cell disease. In a study of 22 patients under the age of 16 who received HLA transplants between 1991 and 1995, 20 survived. The two that died had a central nervous system hemorrhage or graft-versus host disease (GVHD) which sometimes develops when white blood cells from the donor of the graft identify cells in the patient's body (the host) as foreign and attack them. In four patients the graft was rejected and in 3 of those 4 sickle disease reoccurred. Sixteen of the patients had a stable engraftment and 1 of the 16 had stable mixed chimerism (meaning

stable amounts of HbS/HbA or HbA after the transplant).[60] A study done in 2001 on 59 children ages 3.3 to 15.9 tracked the results of their bone marrow transplants from HLA identical sibling marrow allografts. The higher the number of matching HLA antigens, the greater the chance that the patient's body will accept the donor stem cells. Fifty five patients survived the procedure and 50 survived free from sickle cell disease. Thirteen patients had stable mixed donor host hematopoietic chimerism; meaning they had stable amounts of HbS/HbA red blood cells being produced based on whether their donor had sickle trait or just HbA.[61] Although bone marrow transplant can cure Sickle Cell disease, there remain some limiting factors. First, an identical HLA donor must be found to ensure the highest probability of success. For many with SCD there may not be an acceptable donor. Second, to also ensure a higher probability of healthy recovery following grafting, the patient must have vital organs which have not been too greatly damaged from SCD. Finally, even with the above criteria, there is still a 5-10% risk of death, and also a risk that the graft will be rejected. Not many with SCD can or are willing to risk a bone marrow transplant.

Routine blood transfusions are another common therapy for SCD. There are three main types of transfusions, simple transfusion, partial exchange and chronic exchange. Simple transfusion is best for those who are severely anemic because it increases the amount of HbA RBC's without removing any blood from the patient. An exchange transfusion is best for removing HbS RBCs from the patient. Usually exchange transfusions

---

[60] Walters, M.C. et. al. (1996). Bone marrow transplantation for sickle cell disease. *New Eng. J. of Med.* 335(6):369-376.

[61] Walters, M. C. et. al. (2001). Stable mixed hematopoietic chimerism after bone marrow transplantation for sickle cell anemia. *Biol. Blood Marrow Transplant*. 7(12):665-673.

are used for those with acute cerebrovascular accidents, multiorgan failure syndrome, acute chest syndrome (or other lung disease) and before surgery or anesthesia. Chronic transfusions are transfusion programs that will aim to keep the percentage of HbA in the patient above 50 to 70% which means an exchange every 3 to 4 weeks. Usually this therapy will be used for children who had cerebral vascular occlusions, stroke or those with chronic congestive heart failure. Transfusions have been used to try to treat other symptoms of the disease such as frequent crisis events, deterioration of health when all other treatments have been unsuccessful, adults with cerebrovascular accidents, leg ulcers and chronic organ failure. However, it has not been shown that transfusions remedied any of those symptoms. If chronic transfusions are used to treat these symptoms, the patient will usually have a relapse or exacerbation of symptoms once treatment is stopped especially if treatment is suddenly terminated. Sickle patients will still have the same complications as anyone undergoing transfusions. This includes volume overload, which is when too much blood has been transfused too quickly. This can cause congestive heart failure and pulmonary edema. They are also at risk for iron overload (whose treatment also carries side effects) and alloimmunization to red blood cell antigens, making compatible blood difficult to obtain as well as increasing the probability of having a life threatening allergic reaction to the transfused blood.[62] They are also at risk for contracting Hepatitis B and C, as well as at risk for contracting HIV if receiving transfusions in a country that does not thoroughly screen their donated blood for HIV antigens.[63]

---

[62] Clarice, D. R. et. al. (1995). Management and therapy of sickle cell disease. *NIH publication.* Third ed. 59-67.

[63] Yhaya, A. H. et. al. (2011). 203 Donation or infection: retrospective assessment of transfusion transmissible HIV among sickle cell anemia patients. Journal of Acquired Immune Deficiency Syndromes. 56:86.

Hydroxyurea (HU) is a daily dose prescription drug used to treat those with SCD. Originally it was used to treat cancer, but is beneficial for sickle patients because it increases the amount of HbF produced by the body. HU increases the count of F-cells (cells with only HbF) and the overall percent of HbF in other erythrocytes. Since there is a higher amount of non-polymerizing Hb species, patients see improvements in several symptoms such as frequency of crisis episodes and acute chest syndrome. They will also need fewer blood transfusions and will have less hospital visits. A study reported in 2003 also found that children on regular long term HU treatment had growth rates comparable to normal children, whereas untreated children with SCD have below average growth.[64] Nevertheless the efficacy of this drug varies for each person taking it. In a study completed in 1996, 150 patients were tracked for their response to HU for 2 years. Half the patients had long-term increments in HbF, with the top two quartiles seeing an increase of 18.1% and 8.8%. The lower two quartiles changed little from baseline, having 4.2% and 3.9% HbF. Only the top three quartiles saw a substantial increase in F cells which persisted for two years, with the lowest quartile returning to baseline level after the first year.[65] The effectiveness of this drug also depends on the patient taking it daily in the prescribed regime. HU also has some side effects, which are alleviated once treatment is stopped, such as bone marrow suppression and mild neutopenia; i.e. decreased white cell count.

Pain medications are another important treatment for SCD. The pain associated with sickle cell can be intense and last for many days as in a crisis, or mild but still enough to interfere with everyday functionality. Severe pain is treated with either prescription pain

---

[64] Zimmerman, S. A. et. al. (2004). Sustained long-term hematologic efficacy of hydroxyurea at maximum tolerated does in children with sickle cell disease. *Blood*. 103: 2039-2045.
[65] Steinberg, M. H. et. at. (1997). Fetal hemoglobin in sickle cell anemia: determinants of response to hydroxyurea. *Blood.* 89:1078-1088.

killers such as naproxen, codeine and morphine, while more mild pain can be treated with acetaminophen or ibuprofen. Other common treatments for SCD include: breathing in of supplemental oxygen for low oxygen levels as well as receiving fluids through an IV to reduced blockage of vessels. It is also important for sickle patients to receive antibiotics when they get an infection especially pneumonia or acute chest syndrome, since these complications can lead to morbidity.[66] There are other experimental treatments for SCD whose efficacy has not been studied. This includes gene therapy (turning off the sickle gene) as well as drugs which work similarly to HU such as Butyric acid and Decitabine (which may have less side effects). Finally, Nitric oxide (NO) is also an experimental treatment which has been found to dilate blood vessels, reduce the stickiness of RBCs, reduce sickling of HbS, but inhalation of NO does not aid in alleviating a crisis once it has already begun.[67]

Although several treatments described here are proven to help prevent complications and improve the patient's condition, the median survival age for those with SCD remains in the early 40's. In a massive study done on 3764 patients with SCD, 18% of deaths were due to overt organ failure (mostly renal) and 33% due to acute sickle crisis (with 78% of those having pain or acute chest syndrome and the rest having had a stroke). Early mortality was highest in patients who were symptomatic, and life expectancy could be improved if there is a high level of HbF.[68] Clearly, there is still a great need for better treatments with less side effects especially for those who are unresponsive to the current therapies or unable to maintain a strict regimen of transfusions or medication.

---

[66] Gray, A. et. al. (1991). Patterns of mortality in sickle cell disease in the United Kingdom. *J Clin Pathol*. 44:459-463.
[67] Gladwin, M. T. et. al. (2011). Nitric oxide for inhalation in the acute treatment of sickle cell pain crisis. *J of the Amer Med. Ass.* 305(9):893-902.
[68] Platt, O.S. et. al. (1994). Mortality in sickle cell disease. Life expectancy and risk factors for early death. *N Engl J Med*. 330(23):1639-44.

1.3.6 Sickle hemoglobin – trait

About 300 million individuals worldwide have sickle cell trait (SCT). If they are expressing the normal Hb α genes, they will have about 42% HbS in their blood as opposed to those with α gene deletions who have 29% HbS. [69] HbS heterozygotes are generally held to be asymptomatic in the medical community. However, it is important to note that much of the information on sickle trait complications is anecdotal and not part of a rigorous scientific study. There are some side effects that are generally accepted to be present in those with SCT, namely, anatomic and functional differences in the cerebral vasculature, urine concentrating ability, and red cell rigidity.[70] However none of these symptoms are life threatening. There are other more serious complications that have been shown to occur with a slightly higher frequency in those with SCT when compared to the general population. Those are renal medullary cancer, hematuria, renal papillary necrosis, hyposthenuria, splenic infarction, exertional rhabdomyolysis and exercise related sudden death.

Renal medullary carcinoma is an aggressive tumor of the kidney observed almost exclusively in young individuals with SCT. After diagnosis the medium survival is about 15 weeks. Hematuria, blood in the urine, was found to occur in 4% of SCT males admitted to a Veterans Administration hospital, compared to 2% for African American males with normal Hb. It can range from mild to severe and could be caused by polymerization in the long vasa recta of the renal medulla. Hyposthenuria is the loss of the kidney to concentrate urine and

---

[69] Gupta, A. K. et. al. (1991). Effects of alpha-thalassemia and sickle polymerization tendency on the urine-concentrating defect of individuals with sickle cell trait. *J Clin Invest.* 88(6):1963-1968.
[70] Thogmartin, J. R. et. al.: (2011). Sickle cell trait associated deaths: a case series with a review of the literature. *Journal of Forensic Sciences.*

may be related to microinfarctions in the renal medulla. Splenic infarcts are rather uncommon and have been mostly seen to occur in males with over 40% HbS who were in a low oxygen environment. Finally, rhabdomyolysis is the breakdown of muscle fibers and the release of the fiber contents (like myoglobin) into the blood stream. This usually occurs from exercise, lack of oxygen supply, hypothermia, dehydration, overheating, exertion at high altitudes and exertion in non-conditioned individuals. [71]

Rhabdomyolysis is often found as the cause of death in cases of sudden morbidity in those with SCT. A case report of 16 SCT related deaths found that although the circumstances varied greatly, there were several triggers in common: mild to moderate exertion, dehydration and hyperthermia. Several of the people were physically exerting themselves when they suddenly felt lethargic or pain. Post mortem examination revealed rhabdomyolysis and/or micro occlusion as the cause of death. It is believed that cells sickling in the muscles could be the start of these complications by changing the pH of the body. The time from the onset of symptoms to morbidity varied greatly from 20 minutes to 2 weeks in one case. The most precise information on rhabdomyolysis related deaths comes from US Army recruit data, where the rate of sudden unexplained deaths in those with SCT was 32.2 per 100,000; compared to 1.2 per 100,000 for African-American recruits without SCT. However, with implementation of better hydration methods and more breaks to allow the core body temperature to decrease during exertion, the number of unexplained SCT recruit deaths decreased.[72]

---

[71] Tsaras, G. et. al. (2009). Complications associated with sickle cell trait: a brief narrative overview. *The American Journal of Medicine.* 507-512.

[72] Key, N. S. and V. K. Derebail. Sickle-cell trait: novel clinical significance. *American Society of Hemato*logy. 418-422.

1.4 Motivation of thesis

Although sickle cell anemia is symptomatically complex, it is simply the consequence of a point-site molecular mutation of the glutamic acid residue by a valine in the two β subunits of Hb. However, such a substitution causes the deoxygenated form of the molecule to polymerize. There have been many studies done on how other species of Hb or molecules affect polymerization. For example, studies done on the solubility of HbA and HbS mixtures found that HbAS molecules can enter a polymer. This gives information about how polymers form, i.e. a polymer can still form and include HbAS hybrids with only one mutation site (but at a large energetic penalty).[73] [74] Likewise there were studies done on deoxygenated HbS at equilibrium, which found that there was little oxygen or CO bound to the polymer.[75] [76] The equilibrium studies can give information such as the probability for a partially saturated HbS molecule to be in a polymer, but they do not provide information on how that molecule affects the polymerization or nucleation rates. Until now, there have been no studies which measure the homogeneous and heterogeneous nucleation rates of a partially saturated CO or oxy HbS solution.

Studying nucleation rates gives an important piece of information that is applicable to understanding the structural formation of nuclei as well as a therapeutic understanding of how quickly polymer masses grow under these conditions. Nevertheless, most of the studies done on the nucleation rates of HbS have been for pure HbS solutions, such as

---

[73] Eaton, W. A. and J. Hofrichter. (1990). Sickle cell hemoglobin polymerization. *In Advances in Protein Chemistry.* 40:63-262.
[74] Roufberg, A. and F. A. Ferrone. (2000). A model for the sickle hemoglobin fiber using both mutation sites. *Protein Science.* 9:1031-1034.
[75] Hofrichter, J. (1979). Ligand binding and the gelation of sickle cell hemoglobin. *J. Mol. Biol.* 128:335.
[76] Sunshine, H. R., J. Hofrichter, F. A. Ferrone, W. A. Eaton. (1982). Oxygen binding by sickle cell hemoglobin polymers. *J. Mol. Biol.* 158:251.

completely deoxygenated HbS. There are some studies done on hybrid molecules, such as HbS and HbF mixtures, and HbS and HbA mixtures.[77] [78] The hybrid studies have shown that the rate of formation of the HbS nuclei were different from what was predicted. In the case of HbS and HbF mixtures, the benefit of having a non polymerizing species (HbF and HbSF hybrids) was partially counteracted by the crowding of the HbF and HbSF molecules. This meant that polymerization did not decrease by as much as had been expected. In the case of HbS and HbA mixtures, HbAS hybrids can enter the polymer, while HbA cannot. It was found that to form a homogeneous nucleus, there must be at least one pure HbS molecule, while for the heterogeneous nucleus, even a greater number are required. However, despite this the overall nucleation rates of HbS and HbA mixtures were faster than predicted.

Considering this, the objective of this thesis is two-fold, first, to measure the nucleation rates of partially saturated CO HbS; and second, to measure the nucleation rates of partially saturated oxy HbS. Due to the ability of photo dissociating CO from HbS, multiple saturations can be measured on one sample and a larger amount of data can be collected. How will the homogeneous and heterogeneous nucleation rates of oxy and CO HbS compare? Once the nucleation rates are understood, therapeutic questions which can be answered with this information. The motivation for the thesis work will be discussed again after the literature review.

---

[77] Rotter, Maria. Et. al. (2005). Molecular crowding limits the role of fetal hemoglobin in therapy for sickle cell disease. *Biophysical Journal.* (347). 1015-1023.

[78] Rotter, Maria. Et. al. (2011). Nucleation of Sickle Hemoglobin Mixed with Hemoglobin A: Experimental and Theoretical Studies of Hybrid-Forming Mixtures. *Biophysical Journal.* (101) 2790-2797.

1.5 Clarification of Language, Mixtures and Partials

Hybrids refer to HbS and another species of Hb such as HbA or HbF which has dimerized and recombined into a new molecule such as HBSF or HBSA. Where one α β dimer is HbS and the other is from the HbA or HbF.

Partial ligands refer to a Hb molecule that is carrying less than the total 4 ligands, i.e. either 3, 2, or 1. Zero ligands are referred to as the unliganded state, or deoxy-Hb. Deoxy Hb is the term used for the unliganded form of oxy Hb or CO Hb.

Chapter 2: Hemoglobin Allostery and Kinetics

2.1 Derivation of polymerization equations

Sickle hemoglobin polymers grow through a double nucleation pathway.[79] Initially, there are deoxygenated HbS monomers in a solution that will start to form small aggregates. Aggregation is not favored by entropy due to the loss of motional freedom, but is energetically favored by the decrease in free energy caused by the intermolecular bonds made by the HbS monomers. Once an aggregate reaches a certain minimum size (the nucleus), more contacts are available to each molecule and aggregation becomes favorable (figure [2.1]). This process produces a homogeneous nucleus (a nucleus that is formed only from the monomers in the solution). Forming a homogeneous nucleus is a stochastic process; therefore, it is characterized by a variable delay time, before which aggregates cannot be detected. If however the volume of the solution is high enough, the formation of a nucleus can be deterministic, appearing to not have stochastic behavior.

Heterogeneous nucleation occurs through nucleation on preexisting polymer surfaces. It cannot occur until homogeneous nucleation has already taken place. The more polymer surface which becomes present, the more sites that are available for a heterogeneous nucleus. This accounts for the exponential growth that occurs after a nucleus is formed. Polymers will form until solubility is reached (when polymer and

---

[79] Ferrone, F. A. (1985). Kinetics of sickle hemoglobin polymerization II. A double nucleation mechanism. *J. Mol. Biol.* 183:611-631.

monomer are in equilibrium with each other), or until polymers can no longer grow due to end obstruction.[80]

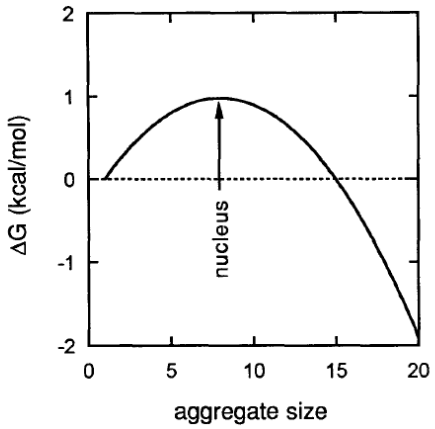

Figure [2.1]: Energy barrier for the formation of the critical nucleus.[81]

When describing polymer kinetics and thermodynamics, it is necessary to consider solution non-ideality. Non-ideality occurs when a mixture of chemical substances deviates from ideal behavior. In ideal mixtures, the interactions between each pair of chemical species are the same as though it is interacting with itself. Therefore, the mixtures can be expressed in terms of their concentrations (or partial pressures) much like an ideal gas in thermodynamics. However, if the molecules of the mixture interact with each other, by attracting or repelling for example, the concentration will not be an accurate description of the species in the mixture. Instead, a modified concentration must be used to describe the

[80] Aprelev, A. et. al. (2007). Metastable polymerization of sickle hemoglobin in droplets. *J. Mol. Biol.* 369:1170-1174

[81] Ferrone, F.A. (1999). Protein aggregation kinetics. *Methods of Enzymology.* 309:259.

mixture, which is done by multiplying the concentration by an activity coefficient. For ideal solutions the activity coefficient = 1, and for non-ideal solutions the coefficient can be > or < 1 (with > 1 being more volatile and <1 being less interactive). For HbS polymerization to occur, the solution concentration must be high. Since the monomers occupy a large portion of the solution volume, the total solution volume is not accessible to all the monomers and the aggregates. This excluded volume causes the activity coefficients to be large.

Table [2.1]: Definition of terms:

Symbol	Definition
c_p	Concentration of polymer ends
c	Concentration of monomer
f_0	Rate of Homogeneous Nucleation
gΔ	Rate of Heterogeneous Nucleation
$\gamma_{i^*+1}, \gamma^{\ddagger}$	Activity coefficient of the nucleus plus 1; Activated complex
γ	Activity coefficient for monomers
γ_{i^*}	Activity coefficient for the nucleus
γ_s	Activity coefficient for solubility (monomer activity in equilibrium with the infinite polymer)
c_s	Solubility concentration
k+	Monomer addition rate
c_{i^*}	Concentration of homogeneous nuclei of size i*
Δ	Concentration of monomers in polymers
J	Elongation rate of the polymer
K_i	Equilibrium constant for formation of the i-mer
c_0	Initial concentration of monomers
ϕ	Proportionality constant of nucleation sites per polymer
δ_1	Fraction of intermolecular bonds relative to the infinite polymer

The derivation of the homogeneous and heterogeneous rate equations have been described in great detail elsewhere.[82] [83] Here, key parts of the derivation will be shown and elaborated upon. Below follows the derivation found in chapter 23 of Disorders of hemoglobin: kinetics, pathophysiology, and clinical management, page 596.[84]

The concentration of polymers (c_p) changes over time, due to contributions from homogeneous and heterogeneous nucleation. Below is the main kinetic equation:

$$\frac{dc_p}{dt} = \left[\frac{dc_p}{dt}\right]_{hom} + \left[\frac{dc_p}{dt}\right]_{het} = f(c) + g(c)\Delta \tag{2.1}$$

The formation of polymers through the homogeneous pathway depends on the monomer addition rate, the activity coefficients of the nucleus, and the monomer, and nucleus plus 1. For the homogeneous nucleus, the activity coefficients can be assumed to be for a spherical object and calculated from scaled particle theory:[85]

$$\left[\frac{dc_p}{dt}\right]_{hom} = f(c) = \frac{k_+ \gamma c \gamma_{i^*} c_{i^*}}{\gamma_{i^*+1}} \tag{2.2}$$

With the equilibrium condition between the nucleus and the monomers as:

$$\gamma_{i^*} c_{i^*} = K_{i^*} (\gamma c)^{i^*} \tag{2.3}$$

---

[82] Ferrone, F. A., Hofrichter, J., Eaton, W. A. (1985). Kinetics of Sickle Hemoglobin Polymerization, II. A double nucleation mechanism. *J. Mol. Biol.* 183:611-631.
[83] Rotter, M. A., Suzanna, K., Briehl, R. W., Ferrone, F.A. (2005). Heterogeneous nucleation in sickle hemoglobin: experimental validation of a structural mechanism. *Bio. J.* 89:2677-2684.
[84] Steinberg, M. H. Forget, B. G., Higgs, D. R., Nagel, R. L. (2001). Disorders of hemoglobin: genetics, pathophysiology, and clinical management. Ferrone, F. A., Nagel, R. L.: Polymer structure and polymerization of deoxyhemoglobin S. Cambridge University Press. Chapter 23. 577-610.
[85] Ferrone, F. A. et al. (2002). Heterogeneous nucleation and crowding in sickle hemoglobin: An analytic approach. *Bio. J.* 82:399-406.

and K_{i^*} as defined in table [2.1].

The heterogeneous growth rate is similar to the homogeneous rate (the i is replaced with a j to show that this is heterogeneous) except that the nucleus is now attached to the polymer and is no longer a spherical object, this is indicated by the prime.

$$\left[\frac{dc_p}{dt}\right]_{het} = f(c) = \frac{k_+ \gamma c \gamma'_{j^*} c'_{j^*}}{\gamma'_{j^*+1}} \tag{2.4}$$

The concentration of homogeneous nuclei, c_{j^*} can be written as:

$$c_{j^*} = K_{j^*} K_{\tilde{j^*}} \phi (c_0 - c)(\gamma c)^{j^*} \tag{2.5}$$

This is a consequence of the two step heterogeneous nucleation. First, the formation of a j^*-mer in solution with equilibrium constant $K_{\tilde{j^*}}$. Second, attachment of the j^*-mer to the polymer with an equilibrium constant K_{j^*}. With c_0 as defined in table [2.1] and ϕ is the proportionality constant which gives the number of nucleation sites per polymerized monomer.

The concentration of monomers in polymers can be written as:

$$\frac{d\Delta}{dt} = k_+(\gamma c - \gamma_s c_s)c_p \tag{2.6}$$

Defining the elongation rate of a polymer as:

$$J(c) = k_+(\gamma c - \gamma_s c_s) \tag{2.7}$$

allows one to write equation (2.6) as:

$$\frac{d\Delta}{dt} = J(c)c_p \tag{2.8}$$

The equations can be expanded about the initial concentrations, and keeping the first order terms gives:[86]

$$\frac{dc_p}{dt} = f(c_0) + \left[g(c_0) - \frac{df(c_0)}{dc_0}\right]\Delta \tag{2.9}$$

From there the growth rates can be separated and solved:

$$f_0 = \left[\frac{k_+ K_{i^*}}{\gamma_{i^*+1}}\right](\gamma_0 c_0)^{i^*+1} \tag{2.10}$$

$$g_0 = k_+ \varphi \Gamma K_{j^*} K_{j^*} (\gamma_0 c_0)^{i^*+1} \tag{2.11}$$

With Γ as the ratio of activity coefficient for a polymer without polymer attached to the activity coefficient of a polymer with aggregate size $j^* + 1$ ($\Gamma = \gamma_p/\gamma^*_{j+1}$). The analytic solution to equations (2.10) and (2.11) are:

$$\Delta(t) = A[\cosh(Bt) - 1] = \begin{cases} \frac{1}{2}Ae^{Bt}, Bt \gg 1 \\ \frac{1}{2}AB^2t^2, Bt \ll 1 \end{cases} \tag{2.12}$$

---

[86] Bishop, M. F., Ferrone, F. A.: Kinetics of nucleation-controlled polymerization. A perturbation treatment for use with a secondary pathway. Biophysical Journal. 1984. 46(5) 631-644.

With the A and B terms then given by:

$$A = f_0 \left[g_0 \frac{df_0}{dc} \right] \tag{2.13}$$

$$B^2 = J_0 \left[g_0 \frac{df_0}{dc} \right] \tag{2.14}$$

$B^2 A$ is independent of heterogeneous nucleation, and can be defined as:

$$B^2 A = J_0 f_0 \tag{2.15}$$

Below is a plot of B^2A at 25° Celsius for different concentrations of HbS solutions. B^2A is only dependent on homogeneous nucleation.

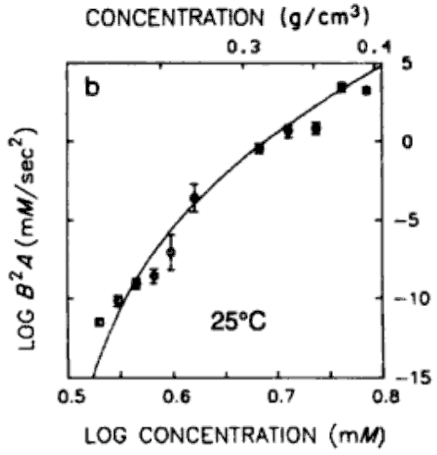

Figure [2.2]: B^2A dependence on concentration for 25° Celsius.[87]

[87] Ferrone, F. A. (1985). Kinetics of sickle hemoglobin polymerization II. A double nucleation mechanism. *J. Mol. Biol.* 183:611-631.

2.2 Derivation of chemical potential of HbS nucleation

When deoxygenated HbS polymerizes in solution, it will eventually reach equilibrium between the monomer and the polymer phase (figure [2.1]). The concentration of the monomers left in the solution is called the equilibrium solubility, c_s. The activity coefficient, γ_i describes how the interactions between the monomers change with concentration, i.e. as concentration increases to solubility, there is crowding in the solution and the surface to surface rather than the center to center interactions must be taken into account. So in terms of the chemical potential, the equilibrium between polymer and monomer can be written as:

$$i\mu_1 = \mu_i \tag{2.16}$$

Where μ_1 is the chemical potential of the monomer and μ_i is the chemical potential of the i-mer.

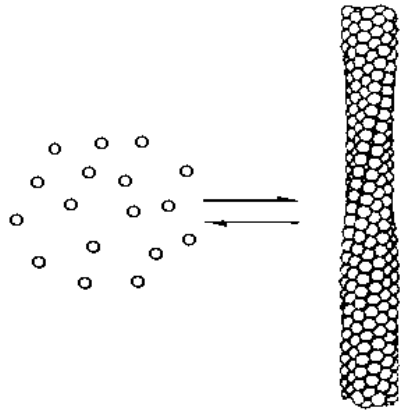

Figure [2.3]: Equilibrium between monomer and polymer states.

The chemical potential of monomer is expanded into the rotational μ_R, and translational μ_T terms; while the i-mer is expanded into rotational, translational, intermolecular bonding between monomers, and vibrational terms ($\mu_{iR}, \mu_{iT}, \mu_{iC}, \mu_{iV}$ respectively). The monomer chemical potential and i-mer chemical potential then become:

$$\mu_1 = \mu_R + \mu_T + kTln(\gamma c) \tag{2.17}$$

Where γ is the activity coefficent of the monomer; T is the temperature and k is the gas constant. Generalizing this to the i-mer:

$$\mu_i = \mu_{iR} + \mu_{iT} + \mu_{iC} + \mu_{iV} + kTln(\gamma_i c_i) \tag{2.18}$$

Expanding equation 2.16 with these terms and separating the $ln(\gamma_i c_i)$ term:

$$i\mu_R + i\mu_T + ikTln(\gamma c) = \mu_{iR} + \mu_{iT} + \mu_{iC} + \mu_{iV} + kTln(\gamma_i c_i) \tag{2.19}$$

$$\ln(\gamma_i c_i) = iln(\gamma c) + i(\mu_R + \mu_T) - \mu_{iR} + \mu_{iT} + \mu_{iC} + \mu_{iV}/kT \tag{2.20}$$

Since the chemical potentials are constants, this equation can be written as:

$$\gamma_i c_i = K(\gamma c)^i \tag{2.21}$$

where K contains the constant terms, thus making it the equilibrium constant between monomers and i-mers. So equation 2.16 can be written as:

$$RTln\, K_i + iRTln\, \gamma c = RTln\, \gamma_i c_i \tag{2.22}$$

Finally, it is important to define the critical nucleus size referred to in figure [2.1]. Clearly,

the critical nucleus is reached when the derivative of the Gibbs energy over the number of monomers is zero. This means that the chemical potential of the i-mer, i.e. $RTln\,\gamma_i c_i$ can be set equal to zero and solved in terms of the supersaturation:

$$i^* = \frac{\xi}{\ln S} \tag{2.23}$$

Where S as the ratio of the HbS concentration to the solubility concentration,

$$S = \gamma c/\gamma_S c_S \tag{2.24}$$

When the concentration at which solubility occurs is low, then the supersaturation is high, and the critical nucleus size is small. The term ξ is a constant which is:

$$\xi = -4 - \frac{\delta_1 \mu_{pc}}{RT} \tag{2.25}$$

Where δ_1 is the parameter which describes the fraction of intermolecular bonds in the nucleus relative to the infinite polymer.

2.2.1 Understanding HbS growth curve distributions

The nucleating event of HbS is governed by stochastic behavior, therefore to appropriately analyze the system, a large amount of data must be collected. In vivo, the loss of oxygen from the RBC is not instantaneous. This is because oxygenated HbS monomers will be mixed with deoxy HbS, thereby lowering the rate of polymer formation. However, in

vitro it is possible to deoxygentate a sample of CO-HbS within milliseconds,[88] almost instantaneously in comparison to the time it takes the first nucleus to form (which can be from a half second to several minutes).[89] It was found that polymerization could be induced in HbS samples saturated in carbon monoxide, via photolysis with 1 Watt 428 nm laser (with a maximum of 3.1 kW/cm^2 intensity). This method has the advantage of allowing the polymers to melt when the laser is turned off, by allowing the CO to rebind to the HbS. The experiment can then be repeated in the same area many times. In addition to this, the laser used is passed through a mesh with many small holes. Such a device creates many sample areas that each will produce nuclei and polymers independent of its neighbors. As each spot grows polymers, they will in turn scatter some of the laser light used to create them. This scattered light is collected and are the data for "growth curves" of the polymers. An example of the kinetic growth curves is pictured in figure [2.4]:

[88] Ferrone, F. A., Hofrichter, J., Eaton, W. A.:(1985). Kinetics of Sickle Hemoglobin Polymerization, II. A double nucleation mechanism. *J. Mol.* 183:611-631.

[89] Hofrichter, J. (1986). Kinetics of sickle hemoglobin polymerization: III. Nucleation rates determined from stochastic fluctuations in polymerization progress curves. *J. Mol. Biol.* 189:553-571.

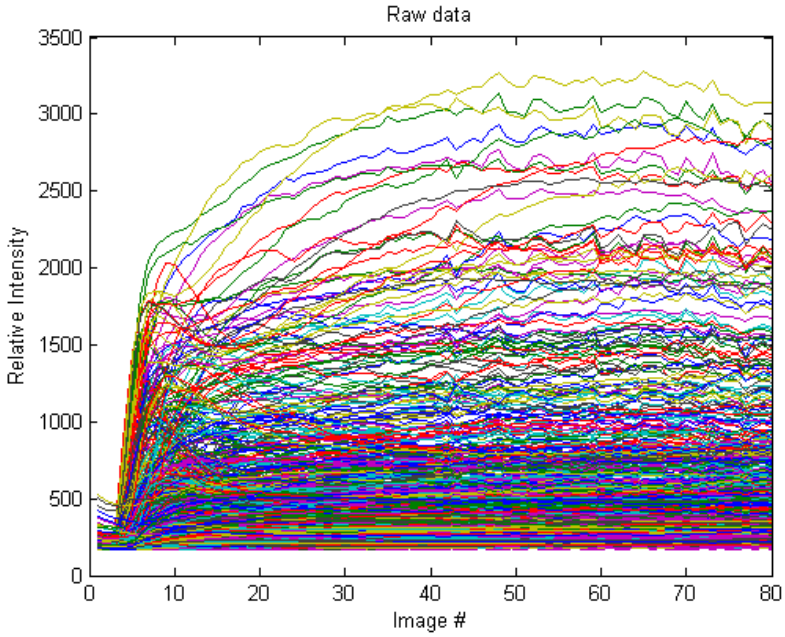

Figure [2.4]: Growth curves of polymers via scattered light.

The data in figure [2.4] can be used to find the exponential growth B of the curves by fitting the first 10% of the curve to an exponential function:

$$f(t) = \frac{A}{2}[e^{Bt} - 1] \tag{2.26}$$

where A is a constant. By plotting a histogram of the tenth times, a curve can be fit to the distribution (figure [2.5]) and the homogeneous nucleation rate, f_0 can be found (more details on this in section 2.3.2).

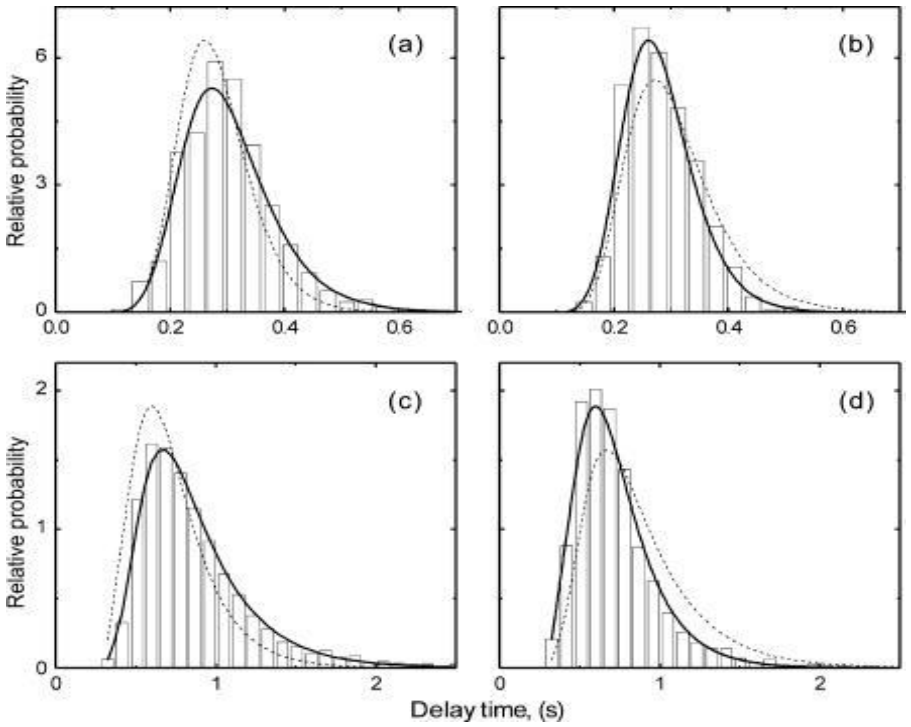

Figure [2.5]: Examples of t_{10} probability distributions.[90]

As an example of how the B and f_0 parameters affect the probability distribution, observe the top two figures in [2.5] above. In figure (a), the solid curve extends further then the dotted line (which is the solid curve in figure (b)), likewise in (c) and (d). This stretching of the t_{10}'s is due to the increase in the homogeneous rate. If the nucleus takes a longer time to appear, the probability distribution will stretch, due to the increased number of possible times for the nucleus event to occur in. Now compare the axis of the two figures on the left of [2.5]. The center of the distribution in (a) it is ~0.3. In figure (c) it is ~0.8. The

[90] Aprelev, A. et al. (2005). The effects of erythrocyte membranes on the nucleation of sickle hemoglobin. *Bio. J*. 88:2815-2822.

center of the distribution will shift right due to heterogeneous growth taking a longer time to occur.

2.2.2 Fitting stochastic growth curves through the Szabo formulation

HbS polymerization can be related to classical stochastic nucleation theory. However, in our system we have a heterogeneous nucleation and growth that can, for example, prevent more than one homogeneous event from occurring. This is because all the available HbS could have been used in making heterogenous polymers, therefore not allowing a second homogeneous event to occur. A stochastic nucleation theory would have to take this into account when describing our system.

In 1988, Szabo laid the groundwork for the analytic model we use to describe HbS nucleation[91]. He began by defining the average number of monomers incorporated into a polymer as the sum of n times the probability that there are n monomers incorporated:

$$\langle n(t) \rangle = \sum_{n=0}^{\infty} n P_n(t) \tag{2.27}$$

For our system, if ζ_0 is the homogeneous rate of polymer formation and B is the heterogeneous rate, then if there are n monomers incorporated in a polymer at time t, then in $t + dt$, either a new nucleus can form, or a present nucleus can grow. Note that a larger nucleus has more contacts and can grow proportional to n. The probability that there are n monomers in a polymer at time $t + dt$ is the sum of the probabilities of those two growth

[91] Szabo, A. (1988). Fluctuations in the polymerization of sickle hemoglobin: A simple analytic model. *J. of Mol. Biol.* 199:539-542.

rates. However, there is also the possibility that no new monomers were absorbed in time t. Considering this, the equation then becomes:

$$P_n(t+dt) = P_{n-1}(t)\big(\zeta_0 + B(n-1)\big)dt + P_n(t)(1-(\zeta_0 + Bn)dt \tag{2.28}$$

Szabo uses mean first passage time theorem to find an expression for n_c, the critical nucleus. Letting $Q_k(t)$ be the probability that n_c has not been reached by time t ($Q_{n_c}(t) = 0$), with k as the number of monomers in a polymer. Then, $Q_k(0) = 1$ and:

$$\frac{dQ_n(t)}{dt} = (\zeta_0 + Bn)(Q_{n+1}(t) - Q_n(t)) \tag{2.29}$$

The distribution of the times to reach n_c from n can be written:

$$T_n(t) = -\frac{dQ_n(t)}{dt} \tag{2.30}$$

Szabo differentiates (2.29) with respect to t, and uses a Laplace transform to find an integral form for$T_n(s)$, and lets $T_{n_c}(s) = 1$. He uses this and solves the recurring series solution of the Laplace transform to obtain:

$$T_0(t) = \frac{B\Gamma(n_c+\zeta_0/B)}{\Gamma(n_c)\Gamma(\zeta_0/B)} e^{-\zeta_0 t}(1-e^{-Bt})^{n_c-1} \tag{2.31}$$

where Γ() is the gamma function. For our system we can only observe the nucleus when it is already grown to an amount much larger then n_c. When n_c is taken to be large ($n_c \approx n$) this expression becomes:

$$T(t) = \frac{Bn^{\zeta/B}}{\Gamma(\zeta/B)}(1-e^{-Bt})^n e^{-\zeta t} \tag{2.32}$$

In our system, $\zeta = f_0 N_0 V$. Where N_0 is Avogadro's number and f_0 is the rate constant for

primary nucleation. When this equation is fit to the distribution of tenth times for a given sample, the f_0 can be solved. From Szabo's expression for tenth times, the B term dominates until some time when t > 1/B when the f_0 term will dominate the distribution.

2.3 Hemoglobin allostery, occupied ligand populations calculations

Allostery refers to the changes in the shape and activity of a molecule due to the binding of ligands to that molecule. The partially saturated HbS experiments conducted in this thesis required the allostery of HbS to be defined in order to fully analyze the data. The CO and oxy samples are measured at different partial pressures and the ligand populations at each of these partial pressures can be solved through the allosteric model for hemoglobin. Hb exhibits positive cooperatively when binding ligands. This means that the presence of the first ligand will assist in the binding of the second and so forth for the four ligands. Cooperativity is what gives the binding curve of oxygen it's well recognized "S" shape (figure [1.6] left). The MWC (Monod, Wyman and Changeux) model is used to describe the binding kinetics of a molecule which can be in two states, R (relaxed) and T (tense) state and is used to describe the cooperative binding of ligands to Hb. In any single molecule all the subunits must be in the same state, either R or T. The R state has a higher affinity for the ligand than the T state. However, the binding of any ligand is assumed to take place at identical sites whose affinity is only determined by the allosteric form, R or T. This model can affectively be used to illustrate the binding of ligands to HbS and is supported by structural studies which also show that Hb does have two forms, R and T.

The generalized form for the derivation of the binding polynomial is obtained from Gill and Wyman's book Binding and Linkage (p 133) through the formulation of the MWC model.[92] However, the Adair binding constants, the liganded HbS populations, and the special case for DPG, are all uniquely derived for this thesis work.

Unliganded R and T forms are denoted with an R or T subscript and the equilibrium constant for the unliganded reaction is given as:

$$M_R \rightarrow M_T \tag{2.33}$$

The equilibrium constant L_o describes the transition between the two unliganded allosteric forms:

$$L_o = \frac{[M_T]}{[M_R]} \tag{2.34}$$

The binding of ligand "X" in each of the forms may be expressed in a two column array. Where the arrows show that the macromolecule can transition between R and T states, as well as bind ligands:

$$\begin{array}{ll} M_R \rightarrow M_T \\ \downarrow \quad \downarrow \\ M_R X \rightarrow M_T X \\ \downarrow \quad \downarrow \\ M_R X_2 \rightarrow M_T X_2 \\ \downarrow \quad \downarrow \\ \vdots \quad \vdots \\ \downarrow \quad \downarrow \\ M_R X_t \rightarrow M_T X_t \end{array}$$

[92] Wyman, J., Gill, S. (1990). Binding and Linkage: Functional Chemistry of Biological Macromolecules. University Science Books.

This shows a system that can bind up to *t* ligands of molecule X. The two binding equations can be written as:

$$M_R + X \rightarrow M_R X, \qquad \kappa_R = \frac{[M_R X]}{[M_R]x} \tag{2.35}$$

$$M_T + X \rightarrow M_T X, \qquad \kappa_T = \frac{[M_T X]}{[M_T]x} \tag{2.36}$$

Where $\kappa_R$and κ_T are the equilibrium constants of binding ligand X to the R or T state respectively. The degree of binding of the first ligand (in both the R and T state of the molecule) can be written as:

$$\bar{X} = \frac{[M_R X]+[M_T X]}{[M_R]+[M_T]+[M_R X]+[M_T X]+[M_R X_2]+[M_T X_2]+[M_R X_3]+[M_T X_3]+[M_R X_4]+[M_T X_4]} \tag{2.37}$$

Substituting the equilibrium equations gives:

$$\bar{X} = \frac{\kappa_R + L_0 \kappa_T}{1+L_0+\kappa_R x+L_0\kappa_T x+\kappa_R x^2+L_0\kappa_T x^2+\kappa_R x^3+L_0\kappa_T x^3+\kappa_R x^4+L_0\kappa_T x^4} \tag{2.38}$$

The binding partition function Q, can then be written as:

$$Q = (1 + \kappa_R x)^t + L_0(1 + \kappa_T x)^t \tag{2.39}$$

where t is the total number of possible bound ligands (4 for hemoglobin). The binding polynomials for R and T can be simplified as:

$$P_R = (1 + \kappa_R x)^t \tag{2.40}$$

$$P_T = (1 + \kappa_T x)^t \tag{2.41}$$

And the binding partition function can then be written as:

$$Q = P_R + L_o P_T \tag{2.42}$$

Until now, the derivation of the binding polynomial has loosely followed what was presented by Gill and Wyman in the book, Binding and Linkage. However, for our system, we will derive the number of each Hb species with each amount of ligands (zero to four) in the R and T forms, and we will also consider the special case of additional DPG. DPG only affects the binding of ligands when Hb is in the T-state, and so the equilibrium of the binding of DPG: L_{DPG} is only multiplied by P_T. This changes the binding partition function to:

$$Q = P_R + L_0 P_T + L_{DPG} P_T \tag{2.43}$$

where L_{DPG} is equal to the equilibrium between R and T multiplied by the binding rate of DPG and the concentration of DPG:

$$L_{DPG} = L_o \kappa_{DPG} [DPG] \tag{2.44}$$

This binding polynomial can be written out for t =4 ligands, which is the case for Hb:

$$Q = (1 + \kappa_R x)^4 + L_o (1 + \kappa_T x)^4 + L_{DPG} (1 + \kappa_T x)^4 \tag{2.45}$$

Once the total binding polynomial is obtained, it should be normalized to the sum of all unligated species: i.e when t=0:

$$P = \frac{(1+\kappa_R x)^4 + L_o(1+\kappa_T x)^4 + L_{DPG}(1+\kappa_T x)^4}{1+L_o+L_{DPG}} \tag{2.46}$$

For simplicity let the normalization be replaced by N:

$$N = 1 + L_o + L_{DPG} \tag{2.47}$$

From the binding polynomial a lot of useful information can be extracted about the system, including the Adair constants, the binding curve, the Hill Plot, as well as the species fractions in R and T at a given saturation of x. With a little bit more work, one can also extract the species fractions that are in R or T with 0, 1, 2, 3 or 4 ligands (i.e. α_{R0}, α_{R1}, α_{R2}, α_{R3}, α_{R4}, α_{T0}, α_{T1}, α_{T2}, α_{T3} & α_{T4}).

An alternative way to describe the binding of a ligand to the molecule is with the Adair binding constants: β_i. They are the stoichiometeric coefficients that describe the binding process in terms of overall reactions to the unliganded molecule. Here are they are for the R0 to R1 and R0 to R2 ligand bindings:

$$M_R + X \rightarrow M_R X, \qquad \beta_{R1} = \frac{[M_R X]}{[M]x} \tag{2.48}$$

$$M_R + 2X \rightarrow M_R X_2, \qquad \beta_{R2} = \frac{[M_R X_2]}{[M]x^2} \tag{2.49}$$

The Adair constants are found by expanding the binding polynomial and grouping coefficients of the same powers. Expansion of the terms in P gives:

$$P = \frac{\begin{bmatrix}1+4\kappa_R x+6\kappa_R^2 x^2+4\kappa_R^3 x^3+\kappa_R^4 x^4+L_o\left(1+4\kappa_T x+6\kappa_T^2 x^2+4\kappa_T^3 x^3+\kappa_T^4 x^4\right)\\ +L_{DPG}\left(1+4\kappa_T x+6\kappa_T^2 x^2+4\kappa_T^3 x^3+\kappa_T^4 x^4\right)\end{bmatrix}}{N} \tag{2.43}$$

The Adair binding constants for the T states are:

$$\beta_{T0} = \frac{L_o+L_{DPG}}{N} \tag{2.45}$$

$$\beta_{T1} = \frac{L_o 4\kappa_T+L_{DPG}4\kappa_T}{N}$$

$$\beta_{T2} = \frac{L_o 6\kappa_T^2+L_{DPG}6\kappa_T^2}{N}$$

$$\beta_{T3} = \frac{L_o 4\kappa_T^3+L_{DPG}4\kappa_T^3}{N}$$

$$\beta_{T4} = \frac{L_o \kappa_T^4+L_{DPG}\kappa_T^4}{N}$$

and for the R states:

$$\beta_{R0} = \frac{1}{N} \tag{2.46}$$

$$\beta_{R1} = \frac{4\kappa_R}{N}$$

$$\beta_{R2} = \frac{6\kappa_R^2}{N}$$

$$\beta_{R3} = \frac{4\kappa_R^3}{N}$$

$$\beta_{R4} = \frac{\kappa_R^4}{N}$$

The activity coefficients, $\alpha_{hi}'s$ are the species populations of how many HbS have that number of ligand *i* in form *h* (where *h* is R-state or T-state) for a given oxygen pressure (x).

$$\alpha_{hi} = \frac{\beta_{hi} x^i}{P} \tag{2.46}$$

Solving for $\alpha_i's$:

$$\alpha_{R0} = \frac{1}{P}; \alpha_{T0} = \frac{L_o + L_{DPG}}{P} \tag{2.48}$$

$$\alpha_{R1} = \frac{(4\kappa_R)x}{P};\ \alpha_{T1} = \frac{(L_o 4\kappa_T + L_{DPG} 4\kappa_T)x}{P}$$

$$\alpha_{R2} = \frac{(6\kappa_R^2)x^2}{P};\ \alpha_{T2} = \frac{(L_o 6\kappa_T^2 + L_{DPG} 6\kappa_T^2)x^2}{P}$$

$$\alpha_{R3} = \frac{(4\kappa_R^3)x^3}{P};\ \alpha_{T3} = \frac{(L_o 4\kappa_T^3 + L_{DPG} 4\kappa_T^3)x^3}{P}$$

$$\alpha_{R4} = \frac{(\kappa_R^4)x^4}{P};\ \alpha_{T4} = \frac{(L_o \kappa_T^4 + L_{DPG} \kappa_T^4)x^4}{P}$$

Plotting the α_{hi}'s for CO Hb will show all the Hb to be in state T0 at zero CO pressure. The T states are unpopulated at high CO pressure (figure [2.6]), because most of the Hb will be in the R-state. Figure [2.7] below shows the total α_R plotted with the total in α_T. The values used in creating these plots are: L_0: 3.08e5, $\frac{\kappa_T}{\kappa_R} = 0.01$ and [DPG]=0 (DPG is insignificant in the case of CO Hb binding).

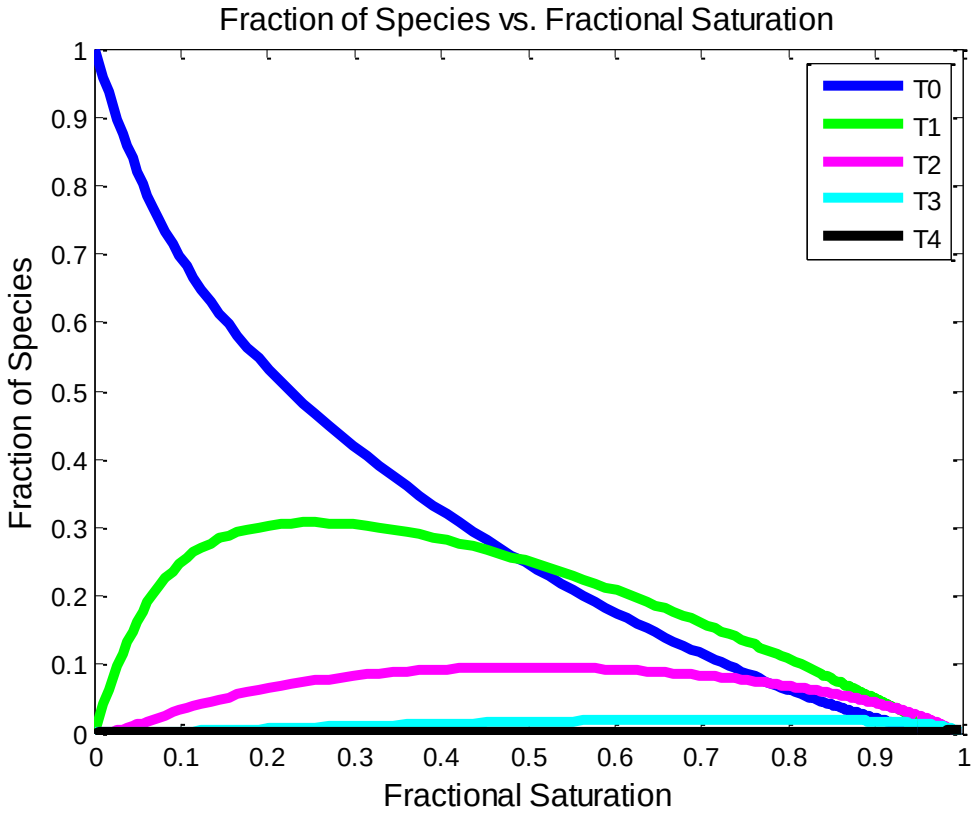

Figure [2.6]: Fraction of HbS in T state

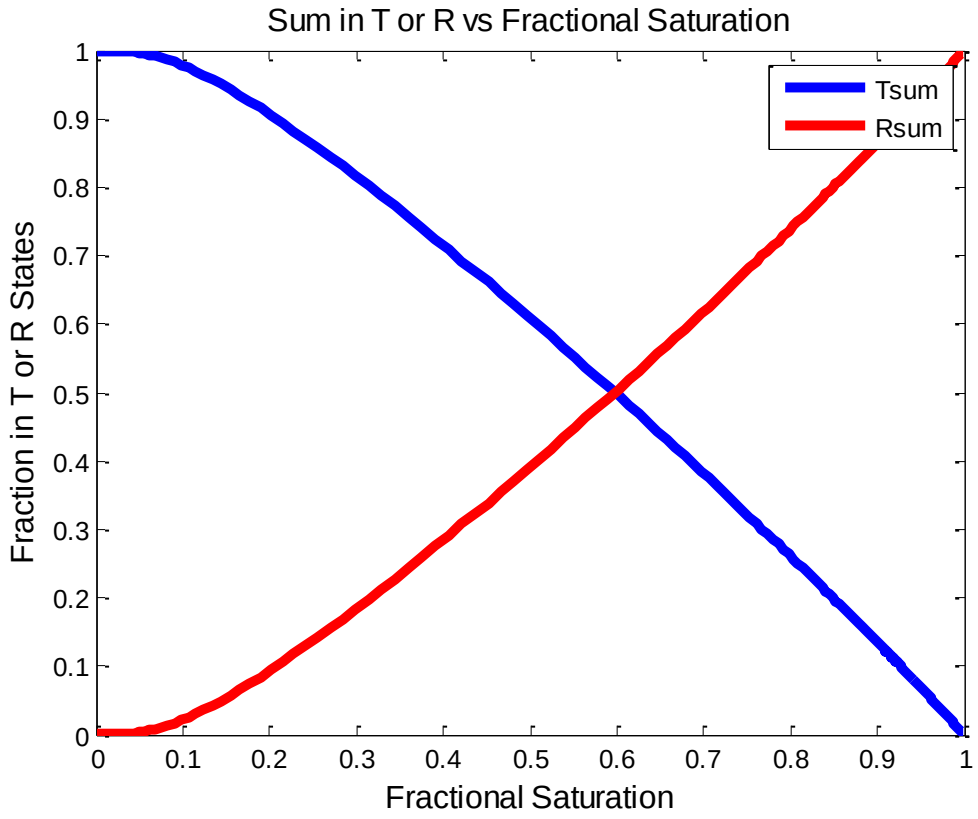

Figure [2.7]: Fraction of Hb in T-state and R-state.

Chapter 3: Literature review

As mentioned in chapter 1 section 4.2, there were already studies done on the equilibrium of partially liganded CO and O_2 HbS. Small amounts of O_2 and CO were found in gelled deoxygenated HbS. In this chapter, two extensive experiments will be reviewed and used as examples for the motivation for this thesis work.

3.1 Ligand binding and the gelation of sickle cell hemoglobin, Hofrichter

In 1979, James Hofrichter would publish an extensive study of CO in gelled HbS solutions.[93] At the time of publication completely deoxygenated HbS gels had already been studied.[94] It was known that there was a delay before polymers would appear,[95] and that this delay was related to the 40th power of the concentration.[96] However, these studies were done on large volume HbS samples, which would nullify the stochastics of homogeneous nucleation. The double nucleation growth pathway was also not defined at this time. Even so, such knowledge was not necessary in order to study the characterization of HbS in gels.

For many years there has been great interest in relating in vitro HbS experiments to the in vivo environment. Studying partially liganded HbS solutions is one approach of many.

---

[93] Hofrichter, J. Ligand binding and the gelation of sickle cell hemoglobin. J. Mol. Biol. 1979. 128, 335-369.
[94] Hofrichter, J. Ross, P. D., Eaton, W. A.: Kinetics and mechanism of deoxyhemoglobin S gelation: A new approach to understanding sickle cell disease. PNAS. 1974. 71(12) 4864-4868.
[95] Eaton, W. A., Hofrichter, J., Ross, P. D., et al. Comparison of sickle cell hemoglobin gelation kinetics measured by NMR and optical methods. *Biochem. Biophys. Res. Commun*, 69 (1976), pp. 538–547.
[96] Eaton, W. A., Hofrichter, J., Ross, P.D.: Delay time of gelation: a possible determinant of clinical severity in sickle cell disease. Blood. 1976. 47, 621-627.

At the time of Hofrichter's publication, there were already some other studies done on oxygen and HbS. It was already shown that HbS cells could sickle at high oxygen fractional saturations.[97] And that oxygen affinity decreases with increasing cellular concentration due to the polymerization of deoxy HbS.[98] Hofrichter's work would show that HbS polymers are composed of mostly unliganded deoxygenated T-state HbS, with a very small fraction of liganded COHbS in the gelled polymers.

Hofrichter used three techniques in his study of CO HbS gelation. These were sedimentation, linear dichroism and turbidity. Sedimentation is a technique which centrifuges large volumes (~330 ul) of deoxygenated HbS. Polymers and monomers will reach equilibrium in solution, and the centrifugation sediments the polymers and allows the supernatant to be measured. For a mixture of deoxy HbS and COHbS, the concentration of CO in the original solution and in the supernatant is used to find how much CO is in the polymer. Linear dichroism is a spectroscopic technique that uses the difference between parallel and perpendicular polarized light to measure the composition of aligned polymers. It is one of the few techniques that can measure the absorption of polymers when there are monomers in the solution, because it is only sensitive to the aligned polymers.

Samples for this experiment were prepared by exposing a small amount of HbS to CO. This was then mixed with a larger amount of oxy HbS. After thorough mixing, the sample's concentration was determined through dilution. The oxy/CO HbS mixture was then mixed with dithionite, which converts the oxy HbS to deoxy HbS as well as kept at a low temperature. The samples were large volume samples of about 350 µl in a sealed

---

[97] Bookchin, R. M., Balazs, T., Landau, L. C.: Determinants of red cell sickling. Effects of varying pH and of increasing intracellular hemoglobin concentration by osmotic shrinkage. J. of Lab. And Clin. Med. 1976. 87(4): 597-616.

[98] May, A., Huehns, E. R., The concentration dependence of the osxygen affinity of haemoglobin S. Brit. J. of Haem. 1975. 30(3) 317-335.

quartz vial. It was possible to measure the spectrum of the samples in the sealed vials to determine the final deoxy HbS concentration, the CO heme concentration of the sample can also be determined. The samples are then allowed to increase in temperature till they gel. They are then centrifuged till there is sedimentation of the polymer. The supernatant can then be measured for the amount of CO. If it less than the amount measured previously, that is an indication of CO present in the polymer. When the sedimentation experiment is concluded, the polymers are melted and mixed at a lower temperature. A small amount of the solution, 1-2 µl was then used to make 3 or 4 slides in a nitrogen atmosphere. These samples were warmed until they gelled and then were measured via linear dichroism.

The solubility experiment is analyzed by studying the supernatant after sedimentation is completed from the centrifugation. The deoxy heme concentration of the supernatant and pellet and the volume fraction of the pellet are measurable quantities. The concentration of deoxy hemes in the supernatant decreased with increasing saturation of CO Figure [3.1] bottom. This was believed to be due the increase of copolymerization of CO HbS and not due to less efficient packing of the pellet at higher concentrations. Linear dichroism can detect spectra changes as small as 0.5%. The dichroism spectra were normalized by dividing through with a pure deoxy polymer spectrum. The samples showed only a small contribution from CO which increased monotonically with fractional CO saturation, data in figure [3.1]top.

The data was analyzed by first defining what the fractional species of CO HbS in the sample are. In figure [3.2], two different sets of allosteric parameters were used to build these curves. Then, when the number species of HbS with 1, 2, 3 or 4 liganded CO is known for each percentage of CO in the sample, it can be compared to what was found in the polymer and solution. For example, a sample with 40% CO initially would have about 8%

with three and two ligands, 21% with one ligand and 38% without ligands (the dotted lines in the left figure). Since the fraction of polymer is known as well as the concentration of deoxy HbS in the supernatant, it is possible to build a model for what liganded species if any are in the polymer. Figure [3.1] top and bottom show different models being fit to the data points.

The top figure of [3.1] shows the results from the analysis of the linear dichroism study and the bottom is the results from the equilibrium experiments. The dotted lines on the two graphs show an analysis for all T states being in the polymer, regardless of degree of ligation. There are two lines because they come from two different sets of allosteric parameters. The upper curve has $L=10^5$, $K_T/K_R=c=0.01$; the lower, $L=10^7$, $K_T/K_R=0.002$ where K_T/K_R is equivalent to c. The long dashed line (almost flat to the x-axis) is the prediction for only unliganded HbS T states entering a polymer. The solid lines represent T0 polymerizing and the other liganded T-states polymerizing with differing probabilities. In the top figure of [3.1], the upper solid line has parameters $L=10^5$, c=0.01, $e_T=0.25$ and the lower line, $L=10^7$, c=0.002, $e_T=0.3$ with e_T being adjusted in increments of 0.05. Where e_T is the partition coefficient for the partially liganded T-state species. The bottom graph has the same parameters for the dotted lines. The long dashed line has $L=10^5$, $K_T/K_R=0.01$, the upper solid line has $L=10^5$, $K_T/K_R=0.002$ and $e_T=0$.

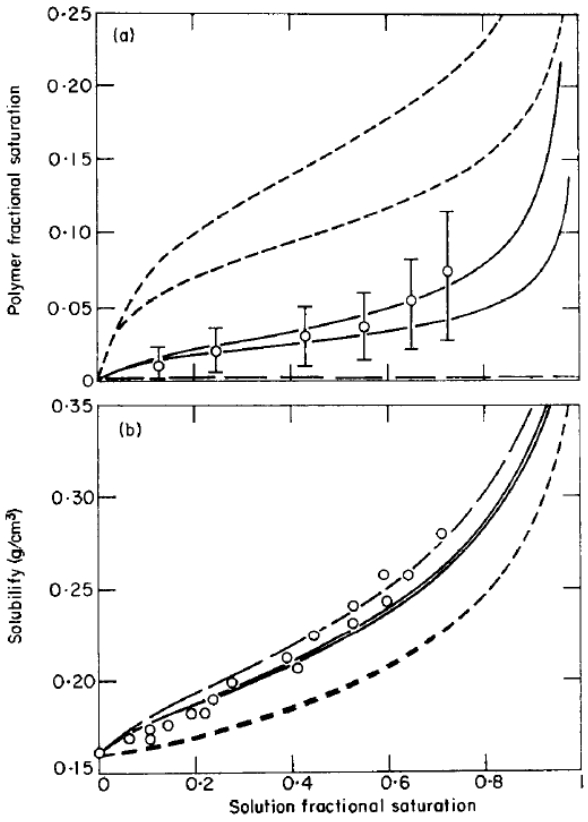

Figure [3.1]: Top: Fitting different theoretical models to the data from the linear dichroism experiment. The error bars increase because as fractional saturation of CO increased, the amount of polymer decreased, and therefore the level of noise in the data increased. Bottom: Fitting different theoretical models to the solubility experiments.

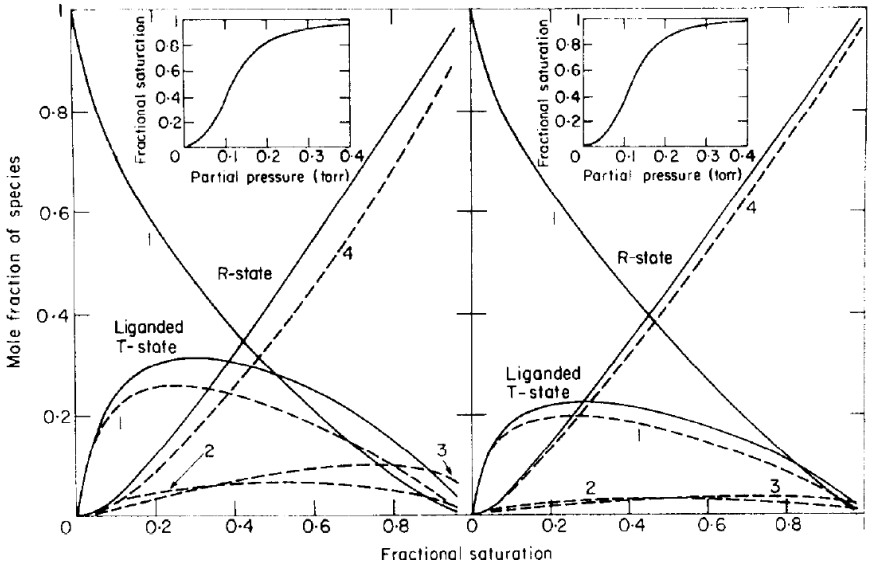

Figure [3.2]: T-state and R-state fraction of species of species versus fractional saturation of CO. Left has allosteric parameters, $L=10^5$, $K_T/K_R=0.01$, $K_R=160$ torr^{-1}. Right has $L=10^7$, $K_T/K_R=0.002$, $K_R=500$ torr^{-1}. The three solid lines depict the fraction of unliganded T-state molecules (T0), total fraction of liganded T-state molecules (T1+T2+T3+T4) and total R-state molecules. The dashed lines show fractions of molecules with 1, 2, 3, or 4 ligands as indicated in the figure.

From figure [3.1] top, it is clear that the best fit is with the liganded T-states polymerizing with differing probabilities. In the bottom graph in the figure, the data appears to be between the differing probability T-states and all T-states entering the polymer up until 20% fractional saturation. Above 60%, the data seems to fit better with the model of only T0 states polymerizing. It is clear that the polymer prefers completely unliganded T-state molecules. In the dichroism experiment in the top graph of figure [3.1] the percent of the fractional saturation of CO in the polymer is not above 5% even at solution fractional saturations of 70% and the CO increased total solubility by 7%. However, it should be noted that in both the solubility and linear dichroism experiment are measured

well after the polymers are completely formed. This is different from the experiment which will be shown in this thesis, which are the nucleation rates.

How a homogeneous and heterogeneous nucleus form in the presence of partially liganded T-states may be different from what is ultimately found in completely grown polymers. However, these experiments show conclusively that there are liganded T-state Hb found in polymers. There is one final experiment that was described in the Hofrichter paper. Each sample was also measured for a delay time in polymerizing. This was done via turbidity measurements on the solubility samples. As described elsewhere,[99] the samples were kept in an ice bath and then had their temperatures raised until they could gel. The optical density was then monitored. Gelation would cause an increase in the optical density at 800 nm. The shortest gelation time measureable is the time it takes for thermal equilibrium of the sample. Figure [3.3] shows how the delay changed with different samples at the same total HbS concentration with different fractional saturations of CO. The data with open circles (O) was taken at 35°C and the triangles (Δ) were taken at 20°C. Between 0 and 18% saturation increases by a factor of 30 in the high temperature sample and increases by 30 between 17 and 36% in the low temperature sample. The slopes for the two samples are identical and for an increase in the fractional saturation from 0 to 40%, the delay time increases by about 10^4. There seems to be a decrease in slope between 10 and 20% fractional saturation, but there is not sufficient data to show this explicitly.

[99] Hofrichter, J. Ross, P. D., Eaton, W. A. Supersaturation in sickle cell hemoglobin solutions. Proc. Natl. Acad. Sci. 1976. 73 (9) 3035-3039.

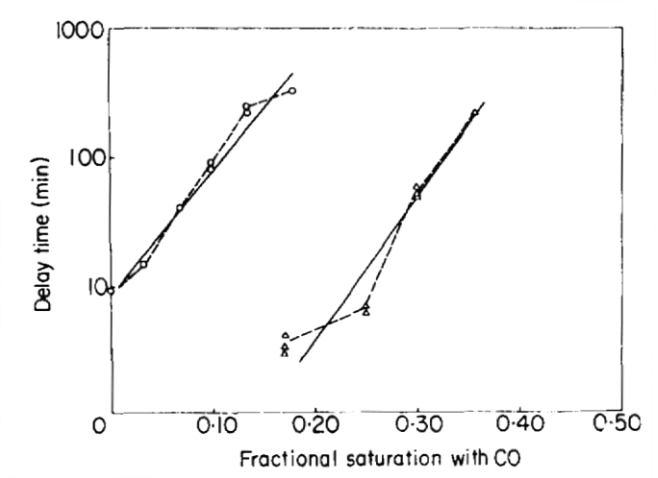

Figure [3.3]: log of gelation delay times versus fractional CO saturations for two different sample concentrations.

The delay time experiment results are directly relatable to the kinetics experiments conducted in this thesis. The CO partial photolysis experiments have tenth times measured for each % photolysis and concentration. Tenth times are the time it takes for the mass of polymers to scatter $1/10^{th}$ of the maximum scattered light (or reach $1/10^{th}$ their final size). Since growth of polymers in small volumes is stochastic, the shortest tenth time is the delay time.

3.2 Oxygen binding by sickle cell hemoglobin polymers, Sunshine

In 1982, Helen Sunshine along with Dr. Hofrichter, Dr. Ferrone and Dr. Eaton, would publish her results from experiments on the gelation of sickle hemoglobin in the presence of

oxygen.[100] They would find that the polymer binds oxygen in a non-cooperative manner, and has an affinity to bind oxygen which is similar to T-state Hb. They did two experiments on oxy HbS, solubility and linear dichroism. The solubility and linear dichroism were conducted with the same methodology as in the CO HbS experiment. Before this study, experiments on the effect of oxygen on HbS solubility had been conducted on red blood cells and whole blood.[101] [102] These studies showed that inside RBC's HbS gels had a decreased affinity for oxygen. This was due to formation of polymers inside the gels, because in dilute HbS solutions with the concentration below solubility, polymers cannot form, and the oxygen dissociation curve is the same for HbS and HbA.[103] Although this shows that it is the polymers which have a decreased affinity for oxygen, it does not quantify the oxygen affinity of polymers.

To conduct this experiment, it was necessary to develop a technique to decrease the amount of met HbS. Normally 1-2% of oxygenated Hb is met Hb. However, in a partially oxygenated environment, Hb will rapidly oxidize to met Hb. The met Hb was minimized via a met Hb reductase system, and the amount of met Hb was never more than 4%. However this also caused the amount of oxygen in the sample to slowly be consumed. Due to this, all samples were measured with the amount of oxygen as a function of time. The gelation and solubility experiments used HbS which was stored at a temperature between 0 and 4°C and then raised to 23.5°C to induce the formation of polymers. In order to decrease the time it

---

[100] Sunshine, H. R., Hofrichter, J., Ferrone, F.A., Eaton, W. A.: Oxygen Binding by Sickle Cell Hemoglobin Polymers. J. Mol. Biol. 1982. 158. 251-273.
[101] Becklake, M. R., Griffiths, S. B. et. al.: Oxygen dissociation curves in sickle cell anemia and in subjects with the sickle cell trait. J. Clin. Invest.. 1955. May; 34(5): 751-755.
[102] Mizukami, H. et. al. Hysteresis-like behavior of oxygen association-dissociation equilibrium curves of sickle cells determined by a new method. Exp. Biol. Med. 1977. 154(2) 304-309.
[103] Huehns, M. A.: The mechanism of the low oxygen affinity of red cells in sickle cell disease. Hamatologie und Bluttransfusion. 1972. 10: 279-283.

takes for the formation of polymers in the gelled samples for dichroism measurements, an argon laser of 3kW/cm^2 at 514 nm was focused on the sample which also caused a large domain of polymers to form. In some samples, the amount of polymer formed was so small that the samples still appeared to be liquid. For the solubility measurements the samples were centrifuged for one hour and had their spectrum taken at intervals for 2 hours. To find the amount of oxygen at the time of sedimentation, the data was extrapolated back to 30 minutes after the start of centrifugation.

In the solubility experiment, the supernatant has a decreased concentration due to formation of polymers, yet, the amount of oxygen increases. This shows that the polymer has a lower affinity for oxygen. The solubility was measured for differing concentrations and amounts of oxygen. In figure [3.4], the results of the oxygen experiment are compared to the CO HbS data. The filled circles are the oxygen HbS data and the open circles are the CO HbS data. The upper dotted line is for only T0 states polymerizing the theoretical curve. The lower dotted line is for all oxygen T-states entering a polymer. The solid line is calculated from the thermodynamic equation which relates the total Hb activity in the solution phase to the Hb binding of oxygen in each phase.

$$\ln a_s = \ln a_s^0 + 4\int_{-\infty}^{\ln p} \frac{y_s - y_p}{1-\frac{1/c_p-\bar{v}}{1/c_s-\bar{v}}}\, d\ln p \qquad (3.1)$$

where $a_s = \gamma_s c_s$ is the solution phase hemoglobin activity at oxygen pressure p. a_s^0 is the solution phase hemoglobin activity at zero oxygen pressure. γ is the activity coefficient and $\bar{v}$ is the partial specific volume of Hb. For the solid line c_p =0.69 g/cm^3, $\bar{v}$ = 0.75 cm^3/g and the specific volume V = 0.92 cm^3/g. The long broken curve is equation [3.1] without $\frac{\left[\left(\frac{1}{c_p}\right)-\bar{v}\right]}{\left[\left(\frac{1}{c_s}\right)-\bar{v}\right]}$, which is the solvent term and relates the moles of solvent of Hb in the polymer to the

number of moles of solvent per mole of Hb in the solution. The short broken line comes from the least squares of:

$$c_s = a\ by_s + cy_s^3 + dy_s^{15} \tag{3.2}$$

with a = 0.1826 g/cm3, b = 0.0924 g/cm3, c = 0.0980 g/cm3 and d = 0.2352 g/cm3. This equation is used to solve for y_s, the solution phase saturation.

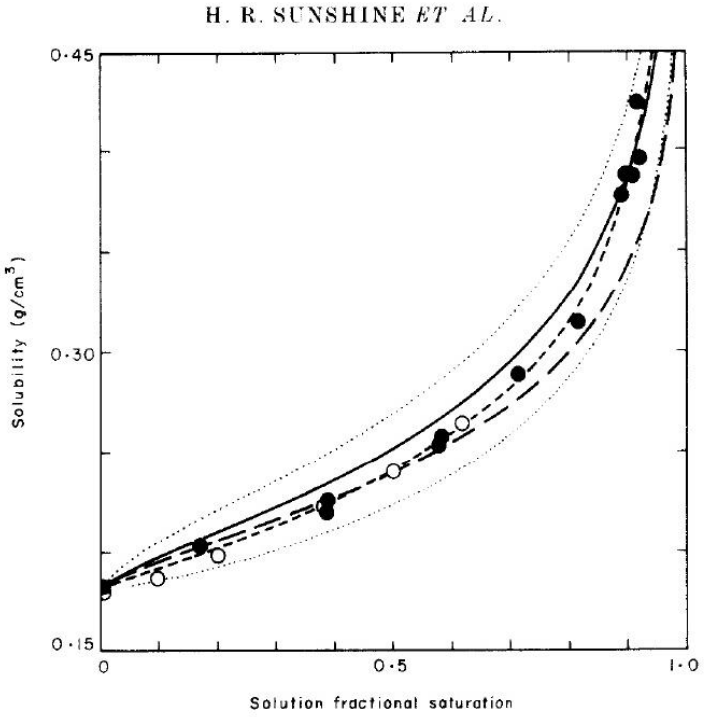

Figure [3.4]: Solubility data for oxygen (filled circles) and COHbS versus fractional saturation.

The solution phase saturation is converted to an oxygen partial pressure using the binding curve from Gill.[104] The oxygen partial pressures were used to make a Hill plot, shown here in figure [3.5]. The figure shows the data for a 16 g/dl solution (open circles) and 37 g/dl gel (squares are oxygenation and triangles are deoxygenation experiments), the crosses are the polymer binding data from the solubility experiment. The straight line has a slope of 0.97 ±0.09. In a Hill plot for hemoglobin shows how many subunits are interacting. A slope of 1 means the hemoglobin is non-cooperative. The polymer phase had a larger affinity for oxygen than for CO. Sunshine found that the fractional saturation of the polymer with oxygen was 1.5 times more than with CO at all saturations of the solution phase. However, they were not sure if the discrepancy could be contributed to the different ligand, or if it could have been an artifact of the sample making technique. The CO samples were gelled for a much longer period of time and could have crystallized. This form could have caused less CO to be in the polymer phase. However, when the data for the dichroism experiments were compared in figure [3.6] there was good agreement for the affinity of the polymer for the different ligands. However, at the time of these experiments, it was not known that gelled samples do not reach complete solubility, whereas in centrifugation experiments, solubility is reached.[105] This could mean that less oxygen is found in the gelled samples because polymers formed with the more favorable unliganded HbS molecules that were available. This could explain why less CO and oxygen is found in the polymer in the linear dichroism experiment.

---

[104] Gill, S.J. et al. Oxygen binding to sickle cell hemoglobin. J. of Mol. Biol. 1979. 130 (2) 175-189.
[105] Aprelev, a., Weng, W., Zakharov, M., Rotter, M., Yosmanovich, D., Kwong, S., Briehl, R., Ferrone, F. A.: Metastable polymerization of sickle hemoglobin in droplets. J. of Mol. Biol. 2007. 369(5) 1170-1174.

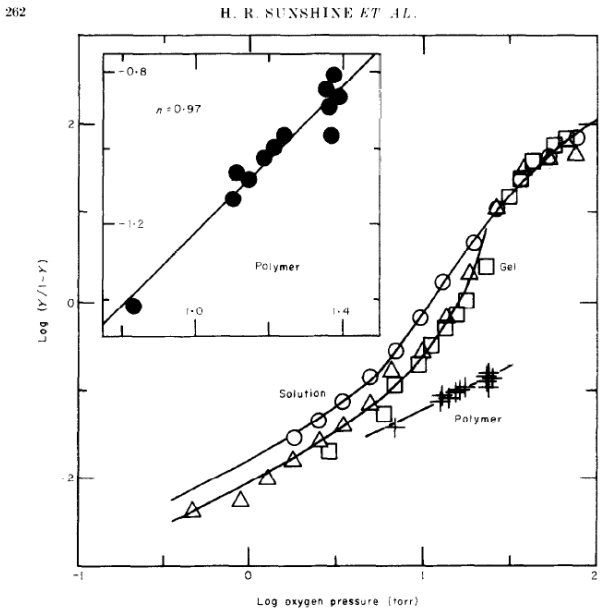

Figure [3.5]: Hill plot of the solubility data for the oxygen experiment.

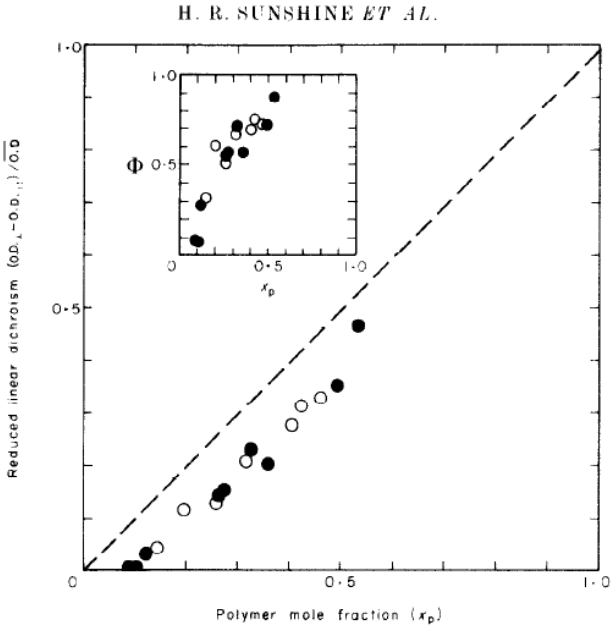

Figure [3.6]: Linear dichroism experiment oxygen experiment. The broken line is for perfectly aligned polymers, open circles are from the CO experiment at 35°C and filled circles are the oxygen experiment at 23.5°C.

In conclusion, the oxygen experiment shows what appears to be a greater affinity of the polymer for oxygen than for CO ligands. Sunshine would calculate that the probability for the oxygen bound T1 state to enter the polymer to be 0.37 and for T2 to be approximately $(0.37)^2$. However, although these studies demonstrate there is oxygen present in already formed polymers, it does not explain how the presence of oxygen and CO affect the nucleation rate of HbS.

3.3 Motivation for thesis work

The two experiments presented in chapter 3 sections 1 and 2, are equilibrium experiments. The polymer and monomer state of HbS and partially liganded HbS are in equilibrium when the measurements are conducted. Such experiments are fundamentally different from measuring the rate at which a homogeneous or a heterogeneous nucleus forms. Although a certain amount of liganded HbS is found in the polymer, it will not necessarily explain how the presence of such partial ligands will affect nucleation. Two examples of this are the mixture experiments performed by Rotter et. al. on deoxygenated fetal[106] and deoxygenated normal adult Hb mixed with HbS.[107] In the case of fetal Hb mixed with HbS, other experiments had already showed that fetal hemoglobin did not polymerize,

[106] Rotter, M., A. Aprelev, K. Adachi, F. A. Ferrone. (2005). Molecular crowding limits the role of fetal hemoglobin in therapy for sickle cell disease. *J Mol. Biol*. 347(5):1015-23.
[107] Rotter, M. A. et. al. (2005). Heterogeneous nucleation in sickle hemoglobin: experimental validation of a structural mechanism. *Biophysical Journal.* 89(4):2677-84.

nor did fetal/HbS hybrids.[108] However, when the nucleation rates were measured, it was found that the rates did not decrease as much as expected based on gelled sample data. This was because although the fetal Hb and HbSF do not polymerize, they crowded the solution. Although having a non-polymerizing species does decrease the nucleation rates, it will be partially counteracted by the crowding species in the solution. This result would have only been a theoretical hypothesis if the experiment had not been done.

Other experiments on deoxygenated HbA and HbS mixtures found that the hybrid species, HBAS does enter polymers. However, nucleation experiments would reveal further information about the formation of the nuclei in the presence of these hybrids. It was found that the homogeneous nucleus requires at least one pure HbS molecule, and the heterogeneous nucleus requires a greater number. That may be due to the larger number of molecules involved in the formation of a heterogeneous nucleus. The nucleation rates of HbAS mixtures were also faster than predicted.

These two results demonstrate that experiments on polymer composition can provide important information when deoxygenated HbS is not the only species. Understanding why polymers can contain HBAS hybrids, but not HBSF is useful in understanding the alignments of the hydrophobic pockets which allow the polymers to form (chapter 1 section 3.3). However, these experiments do not completely predict the behavior of the system in the case of nucleation. Therefore, it is necessary to measure the nucleation rates of partially saturated CO and oxy HbS solutions in order to either reaffirm

[108] Singer, K., and L. Singer. (1953). The gelling phenomenon of sickle cell hemoglobin: Its biological and diagnostic significance. *Blood* 8:1008.

or contribute more information to what is already known. The two experiments conducted in this thesis are on partially saturated CO and oxy HbS samples.

3.4 Nucleation rates of HbS partially saturated with CO and oxygen

The CO HbS experiment is conducted by making samples of HbS in which the only ligands in the system are CO. Laser photolysis, a technique which uses the ability of a laser at a particular frequency (488 nm in this case) to push the CO out of its illuminated or "photolyzed" region, will therefore create an area of deoxygenated HbS (unliganded HbS) in a sample (chapter 4 section 4.2). The deoxygenated HbS will form into polymers, which will then scatter some of the laser light. The scattered laser light is then captured by a CCD camera and related to the polymer's growth. Due to the stochastic nature of the formation of nuclei, a large amount of data needs to be collected. This is done by passing the laser light through a mesh with holes of about 10 um in diameter, with the consequence that 25-35 experiments can be conducted simultaneously. The size of the illuminated laser spots on the sample allow only for only 1 homogeneous event to occur. This is because a polymer mass has already grown (due to the exponential growth) before another homogeneous nuclei will have the opportunity to form. Previously, numerous experiments were done by Ferrone et. al. in which the laser completely deoxygenated, i.e. removed all the CO from the HbS in the photolyzed region. However, prior to this, experiments on partially saturated samples were not done due to the complicated nature of measuring partially saturated areas.

To measure a partially saturated sample, it is necessary to have a range of laser intensities across the sample, in order to produce varying areas of partial saturation. For example, this may produce a range of 10-20% saturation. This means the next data set which will be measured can have the laser adjusted to produce 20-30% saturation. It is less time consuming to gather a large amount of data through this method, thereby obtaining more varied percentages, as opposed to measuring a single percent at each laser intensity. This also means that the laser intensity at each photolysis area must be measured. This is necessary because the intensity at each area can be related to the amount of saturation which is present in that area. To measure the intensity, the laser light was passed through the optical system and focused at the sample. The mesh was removed and a diaphragm was inserted, creating a single spot of light. The power of the laser light at the sample is measured through an optical power meter. The size of the spot is found by taking pictures of it with the CCD camera and relating the pixels to microns. This was then used to find the area of the spot and the power density. This image is also used to make a relation between the intensity captured in a pixel on the CCD camera image and the intensity in that place in the sample. Finally, the percent of saturation was directly measured through a single wavelength optical technique (chapter 4 section 5.2). The optical absorbance of hemoglobin changes depending on whether it has any ligands, such as CO bound. The best way to measure the composition of a sample is to take its spectrum within a well defined range. However, to do so in this case would take too long (~ 1minute) and within that time polymers will most likely have formed and the composition of the area changes. Therefore, a method of quickly measuring the components of the solution is necessary. Inspired by a technique which had been previously used to measure the complete deoxygenation of HbS, a new technique was created to measure the percent of deoxygenated hemoglobin and CO

saturated hemoglobin. This technique captures images of the sample with the laser on and off and can then use the difference in optical densities to solve for the amount of saturation. Programs were created in IPLab to control the opening of the laser shutter and the imaging capturing with the CCD camera.

After obtaining the images of laser intensity and percent saturations, there also must be a way to analyze this data (chapter 4 section 5.3). Currently there are commercial software packages, such as ImageJ, which can calculate the properties of an area an image highlighted by a user. However, consider the 25-30 saturation spots captured at differing desaturations, as well as each spot evolving over time, its intensity value, and finally its kinetics (scattered light) values evolving over time as well. Such a massive amount of data, which all needs to be sorted, and related (saturation to intensity to kinetics) for each individual spot, cannot be analyzed by a simple software such as ImageJ. Therefore, extensive image analysis programs were written in Matlab to study and tabulate all of the collected data.

The partially saturated oxygen experiments were conducted by making samples with both CO and oxygen ligands. The CO is laser photolyzed off the HbS leaving only the oxygen ligands. The samples for this experiment were made differently than the CO HbS samples. It was found that mixing CO HbS with oxygenated HbS, and diluting with deoxygenated buffer produced a mixture with a very low amount of free CO or oxygen in the solution. This allowed the photolyzed regions to not have free oxygen in the solution rebind with the deoxygenated HbS. To measure the saturation in these samples, a spectrum is taken while the HbS is photolyzed with the laser, in order to find the amount of oxygen left in the photolysis spot. Although measuring the kinetics of the oxygenated sample is

simpler than a partial CO HbS sample, there is a great limitation that each oxygen sample has a fixed percentage of oxygen. For this reason, there are fewer data points for the oxygen experiments.

Chapter 4: Experimental Work

4.1 Chromatography of hemoglobin

Chromatography is a process used to separate mixtures into its constituent components. Cellular Hb is separated into its various components through ion exchange chromatography. This is accomplished via a column, or a tall cylindrical tube filled with a nonreactive medium such as cellulose. The material in the column is equilibrated to a fixed pH. The cellulose in the column remains stationary while a Hb mixture poured into the column will flow down through the cellulose at varying speeds due to differing attractions to the ions in the cellulose.

4.1.1 Preparation of Hb for chromatography

Blood was collected fresh from an anonymous donor undergoing transfusion at the Children's Hospital of Pennsylvania. Approximately 25 ml of blood was transferred into 6-50 ml centrifuge tubes and initially mixed with 25ml of 0.9% NaCl (saline) solution. This was spun at 2,500 RPM (~790 g's) for 20 minutes. The supernatant was then discarded; the tubes were filled again to 50 ml, capped and spun again. This was done for a total of 3 times. After this, the packed RBC's must be diluted and have a final salt concentration of 2%. The packed RBC's were mixed with a small amount of (1.5 ml) of 15% NaCl and then diluted with 2% NaCl to ~60 ml volume. The RBC solution was then transferred to large volume cryogenic vials (15 ml) and

dipped into liquid nitrogen for 30 seconds and then allowed to thaw in the fridge (figure [4.1]). Due to the larger volumes, thawing took several hours. This process ensures lysing of the RBCs.

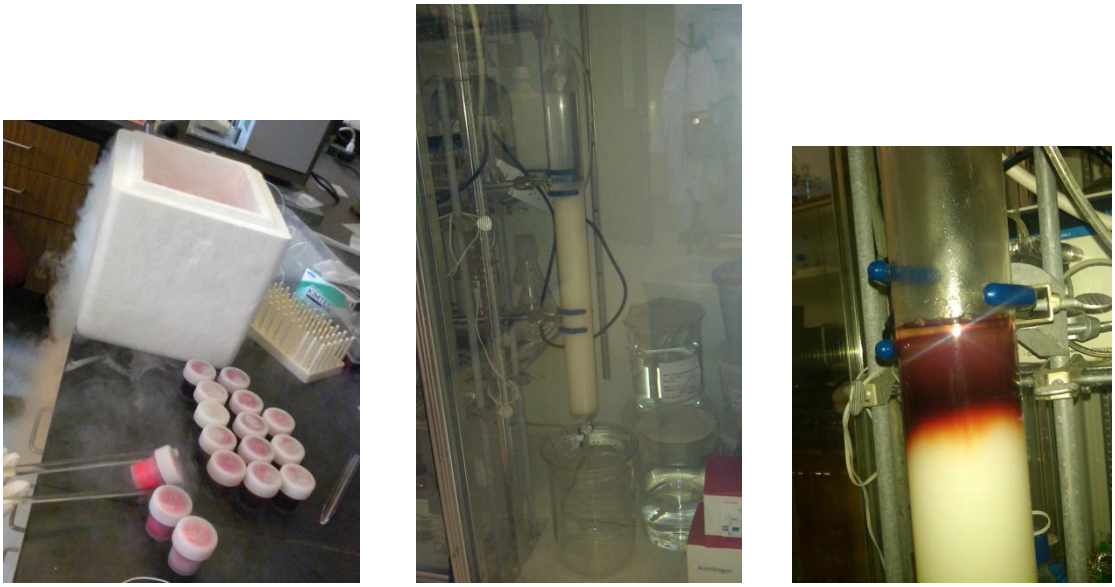

Figure [4.1]: Left: Dipping cryo-vials of blood in liquid nitrogen. Middle: The column in the fridge. Right: the column loaded with Hb.

Hb/lysed RBC mixture is then transferred again into 50 ml vials and spun at a very high velocity, 14,000 RPM for 1 hour. This creates a thickened glob of cellular material at the bottom of the vials. The Hb was poured out, the vials were cleaned and the process was repeated 1 to 2 more times depending on the amount of cellular material which needed to be extracted. After this, the HbS saline solution is mixed with approximately 3 times its volume of Tris buffer that has a pH of 8.0. If the volume of the HbS solution was too large, it was concentrated in a 10K

pore membrane concentrator. The HbS Tris solution was poured into dialysis tubing which had been sterilized by boiling in EDTA and then rinsed in double distilled water. The tubing was then suspended in a large volume beaker (4L). The HbS is then dialyzed against pH 8.5 Tris buffer which is 60 times the volume of the Hb. It is stirred in the cold fridge for 2-3 hours and pH 8.5 Tris buffer is exchanged twice more. When dialyzing the solution inside the dialysis tubing will grow in volume. After this, the Hb was concentrated again so as to facilitate easy loading of the column (figure [4.1] right). In the preparation shown in the pictures above, the column is kept in the cold so as to minimize the formation of met Hb. The Hb solution will be loaded onto the column as a concentrated solution of about 20 ml.

To separate Hb into HbA and HbS, one must first pour pH 8.5 buffered Hb into an equilibrated pH 8.5 Tris column. Equilibration of the cellulose begins with washing it with about 6 times its volume in pH 8.5 Tris buffer. The cellulose and buffer is stirred for 20 minutes on a magnetic stirrer and allowed to settle for 30 minutes. The supernatant is discarded and the process is repeated for a total of 6 times. The supernatant should be almost clear at the conclusion of washing. The column is poured by stirring the cellulose with a small amount of buffer to allow easy flow down a glass rod into the glass column tube. Equilibration of the column's pH is then continued by passing up to 5 liters of buffer through the cellulose. The cellulose in the column will also settle and decrease in volume overnight.

When the column is ready for chromatography, the flow of buffer into the column is halted until the level of buffer on top of the cellulose is barely visible. When this has happened, the column is loaded with Hb by injecting the hemoglobin in a circular motion around the inner walls of the column so as to not disturb the cellulose levels. After loading the column, the Hb will start to separate into a lighter lower band and a darker upper band (HbA2). After the Hb

has fully entered the cellulose, pH 7.35 Tris buffer is added to the column. The difference in pH allows the HbS and HbA to separate further. The HbS will elute from the column first. This is collected and re concentrated to 4 g/dl. At this point, the bulk of the HbS can be stored long term in the Tris buffer at this concentration in liquid nitrogen. This is the case for the CO experiments. For the oxygen experiments, the eluted HbS was never stored in liquid nitrogen; it was used right away in order to minimize the formation of met HbS.

4.1.1.1 A note on concentrators

All concentrators used were either 10K or 30K Centricons, ranging in size from 2ml to 16ml. They were washed with a 70% Ethanol solution 3x's at 4500 RPM for 15 minutes. Then the concentrators were washed with distilled water 3 more times at 3000 RPMs for 15 minutes. Finally, the solution buffer was used to wash them 3 times at 3000 RPM for 15 minutes.

4.1.1.2 A note on buffers

For the HbS separation, a large amount of Tris buffer was used at three different pH's: 8.00, 8.35 and 8.5 at 0.05M. Tris buffer is made by adding the liquid to the solid, then adding small amounts of HCl while being mixed with a magnetic stirrer. However, Tris buffer changes pH with changes in temperature. Also, it is necessary to know approximately what the temperature of the column will be during the chromatography, because this is the temperature at which the three Tris buffers need to have the correct pH. It is not possible to keep the temperature of Tris buffer constant while making it. This is because the addition of HCl increases the solution temperature. To counteract this, HCl and small amounts of cold distilled

water can be added to the buffer until the desired pH at the right temperature is reached. Finally, distilled water is added to obtain the correct final volume and 0.05M. To facilitate this process, just one buffer was made at the right pH and temperature. That buffer's temperature was varied between 18°C and 5.5°C while the pH was monitored so a relation was made between temperature and pH. It was found that pH changed by -0.032 per Celsius degree increase. This method was used to make all the Tris buffers.

Phosphate buffer is made by first making a stock solution of K_2HPO_4 and KH_2PO_4. Two liters of 0.15M K_2HPO_4 were made by adding 52.25g of K_2HPO_4 to a container then filling with twice distilled water to 2 liters. Next, 0.6L of 0.15M KH_2PO_4 was made by adding twice distilled water to 12.25 g of KH_2PO_4. To obtain a pH of 7.35 or 7.05, a freshly calibrated pH meter was placed in the 2L of K_2HPO_4 and the solution was stirred as the KH_2PO_4 was slowly added.

4.1.2 Exchanging HbS buffer

In order to conduct kinetics experiments under pH and salt concentrations similar to in vivo conditions, the HbS will be transferred to pH 7.35 phosphate buffer. To exchange the buffer from Tris to phosphate, a pd-10 desalting column is used. It exchanges through volume exclusion. The column has many tiny pores in which small molecules, such as the molecules in a buffer become trapped. In a vertical column, this means that a large protein such as Hb will flow faster through the column via the force of gravity than its buffer. The buffer that was already in the column, in our case pH 7.35 phosphate will then flow out with the protein. Each column is prepared by initially passing 50 ml of phosphate buffer through. When the column is ready to be loaded with HbS, the buffer level is allowed to settle to the top of the column. Then about 300 –

400 µl of 4 g/dl HbS is pipetted onto the top of the column. The HbS is allowed to enter the column, then immediately 2 ml of phosphate buffer is added to the column. When most of that has entered the column, more buffer is added (~6-10 ml) to increase the velocity of the flow through the column. The HbS is collected at the bottom of the column and now has a volume of ~2 ml. The last few drops of diluted HbS is not collected and allowed to drip into a waste container. The column is then flushed with 50 ml of phosphate buffer and used for no more than six exchanges. To exchange a large amount of HbS quickly, two or three columns are run simultaneously with a buffer reservoir on top. This allows a larger amount of buffer to be placed at the top of the column, therefore causing buffer to flow through the column quicker. At the conclusion of exchange, the HbS will then be concentrated again, this time in a small size concentrator, either 2 ml or 6 ml volume with either a 30K or 10K pore size. The final concentration should be about 39 g/dl. About 60-90 µl of this is placed in a 1.8 ml cryogenic vial and is either stored in the liquid nitrogen, or in a fridge depending on application.

4.2 Sample preparation

4.2.1 CO partial photolysis sample preparations

To prepare a sample for a partial CO photolysis experiment, a vial of hemoglobin in 7.35 pH phosphate buffer is removed from its storage in liquid nitrogen, and thawed inside the CO glove box. The CO glove box is flushed ahead of time with CO for 20-30 minutes. Approximately 2 containers of 40 ml of phosphate buffer are flushed with CO in the glove box for no less than 30 minutes. This removes oxygen from the buffer solution and replaces it with CO. When the buffer is done flushing, three tubes each with 5 ml of CO phosphate buffer are prepared for

testing the Hb composition and concentration. Before the Hb is diluted for spectrum testing, it is stirred and mixed with a micro pipette. This is done by drawing up 5ul of Hb from the bottom center of the conical vial and then releasing it at the top of the 60 µl solution in a circular manner. This is important due to the small volumes in each container (50-100 µl) and the possibility of the settling of contents as well as some drying at the surface/air contact. The measurements conducted here can be greatly affected by small changes in concentration, for example a 1 g/dl difference in concentration (from 26 g/dl to 27 g/dl) could have a tenth time (where the tenth time is one tenth of the time a kinetics growth curve takes to reach its maximum value) decrease from 16 to 5.5 seconds. Similarly, the log f_0 values can then differ by ~1 mM/s (from -8.25 mM/s for 26 g/dl and -7.3 mM/s for 27 g/dl) and the log B by 0.35 s^{-1}(-0.25s^{-1} for 26 g/dl and 0.12 for 27 g/dl).

After mixing, two microliters of Hb are drawn from the container with a Drummond micropipette and, after wiping excess Hb which sticks to the outside of the pipette, the Hb is pipetted into the awaiting 5ml of CO buffer. A spectrum is taken of each solution, and the three values are averaged to give a final Hb concentration. The values of this are shown in table [4.1] for the samples used in the CO partial photolysis experiment.

Table [4.1]: The samples used in the CO partial experiment. Concentration values before dilution with dithionite and phosphate buffer. *A,B,C,D; designates samples from different HbS preparations. Note that higher concentration measurements have a larger standard deviation in comparison to lower concentration measurements, see table [4.2].

Date	Conc (g/dl) 1	Conc (g/dl) 2	Conc (g/dl) 3	Conc Avg	Conc Std	% CO etc	Hb Prep*
9/30/2010	41.65	43.4	41.19	42.08	1.17	95%CO 5% Oxy	A
12/22/2010	41.3	41.86	44.7	42.62	1.82	93% CO 7% Met	B
2/9/2011	45.17	44.05	-	44.61	0.79	88%CO 12% Met	B
2/18/2011	34.36	38.5	-	36.43	2.93	90% CO 10% Met	B
4/29/2011	33.51	33.87	33.12	33.50	0.38	90.4% CO 9.6% Met	C
6/7/2011	37.96	35.67	-	36.82	1.62	93% CO 6.4% Met 0.6% Oxy	D

Once the concentration of the initial Hb is known, the amount of buffer needed to dilute the Hb is calculated. Sodium dithionite needs to be mixed with the buffer and hemoglobin solution so as to have a final concentration of 50 mM. The high molarity of sodium dithionite ensures that any free O_2 in the solution will be reduced. The sodium dithionite is mixed with the CO HbS buffer, which is then used to dilute the HbS. To calculate the amount of sodium dithionite needed, consider the following: suppose there is a hemoglobin stock solution of initial concentration 40 g/dl and it needs to be diluted to 26.6 g/dl. A final sample volume of 15 µl is desired because that is enough to make three samples each with 1.5 µl, and three concentration measurements of 2 µl each. Therefore, 5 µl of buffer is mixed with 10 µl of the 40 g/dl Hb. The final concentration is calculated as:

$$C_f = \frac{C_i \times V_{Hb}}{V_f} \tag{4.1}$$

Where V_{Hb} is the volume of the Hb to be added to the solution, V_f is the final total volume. The calculation is restricted by the final solution having 50 mM of sodium dithionite. The buffer is taken from a stock solution of 2 ml of dithionite buffer mixture. To calculate how many grams of dithionite to add to the 2 ml stock solution:

$$grams\ of\ dithionite = \frac{50mMol \times 10^{-3}\frac{Moles}{mMoles} \times 174g/mol \times 15ul \times 2 \times 10^{-3}Liters}{V_{Buff}} \quad (4.2)$$

where the mMoles are converted to Moles, 174 g/Mol is the molecular weight of dithionite, and V_{Buff} is the volume of the buffer that is added to the final solution, 5ul in this example.

The correct amount of dithionite for this example is 0.0912 grams. The dithionite is taken from a stock amount that is in a sealed container which is kept in an anaerobic chamber filled with nitrogen gas. A small amount is weighted out on a precision mechanical scale and then sealed tightly in a small vial. The vial is then placed in the CO glove box where is mixed with the 2 ml of CO flushed buffer. A measured amount of Hb is pipetted into a new vial and then mixed well with a few microliters of the sodium dithionite taken from the 2 ml stock solution (the amounts of HbS and buffer to be mixed are found from equation 4.1). CO gas is allowed to flow into the vial, and then it is sealed and placed down for about two to three minutes. This assures that the Hb reacts with the dithionite, loses all its oxygen, and binds with the CO gas in the buffer.

Meanwhile, three tubes of 6 ml of CO buffer are prepared for concentration measurements, post dilution. After waiting, the vial with the mixed Hb is opened, mixed again, and then 3 µl is pipetted into each awaiting concentration measurement. The Hb vial is stoppered between each use to prevent drying. The three tubes are then sealed with Parafilm® and immediately inverted and mixed. The concentration measurements post mixing are shown

in table [4.2]. Next, three glass microscope slides and cover glass are wiped clean with a Kimwipe™, and 1.5 µl of the Hb mixture is placed onto the center of each slide. They are then sealed air tight with wax melted on by a soldering iron.

Table [4.2]: Dilution concentration measurements for the samples used in the CO partial photolysis experiment; with final average concentration and standard deviation of measurements. Some samples have only two measurements due to small sample volume.

Date	Conc (g/dl) 1	Conc (g/dl) 2	Conc (g/dl) 3	Conc (g/dl) 4	Avg Conc	Std dev
9/30/2010	28.7	28.89			28.8	0.13
12/22/2010	28.3	27.56			27.9	0.52
2/9/2011	26.89	26.25	26.77		26.64	0.34
2/18/2011	37.38	36.3	35.56	36.07	36.33	0.77
4/29/2011	26.78	26.44	26.37		26.5	0.22
6/7/2011	26.53	26.77			26.65	0.17

4.2.2 Oxygen-carbon monoxide experiment sample preparation

This experiment is often referred to as the “oxygen” experiment; however, these samples contain both oxygen and carbon monoxide. Previously, samples were carefully prepared so as to not have any oxygen. These however, were prepared by mixing oxy HbS with a small amount of CO HbS and diluting with deoxygenated buffer so as to minimize the free CO and oxygen in solution. This method would create a sample with a stable ratio of CO and oxygen. These samples would be tested much like the pure CO HbS samples because laser

photolysis causes HbS to release only the CO ligands. This means that in an oxy HbS sample, only the CO is released while the oxygen population remains stable, allowing the effects of oxygen on HbS polymerization to be measured. Oxygen samples were prepared in pH 7.05 buffer, the pH that 50 mM of dithionite would change a CO HbS sample to.[109] They are prepared similar to CO HbS samples; the HbS is mixed in the same container, as well as spectrum dilution measurements. However that is where the similarities end. For example, the HbS for oxygen experiments was never frozen, but was kept in a fridge and used fresh so as to minimize Met Hb formation. Also, all the HbS used in the oxygen experiments came from a single Hb preparation and completely prepared in the cold fridge as to minimize met Hb.

The HbS for oxygen experiments was divided into five vials which had their concentrations measured and then labeled. Unlike in the CO experiments, the initial volume of HbS does not need to be precisely known before making a sample. This is because the HbS will not be mixed with dithionite to obtain the final 50 mM amount. One vial of HbS was exposed to CO in the CO glove box and was capped tightly and rotated for several hours. The other vials were kept in an oxygen atmosphere. To make a sample, first, a small amount of the CO HbS was placed into a vial (for example, 3 µl). This vial then had any excess CO blown out by N_2 gas. This vial was then placed in a glove box with a nitrogen atmosphere. To this vial was added a small amount of oxy HbS (5 µl for example) and deoxygenated buffer (buffer made by bubbling with N_2) and was stirred with a microliter volume Drummond syringe. The sample was then quickly made and sealed with wax. Two dilution spectrum measurements would be made, one in Deoxygenated buffer and another in CO buffer. The HbS could not be kept in the deoxygenated box for any extended period of time because it would quickly lose any oxygen it contained. The

[109] Galkin, Oleg. Et. al. (2007). The kinetics of nucleation and growth of sickle cell hemoglobin fibers. J. of Mol. Biol. 365. (425-439).

vial of oxy HbS also could not be kept in the box for this same reason, and would only be brought into the box right before the sample was made. Different techniques were tried, and it was found that making a sample in the open atmosphere produced too much excess oxygen in the samples and they would not polymerize. In table [4.3] are the values of the samples concentration when measured by dilution in CO and deoxy buffer. The CO buffer measurement allows a spectral fit of just three parameters (CO, O_2 and met HbS) and should give the more reliable value for the concentration. The percentages of CO, met and oxy HbS are shown from the dilution spectrum measurement in deoxy buffer. The percentages would not be accurate in the CO buffer due to the high binding rate of HbS for CO in comparison to oxygen. The final two columns in table [4.3] contain the percent met and oxy HbS as measured through a spectrum taken on the sample slide.

The spectrum taken on an oxygen sample is much more complex than a CO sample. For a CO sample, a baseline intensity is measured from 400 – 450 nm on a buffer sample, then the HbS sample intensity is measured. However, for an oxygen sample, taking a spectrum with a mixture of CO, oxy and met HbS is not accurate. This is in comparison to fitting a spectrum with deoxy, oxy and met HbS, whose peaks in the 400-450 range are further apart and more precisely resolved. A deoxygenated spectrum is obtained by photolyzing the CO off of the HbS and then measuring the sample absorbance. To obtain a deoxygenated spectrum, a larger area of the sample is exposed to the laser to be photolyzed (this is done by removing the mesh which splits the laser beam into micron sized holes). A diaphragm is inserted in the laser path creating a specific photolyzed region (dark red circle in figure [4.2] left). This produces an area of about 170x170 pixels of photolysis. Another diaphragm is inserted such that an area of 100x100 pixels (20x20 μm) of the photolyzed laser area is illuminated by the monochromator light (small dark

red circle in figure [4.2] on the right is the viewable area after the diaphragm is closed). Then a square region of interest is chosen for measurement. The square area is chosen in the center because the image will shift due to changing wavelengths. Using a diaphragm allows only light from the photolyzed area to enter the camera and greatly decreases the scattered light from unphotolyzed areas of the sample (scattered light from an unphotolyzed region can produce a false signal of CO HbS in the spectrum). While obtaining a deoxygenated spectrum, polymers may have formed during measurement. To try to delay and decrease the amount of polymer formed, the sample is flashed with the laser for 0.2s and then the laser is turned off for 1 second before the next wavelength is taken. Interesting to note, when polymers are formed the percent of oxygen decreases and the percent of met HbS increases slightly and deoxy HbS may increase slightly. This occurred in sample #2 6/8/11 where polymers formed and 59% deoxy, 29% met and 10% oxy HbS were measured, as opposed to 63% deoxy, 16% met and 20% oxy HbS in a spectrum without formed polymer. This also occurred in sample #3 6/9/11 where 59% deoxy, 22% met, and 18% oxy HbS were measured when polymers formed, as opposed to: 59% deoxy, 16.8% met, and 23% oxy HbS without polymers.

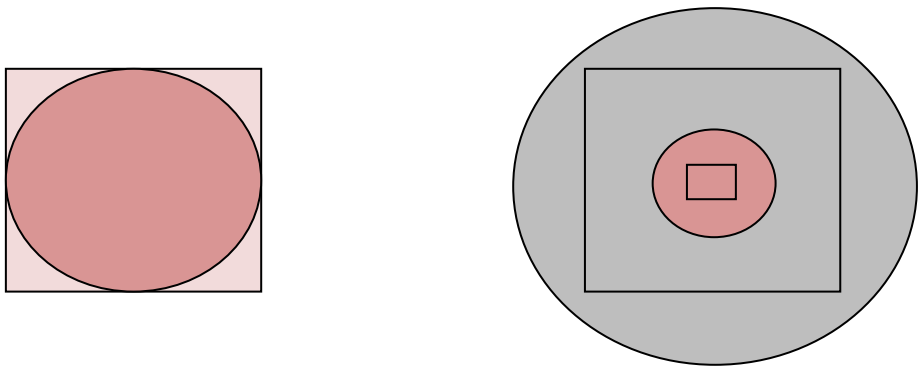

Figure [4.2]: Left: Dark circular area photolyzed is photolyzed by the laser. Right: Diaphragm is placed over the lamp illuminating the sample and only a small circular area of the photolyzed region is viewable. The small square shows the area imaged by the camera.

To analyze the spectrum data, several deoxygenated spectra were taken of each sample in the area of the experiment on the sample. The error of each spectrum measurement is found from the standard deviation of each of these individually measured spectra. To find the average spectra values, the optical densities of each spectrum at each wavelength were averaged together, and fit for the percentages of oxygen, met and deoxy HbS as well as the sample thickness. The thickness is needed to compute the volume of the sample for the kinetics analysis. In CO samples, sample thickness is easy to find, it is just the OD at 420 divided by the molar extinction coefficient (a known constant) and the concentration:

$$OD = \varepsilon c l \tag{4.3}$$

However, when there are several components as there are in oxygen samples, the optical density becomes:

$$final\ OD = \left(OD_{Deoxy} + OD_{Met} + OD_{Oxy}\right) = \tag{4.4}$$

$$\left(\varepsilon_{Deoxy} * c_{Deoxy} + \varepsilon_{Met} * c_{Met} + \varepsilon_{Oxy} * c_{Oxy}\right) * l$$

where:

$$c_{Deoxy} = \%\ of\ Deoxy * c_{tot} \tag{4.5}$$

Table [4.3]: The oxygen experiment samples parameters as given by dilution in CO and deoxygenated buffer; as well as their % oxygen and met as given by spectrum measurements taken on the sample stage.

Date	Sample	Conc (g/dl) dilution (CO buff)	Conc (g/dl) dilution (deoxy buff)	Deoxy buff dilution component	Conc std dev	% Oxygen	% Met
6/7/2011	1	33.42	32.99	73% CO 0.6% DO 10% Oxy 15% Met	0.3	2.93%	10.53%
6/8/2011	1	29.01	29.45	83% CO 1.4% DO 15% Met	0.31	9.14%	9.66%
6/8/2011	2	27.44	27.9	27% CO 53% Oxy 18% Met	0.33	2.47%	25.94%
6/9/2011	2	32.35	32.13	30.6% CO 48% Oxy 20.9% Met	0.16	34.68%	21.5%
6/9/2011	3	34	33.7	45% CO 35% Oxy 19% Met	0.21	20.98%	20%
6/10/2011	1	34.2	35.35	46% CO 34% Oxy 18.9% Met	0.81	22.43%	16.46%
6/10/2011	2.1	34.2	35.35	46% CO 34% Oxy 18.9% Met	0.81	43.75%	17.09%
6/10/2011	2.2	32.45	32.55	38.9% CO 39% Oxy 21% Met	.07	43.75%	17.09%
6/11/2011	1	31.57	30.78	44% CO 30% Oxy 25.25% Met	.56	22.5%	22.9%
6/11/2011	2	35.9	34.3	47.3 % CO 25.6% Oxy 26.9% Met	1.13	19%	22.7%
6/11/2011	3	35.35	33.6	33% CO 37 % Oxy 29.6 % Met	1.24	38.1%	21.64%

Table [4.4]: Comparing the spectrum data of CO and deoxygenated oxygen samples. The % of met Hb in the CO spectrum was used as fixed percentage when fitting the deoxy spectrum.

			CO Spectrum Data				**Deoxy Spectrum Data**			
Date	Sample #	Conc avg (g/dl)	% CO	% MET	% OXY	Thick (um)	% CO	% Met	% O2	% Deoxy
6/7/2011	1	33.21	89.5	10.53	0	4.87	0	10.53	2.93	86.54
6/8/2011	1	29.23	83.66	9.66	6.67	3.32	0	9.66	9.14	81.2
6/8/2011	2	30.34	43.16	25.94	30.9	7.38	6.3	25.94	2.47	65.29
6/9/2011	2	32.24	43.06	21.5	35.44	4.11	0	21.5	34.68	55.8
6/9/2011	3	33.85	54.18	20	25.82	5.29	0	20	20.9	59.02
6/10/2011	1	34.78	59.51	16.46	24.02	3.57	8.86	16.46	22.43	52.25
6/10/2011	2.1	32.5	42.45	17.09	40.45	0.891	2.06	17.09	43.75	37.1
6/10/2011	2.2	32.5	42.45	17.09	40.45	3.46	2.06	17.09	43.75	37.1
6/11/2011	1	31.18	52.18	22.9	24.96	4.261	0.822	22.9	22.5	53.78
6/11/2011	2	35.1	53.17	22.7	24.12	2.58	7.5	22.7	19	50.8
6/11/2011	3	34.475	38.7	27	34.32	2.76	3.01	21.61	38.1	37.3

The CO spectra were analyzed to obtain the thickness of the samples which is used in the kinetics calculations. The CO spectra were also analyzed for the percent of met Hb in the samples. This percentage was forced to remain constant when the spectra were fit for the deoxygenated spectra. The values found from the CO and deoxy spectra are compared in table [4.4]. Note how some of the spectra have a small amount of CO after fit in the deoxygenated spectra. Increasing the laser power does not seem to affect this amount of CO; on the contrary, increasing the laser power too much burns the sample and causes more met HbS.

4.2.2.1 A note on met Hb

Met Hb is Hb with the iron in the heme group in the ferric state, Fe^{3+} instead of Fe^{2+}. Met Hb does not bind oxygen. Typically 1-2% of a person's Hb is met Hb. Met Hb can be reduced with compounds such as sodium dithionite, which returns met Hb to the ferrous 2+ state, and physiologically by enzymes found in the red cell membranes. Sodium dithionite also reduces oxygen which is why it was not used to reduce met Hb in the oxygen experiments conducted in this thesis. The oxygen experiments data had about 20% met Hb as shown in table [4.3]. Reduction of the met Hb was attempted through several means. The first method we attempted was to conduct the Hb chromatography from fresh blood which was never frozen and to do all the steps in the prep in the cold fridge when possible. After all this, the HbS still had about 12% met Hb right after it was eluted from the column. The final amount of met Hb would increase after the buffer was exchanged and the HbS was re-concentrated.

Sodium dithionite reduces the amount of met HbS. This is done by mixing the HbS in CO buffer and adding a small amount of dithionite. For the duration of a one day experiment, the amount of met HbS in a sealed sample is nearly undetectable, but for the HbS in the oxygen experiment, such a method cannot be used. This is because sodium dithionite will reduce all oxygen it comes in contact with, and to use a sufficient quantity to reduce the 20% met Hbs, will also remove all oxygen from the solution. Instead, in an attempt to reduce the amount of met HbS while retaining oxygen, a series of experiments were conducted where deoxygenated buffer was mixed with a small amount of sodium dithionite (~1mM) and HbS --but the amount of met HbS did not decrease. After that result, other experiments were conducted where the amount of sodium dithionite was incremented; however, this actually caused the amount of met Hb to increase, even double in one case to 33%. It was also found that if the sodium

dithionite-HbS mixture was allowed to re-oxygenate, the total amount of met HbS would be more than before adding sodium dithionite. From these tests, we decided that reducing the met HbS was not possible by the usual means. Another experiment was conducted where the HbS was passed through a chromatography column a second time, decreasing the met HbS by 2-3% from 11%. In conclusion, the immense effort expended was not deemed worth the small return in the reduction of met HbS.

4.3 Apparatus

The optical table had been originally designed by others[110] for the purpose of measuring kinetics on completely deoxygenated HbS samples. However, due to the necessity of measuring partial desaturation, laser intensity, and deoxygenated HbS spectrum, several components had to modified and improved. The only elements kept unchanged from the original design were the position of the laser, lamp and sample stage.

[110] Cao, Zhiqi. Et. al. (2002), a 50th order reaction predicted and observed for sickle hemoglobin nucleation. J. Mol. Biol. (256) 219-222.

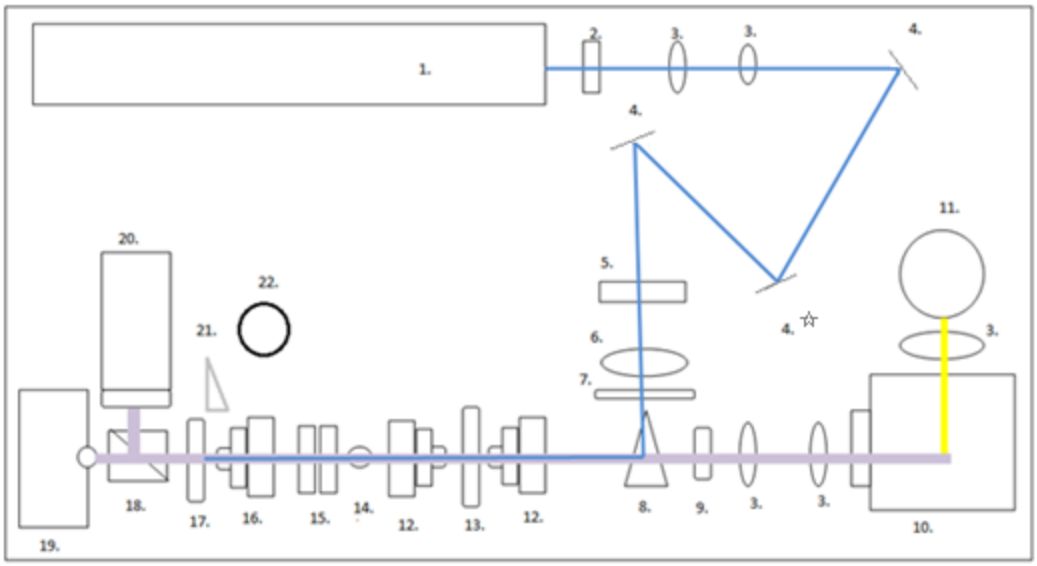

Figure [4.3]: Schematic of the optical table used in the CO and oxygen experiments.

Optical table equipment:

1. 5W Spectra Physics 184 Argon 488nm laser used mainly in the 0.1W to 0.6W range.
2. Laser shutter, controllable by computer and by a push button.
3. Lens.
4. Three reflective mirrors
5. Metal mesh with 0.25um diameter holes spaced about 0.45um apart.
6. Round graded neutral density filter used to decrease the laser intensity.
7. Diaphragm used for laser alignment.
8. Dichroic mirror. Reflective for the laser light and transparent for the monochromator wavelengths.
9. Back aperture, used for focusing the monochromator light on the sample.

10. Monochromator, receives light from the lamp, and outputs single wavelengths of light in the 400-450 nm range. SpectraPro-150, Acton research Corp. 0.150 meter focal length dual grating imaging monochromator/spectrograph.

11. 150 W Xenon arc lamp. The light is focused onto the monochromator slit by the lens.

12. Microscope lens (X amount of magnification needed) one before sample, one after. Before the sample, focuses the lamp and laser light onto sample. After sample, collects the light from sample and sends it towards the eyepiece. Both have adjustable foci and fstop (or aperture).

13. Sample stage with temperature control.

14. Notch filter, blocks specifically in the 488 nm range; used to block laser light in order to measure spectrum and desaturation (in diagram, the blue laser light incorrectly passes through the notch filter). In a kinetics experiment, the notch filter is removed from the optical path and the laser light will be blocked by the dot in order to measure kinetics.

15. Double bandpass colored glass filters (FGB245S), decreases transmittance in the 315-445nm range. Used to lower the intensity of the monochromator light.

16. Projective eyepiece, similar to an eye piece in a stand up microscope, here it focuses the light for the two cameras to view instead of an eye.

17. A thick glass slide with imprinted dots of varying sizes. Used to block straight laser light so only scattered light passes through.

18. Beam splitter box, sends some light to a live action video camera mounted on the optics table, and the rest to the CCD camera.

19. CCD Photometrics Quantix 57 camera. With a 535x512 imaging array and 13x13 μm pixels.

20. Camera used to view sample live on TV screen.

21. Removable mirror, used to direct the laser light towards the laser power meter.
22. Laser power meter.

In reference to figure [4.3], the newly added elements to the optical table include the lenses directly after the laser, as well as an extra mirror (#4 with a star in figure [4.3]). The lenses were placed to expand the laser beams diameter slightly, so the gradient of laser light passing through the mesh would be more even. The extra mirror was placed so as to prevent the laser light from being reflected at too drastic of an angle. Since some lenses were removed from the optical path, the mesh was repositioned so that the laser light underwent a Fourier transform as it passed through the holes. The Fourier transformed light is then refocused onto the sample via the back aperture microscope lens. This is what causes the pattern of the mesh to appear on the sample.

4.4 Data collection programs and devices

4.4.1 Spectrum Data

Spectrum data was collected using a code I wrote in IPLab based on a program originally written by Dr. Rotter. It operated by incrementing the monochromator wavelength by 2 nm from 400 to 450 nm. Images of 250 x 250 pixels were captured at 0.2 sec exposures. The baseline images of the buffer sample were subtracted from these images and then they were averaged and the $\log_{10}$ was taken to find the optical density (OD):

$$OD = -\log\left(\frac{I}{I_o}\right) \tag{4.6}$$

Spectrum data was analyzed using a program based on code written by Dr. Rotter. The spectrum data collected was used to find the thickness of the sample at the local measured area. The thickness is used to calculate the volume of photolyzed spots used in determining f_0, the homogeneous nucleation rate.

My modifications to the program included a new ability to average several spectra together and then fit the data. I also added the capability of forcing a fixed percentage of met Hb while fitting the spectra data. Figure [4.4] shows two CO-oxy-met HbS spectra averaged for sample 6/11/2011 #3. The blue crosses are the optical density measured from the sample.

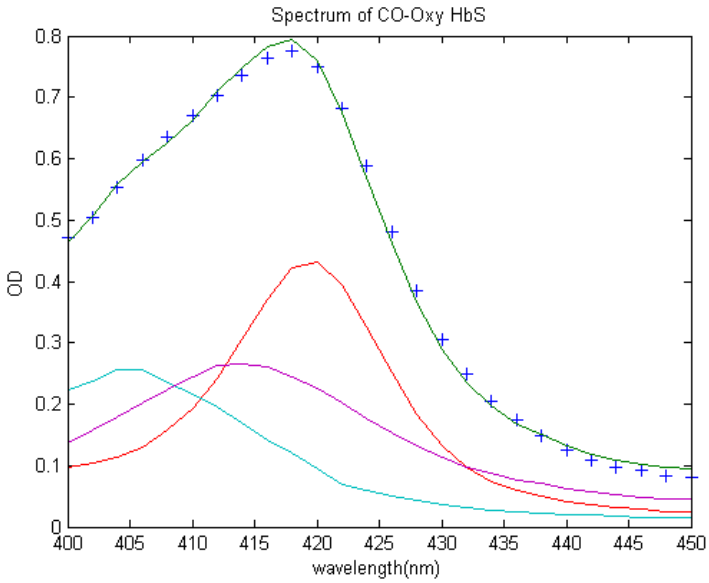

Figure [4.4]: Spectrum of a CO-oxy sample. Blue crosses are the raw data, the green line is the sum of the spectral components. The red, purple and blue lines are the CO, oxy, and met HbS spectral components.

4.4.2 Light Scattering

To measure light scattering, the optical table is setup as follows: Monochromator shutter is closed. Laser light is passed through the mesh and illuminates the sample. Laser light passes directly (straight) through the spots, and it will start to scatter as polymers grow. The direct laser light is blocked by an imprinted spot on a glass slide. The scattered light is refocused into the CCD camera, and the image will reappear as scattered light from multiple distinct spots. The CCD camera will take images in a continuous exposure setting.

Kinetics data was collected using software created in Codewarrior by Dr. Aprelev and Dr. Zakharov. The two programs used were for slow kinetics and fast kinetics. The fast kinetic program operated by binning the pixels in the images collected by the camera, which allowed for faster gathering of images. The image size was 500x500 pixels, with 1 pixel ~0.20 μm and a 10x10 bin. The slow kinetic program operated by capturing single images at predefined exposures and intervals. This was usually 0.2 sec exposure at 0.2 sec intervals. Fast kinetics is an experiment which took less than 90 seconds to be completed. My improvements to the software included an automated collection capability, where the user can input how many data sets to collect, and how long to wait in between each set.

4.5 Analyzing kinetics data

4.5.1 Analyzing kinetics data – CO-oxygen

The process of analyzing CO-oxygen data is discussed first as opposed to the partial CO HbS kinetic experiment. The process for analyzing the partial CO kinetics data is a very similar

process to that described here, but with an added level of complexity that is discussed in the preceding sections. Kinetics are obtained through the CCD camera on a 500x500 pixel area that has been binned to 10x10 bins, therefore the images obtained are 50x50 super pixels. The transfer of collected camera data is limited, in that it can either obtain high spatial-resolution images with a low bin, or lower resolution images at a larger bin, at faster rate. Low resolution at a high rate is necessary for measuring fast kinetics which could have tenth times less than a second. Kinetics data is stored in an array of matrices, the rows in the matrix store each super pixel and the columns are that super pixel changing in time. Areas of scattered light are located by summing all the intensity values in a column and plotting that matrix. The image is shown in figure [4.5] as plotted via Matlab. The islands in the figure show the areas where polymers grew and scattered light. This matrix is used to identify the super pixels which are all part of the same scattered spot. It is also used to identify and zero out scattered light from objects other than polymers, such as dust in or on the sample slide.

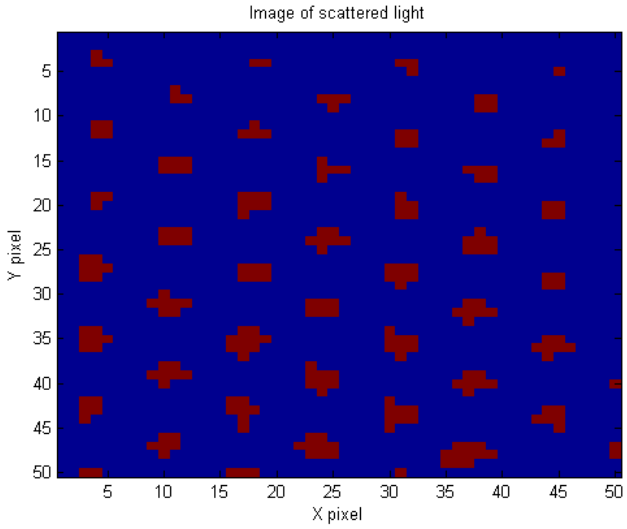

Figure [4.5]: Scattered light summed matrix from the first data run, sample 6/10/2011 #1.

The raw data that is collected from each super pixel when plotted as function of time is shown in figure [4.6] left. Notice in the beginning of the data set there are some data curves that start at a higher value (zoomed in, in figure [4.6] left). These may be spots that have background scattered light and therefore have a baseline which will need to be zeroed out. There are so many curves because they are from each of the 50x50 super pixels. However, the curves which are from the same spots in figure [4.5] will be combined into one curve. Next, the data will then have any spots with maximum intensities less than 30% of the maximum scattered intensity removed (this eliminates data curves that are at widely different intensities). Lastly, the baseline background of each curve is subtrated and the curves are renomalized to the maximum measured intensity value (figure [4.7]).

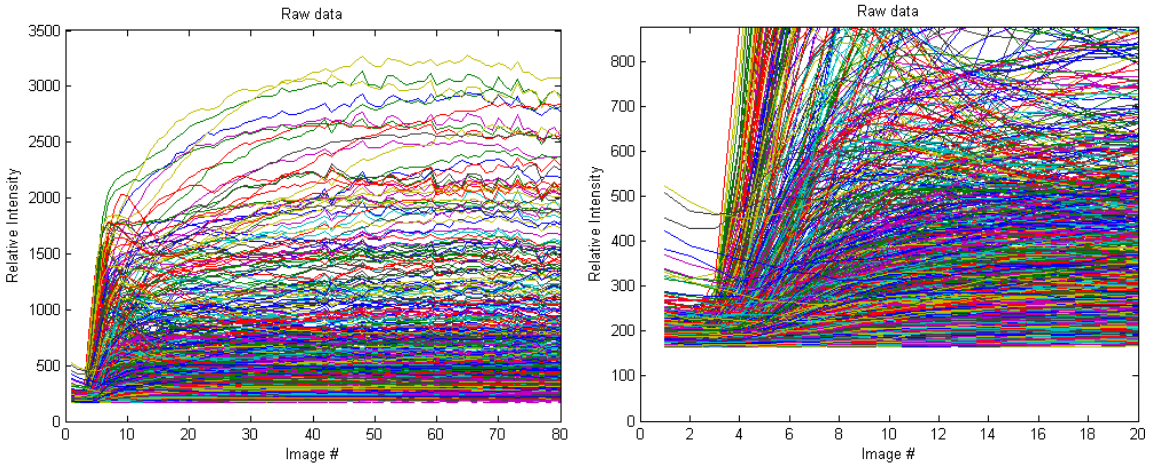

Figure [4.6]: Left: raw intensity data versus image number, each curve is from a super pixel. Right: same data, zoomed in to show detail of curve beginning.

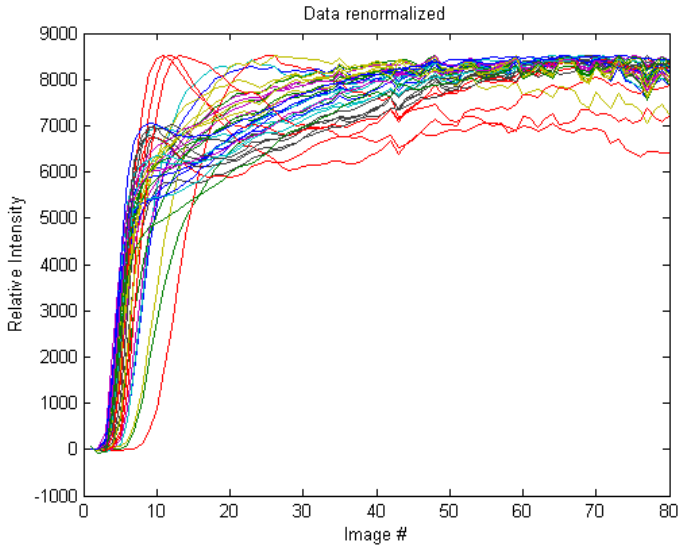

Figure [4.7]: Renormalized data for first data run, sample 6/10/11 #1.

The beginning of each intensity progress curve is an exponential that is fit to find to find the polymer growth rate, B (equation 2.26). The growth curves are solved for their tenth times, t_{10}, i.e. the time it takes for the curve to reach one tenth of its maximum. The tenth times are then plotted in a histogram. The histogram is fit with Szabo's function (equation 2.32) the tail of which is a decaying exponential, which will provide the nucleation growth rate, f_o (equation 2.29). Figure [4.8] shows the histogram of tenth times, with the red curve as the fit to the data. Improvements in the kinetics code for this thesis work, allowed analysis of partially photolyzed samples which scattered different intensities of light in different areas of the sample.

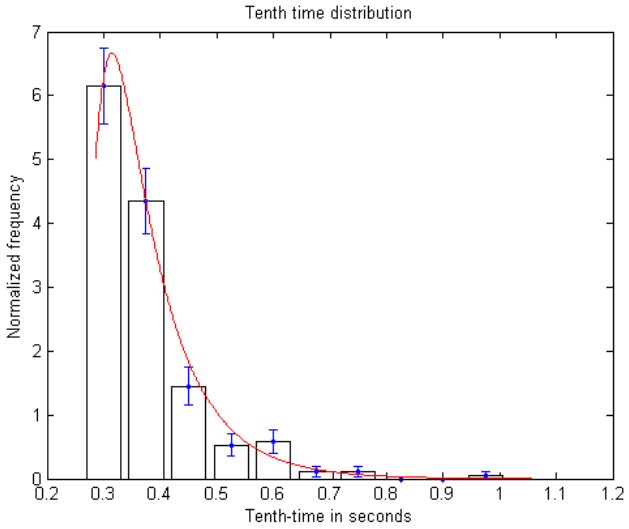

Figure [4.8]: Tenth time distribution for data runs 1-9, sample 6/10/2011 #1.

4.5.2 Analyzing kinetics data –measuring CO HbS desaturation

Desaturation is the opposite of saturation in a sample. Hb which has a gas molecule on each ligand is fully saturated. Deoxygenated Hb is 100 % desaturated. For HbS kinetics experiments, it is common to refer to the desaturation of a sample, since that is the physical state of upmost interest. However, although desaturation will often be referred to in the data analysis, the final theory describing the behavior of the HbS will be in terms of saturation. In this experiment the HbS is saturated with CO. From the allosteric model, the number of HbS molecules with 0, 1, 2, 3 or 4 ligands can be quantified for a given partial pressure. Once the number of each species is known, percent saturation becomes:

$$\%\, saturation = (0 * (X_0) + 0.25 * (X_1) + 0.5 * (X_2) + 0.75 * (X_3) + (X_4))*100 \qquad (4.7)$$

Where X_0, X_1, etc. are the number of HbS molecules with 0 or 1 or 2, etc. ligands. This percent saturation is relatable to the percent CO that is measured when a spectrum is taken of the sample. Since the amounts of X_0, X_1, X_2 and X_3 can be solved for our system, the amounts of each population are known for any percent saturation of the HbS sample.

To find the percent desaturation in partial CO photolysis experiments the relation between deoxy and CO HbS at 432 nm was used as well as the optical density (OD) of the sample at 420 nm. The procedure is as follows, first a CO spectrum is taken of the sample. The OD is found at 420 nm, which is where the CO spectrum peaks between 400 and 450 nm. Next, the sample is illuminated at 432 nm. Four images are taken, first the background with laser and lamp off (image 1). Second, is with only the lamp on (image 2). Third, the laser is turned on with the lamp already on and an image is taken (image 3). Finally, the lamp is turned off and only the laser is on (image 4). Each image is taken at a 0.2 second exposure. Next, the intensity of CO HbS is found by subtracting image 1 from image 2 (removes stray light intensity) and the intensity of the Deoxy HbS is found by subtracting image 3 from image 4:

$$I_{CO} = Image\ of\ CO\ HBS\ at\ 432\ nm - Image\ of\ background\ (lamp\ off)$$

$$I_{DO} = Image\ of\ Deoxy\ HBS\ at\ 432\ nm\ (laser\ on) - Image\ of\ background\ (lamp\ off, laser\ on)$$

Dividing the intensity of CO HbS by Deoxy HbS at 432, and then taking the log is equivalent to finding the difference in their optical densities at 432. However, to obtain an optical density, the intensity of lamp light through a buffer sample must be measured. This would require removing the sample and then placing it back for each measurement. To avoid moving the

sample after the experiment was begun, the mathematical relation was used. Doing this will give a constant in each pixel of the image, K:

$$\frac{OD_{CO\ 432} - OD_{DO\ 432}}{OD_{CO\ 420}} = -\frac{log\left(\frac{I_{CO\ 432}}{I_{DO\ 432}}\right)}{OD_{CO\ 420}} = K \tag{4.8}$$

Optical density (absorbance) is the negative of the log of the intensity divided by the background intensity (this ratio is also called transmittance), and is equal to the molar extinction coefficient multiplied by concentration and the sample path length:

$$OD = -\log\left(\frac{I}{I_o}\right) = \varepsilon c l \tag{4.9}$$

Expanding equation (4.8) using (4.9) gives:

$$\frac{\varepsilon_{CO\ 432} c_{CO} l - \varepsilon_{DO\ 432} c_{DO} l}{\varepsilon_{CO\ 420} c_{CO} l} = K \tag{4.10}$$

where K is a known experimental quantity that comes from the measured images. Letting the concentration of deoxy HbS be:

$$c_{DO} = x * c_{CO} \tag{4.11}$$

where x is the fraction of deoxy HbS and C_{co} is the concentration of full CO sample. Solving for x gives:

$$x = \frac{\varepsilon_{CO\ 432} - K * \varepsilon_{CO\ 420}}{\varepsilon_{DO\ 432}} \tag{4.12}$$

and multiplying x by 100 will give the percent of deoxy or desaturation. The values used for the molar extinction coefficients were: [111]

$$\varepsilon_{CO\ 432} = 43.17;\ \varepsilon_{DO\ 432} = 130.59;\ \varepsilon_{CO\ 420} = 190.29$$

4.5.3 Analyzing CO desaturation

The analysis of the CO data is similar to that of the oxygen experiment, except for the addition of analyzing partially photolyzed areas. The laser's center was off set so that an array of different intensities were created on a single sample. The spots were analyzed for their intensities, which reached a maximum of ~2.8 kW/cm^2. The photolyzed areas were measured for their desaturation (or percent deoxygenation). This was done by first thresholding the image to 4% desaturation, i.e. subtracting out the background noise in the 500x500 pixel image to leave "islands" of desaturation (figure [4.9], right). Next, the locations of the desaturation areas are identified as well as the center of mass of each spot. The center area of each spot should receive the highest laser intensity as well be the most desaturated. However, the program will sweep out to a radius of 6 pixels to find the maximum desaturation value in the center area. Then it will sweep out 8 pixels to find an average desaturation value for the immediate area. The program will then locate all the pixels in the photolysis spot which are within 10% of that averaged value (multiplying the new max by 0.9 and excluding values below this). Since the laser power drops off exponentially excluding the lowest 90% decreases the area of photolysis (figure [4.9] left and figure [4.10]). The final desaturation value for each spot was calculated by

---

[111] Van Assendelft, O.W. et. al. (1970). Extinction coeffients for use in equations for the spectrophotometris analysis of haemoglobin mixtures. Analytical Biochemistry. (69) 43-48.

averaging the remaining pixels within the original 10%. These pixels along with the sample thickness are used to calculate the volume of the desaturation area.

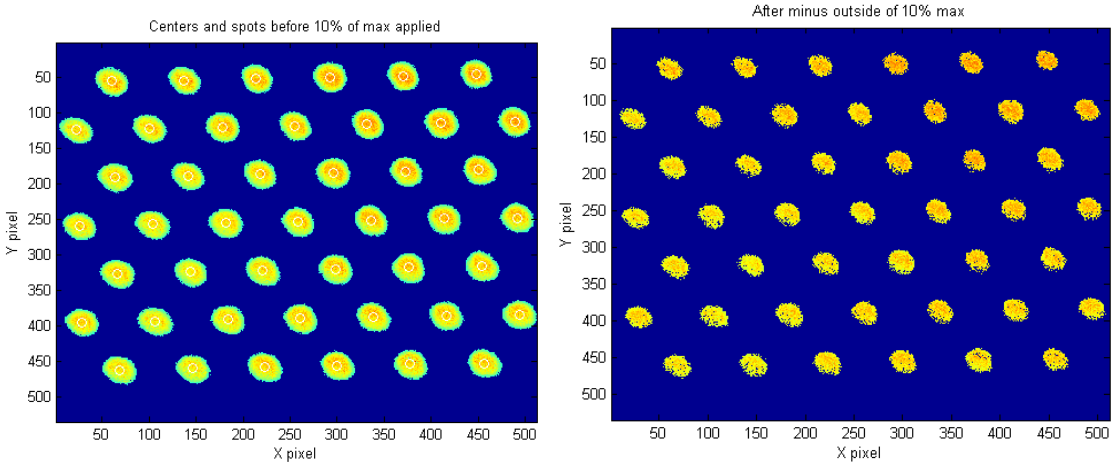

Figure [4.9]: Left: Desaturation image with threshold applied for noise. Center of circles maximum is 0.3 (where 0.45 is maximum desaturation value). Right: After subtracting out pixels outside of 10% maximum averaged desaturation.

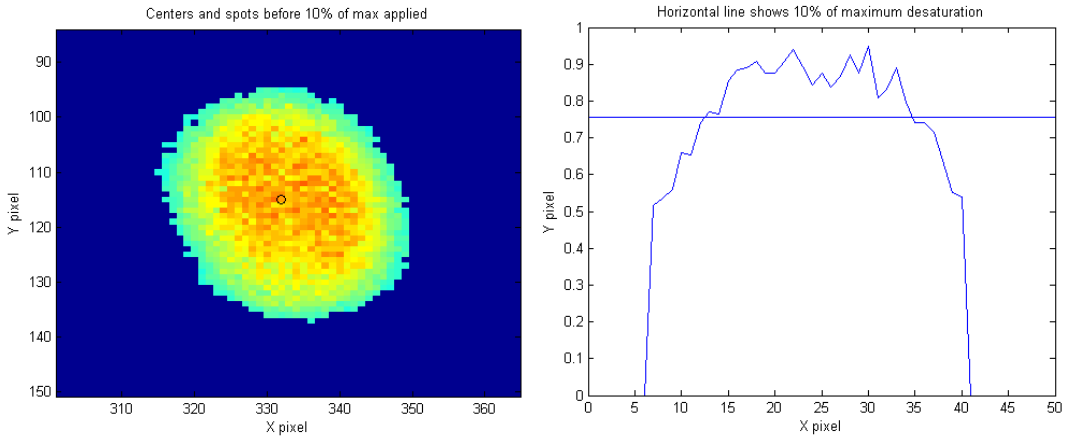

Figure [4.10]: Left: Zoomed in view of a single desaturation spot, black circle shows center of mass position. Right: Same spot along the y=244 axis. Horizontal line shows the cut off for 10% of maximum average.

To conduct a full experiment, multiple desaturations images are taken as a defined amount of time passes, for different laser intensity values. This was done to ensure that the percent desaturation remained constant until polymerization occurred. Using different laser intensities also allowed for comparing of similar percentages of desaturation from different laser intensities. Such comparisons are useful to show that the kinetics are related to the percent desaturation and not an artifact of heating of the sample. Data tables [5.1] to [5.6] list laser power along with percent saturation, log fo and log B values. It is clear from the data that there is no relation between a higher laser power setting and increased kinetics for the lowest saturations (full desaturation). Figure [4.11] shows an example of percent desaturations as they evolve in time. The laser power was set at 0.01 Watts and a filter was used to further decrease the laser intensity.

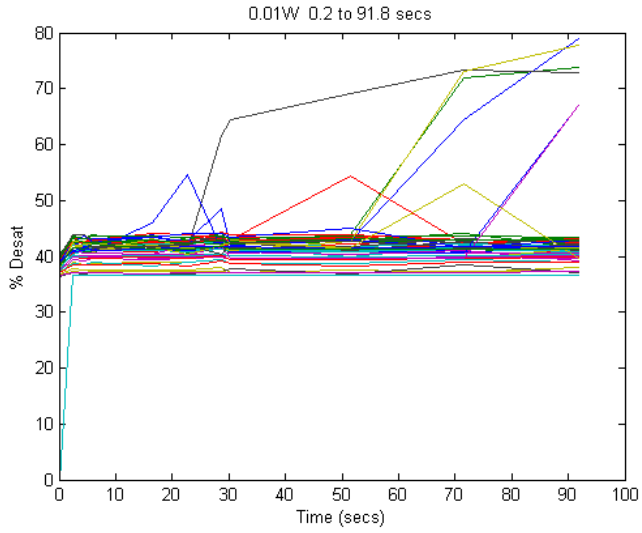

Figure [4.11]: The percent of desaturation as a function of time for sample 2/18/2011, at 0.01W laser power with an additional filter. The delay time for this laser power was ~35 seconds.

The desaturation image evolves over time, so a time is picked (usually the first or second image taken) and the volume and desaturation values for that image are used in data analysis. After the desaturation in each spot is located and tabulated, the image is scaled from 500x500 to 50x50 which is the size of the kinetics image. The desaturation spots are correlation to kinetics areas in a different program. At this point, it is possible to pick a range of desaturation values, 40-45% for example, and to only pick the kinetics curves that come from that range of desaturation areas. The kinetic progress curves from several experiments are all combined into a single data file which will then be analyzed like the oxygen data described in section 4.5.1.

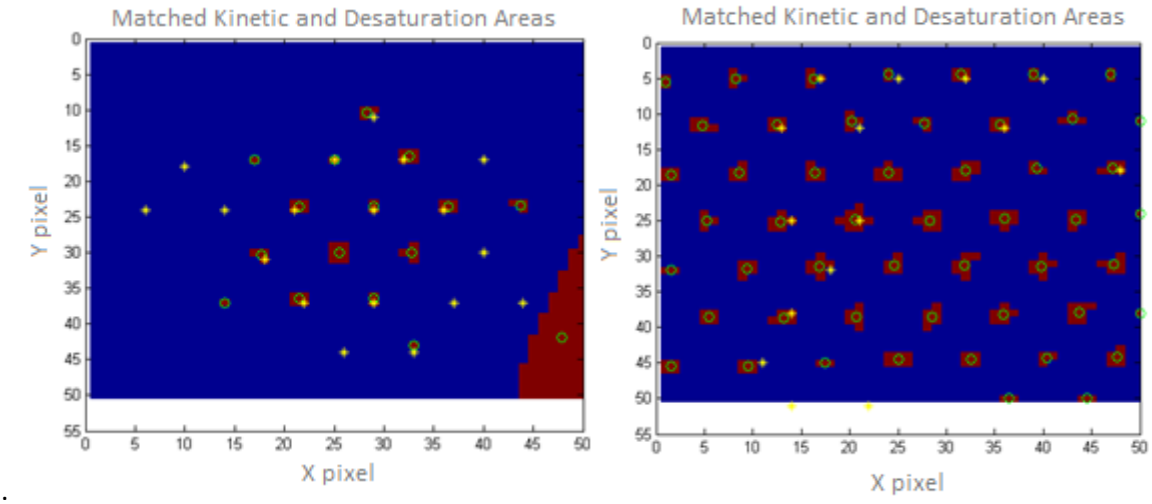

.

Figure [4.12]: Left: 0.01W (with filter) data from sample 4/29/2011. Green circles identify kinetics spots. Yellow stars are desaturation spots in the range of 55-60%. Areas where the circles and stars are within 2 pixels are a match between kinetics and desaturation. Right: Same sample with 0.1W laser power. The red areas are more numerous, meaning that more kinetic events occurred at the higher laser power. The yellow stars indicate 70-75% desaturation.

4.5.4 CO diffusion in photolyzed CO HbS samples

The measured quantity used to analyze data in this experiment, percent desaturation, arises from the combination of two effects. The first is the CO released by photolysis, which depends on the intensity of the laser light, the concentration of the HbS, etc. The relation between the amount of CO released and the fraction of deoxygenated Hb was quantified through a series of experiments conducted by Ferrone, et. al.[112] The optical density of HbA was measured with a PMT while a laser at 514 nm photolyzed the HbA at different intensities. The optical density is measured at times less than 10 ms, because times longer than 10 ms were shown to exhibit changes due to diffusion of CO out of the photolyzed area. A relation was made between the fraction of deoxy Hb and the power density of the laser (kW/cm^2). The results of that experiment are shown in figure [4.13]. The fraction of deoxygenated Hb and its relation to the amount of CO is given by the following two equations:

$$1 - f = \frac{K_R[CO](1+K_R[CO])^3 + L_0 K_T[CO](1+K_T[CO])^3}{(1+K_R[CO])^4 + L_0(1+K_T[CO])^4} \tag{4.13}$$

and

$$[CO] = \gamma c_0 f \tag{4.14}$$

where *f* is the fraction of deoxygenated Hb, [CO] is the free CO released by photolysis, K_R and K_T are binding constants which are the ratio of the association rates divided by the dissociation rates for Hb. L_0 is the equilibrium constant for none liganded Hb, γ is a factor which describes

[112] Ferrone, F. A. (1985). Kinetics of sickle hemoglobin polymerization I. Studies using temperature-jump and laser photolysis techniques. J. Mol. Biol. (183), 591-610.

the reduced solution volume accessible to the CO (which is 1.4 for 40g/dl) and c_0 is the hemoglobin concentration in mM. K_R and K_T are given by:

$$K_R = {}^{R}k_{on}/k_{off} \tag{4.15}$$

$$K_T = {}^{T}k_{on}/k_{off} \tag{4.16}$$

With ${}^{T}k_{on}=2\text{x}10^{5}\ M^{-1}\ s^{-1}$ and ${}^{R}k_{on}=1.2\text{x}10^{7}\ M^{-1}\ s^{-1}$ and k_{off} is defined as:

$$k_{off} = \frac{2.3\varepsilon_{514}\phi I}{NE_{514}} \tag{4.17}$$

where ε_{514} is the molar extinction coefficient for CO HbS (5,500 $M^{-1}\,cm^{-1}$), ϕ is the apparent photochemical yield and is less than one (0.47), I is the intensity of the laser, N is Avogadro's number, and E is the energy of a photon at 514 nm. These values were used to calculate the solid red line in figure [4.14].

However, the measured percent desaturation in this experiment also arises from a second effect, CO diffusion. The rate of CO diffusion from a photolyzed region has also been studied by Ferrone, et. al. and a relation was made between the fraction of CO (F(t) in the equation) remaining at the center of the photolyzed spot and the radius of the spot as well as the time of measurement:

$$F(t) = 1 - e^{-R^2/4Dt} \tag{4.18}$$

with D as the diffusion constant for CO and t is the time passed in seconds.

Using the following values, a curve was produced which predicts the percent deoxy HbS versus the laser intensity (figure [4.14]). The wavelength of the laser light was 488 nm,

therefore ε is 5400 M^{-1} cm^{-1},[113] the concentration of the sample was 26.65 g/dl, the diffusion constant was extrapolated from given data values to be approximately 4.2x10-6 cm^2/s[114] (at this concentration) and the radius of the laser spot was 3.4 µm. The blue line in figure [4.13] is the result of this calculation and it shows that the photolyzed areas had reached equilibrium with diffusion at the time they were measured. Also, they had reached equilibrium with CO diffusion long before any kinetics occurred. However, as the colored dotted points in figure [4.14] shows, the raw data measured in this experiment had maximum desaturation values around 87%. This is due to diffracted light in the optical system which made the desaturation values appear lower than they should have been.

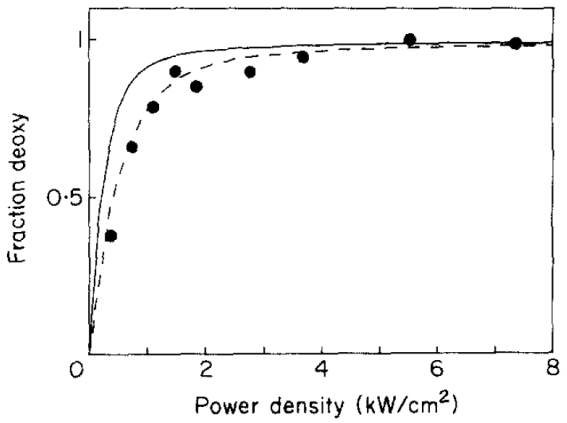

Figure [4.13]: Effect of laser intensity on fractional saturation at a photolysis time of 2ms.

[113] Parkhurst, L. J. (1979). Hemoglobin and myoglobin ligand kinetics. Annu. Rev. Phys. Chem. (30) 503-546.

[114] Longmuir, I. S. et. al. (1952). The diffusion coefficients of carbon monoxide and nitrogen in haemoglobin solutions. J. Physiol. (118) 264-275.

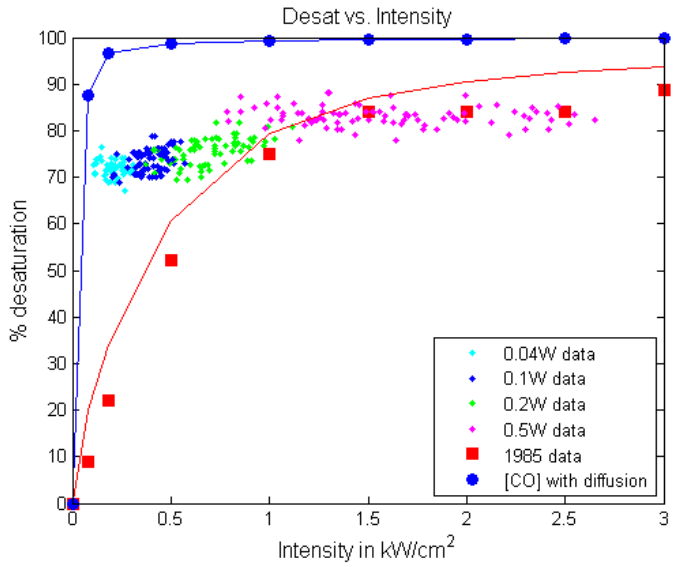

Figure [4.14]: Laser Intensity versus percent desaturation for sample 6/7/2011 and for the data in Ferrone et. al. 1985 paper.

4.5.5 Diffracted monochromator light

It was known that there was diffracted monochromator light in the optical system. This stray light would cause images captured by the CCD camera to appear slightly brighter than they should have been. Several control experiments were done to quantify the effect this would have on capturing images. First, it was necessary to establish that full desaturation was reached through laser photolysis. This was accomplished through a process similar to that described in section 4.2.2 and figure [4.2]. The mesh in front of the laser was removed, and a single large photolysis spot was created on a low concentration CO HbS sample. A diaphragm which is at the position equivalent to the back aperture of a microscope and is in the path of the monochromator and not the laser (#9 in figure [4.3]) is closed until it overlaps some the laser

area. Then a single wavelength desaturation measurement is conducted. The results show two things, first that full desaturation is successfully reached, and second, that stray light causes the desaturation measurement to be off by a factor related to the amount of stray light. The next experiments which were conducted were a series of measurements of how much the level of the diffracted light changed when a diaphragm was opened and closed on a CO HbS sample at 432 nm. It was found that the usual set up of using three filters and a notch filter for measuring desaturation actually minimized the effects of the diffracted light. It was also found that the stray light was about 11% of the measured sample light intensity.

To account for the stray light in the desaturation measurement, a calculation was done in Matlab to relate the measured desaturation to the actual desaturation. First, a relation was made between the ideal (or actual) desaturation and the intensity of the laser light on a CO HbS area and a deoxy HbS area. Consider equation (4.8), the definitions for the intensities in the text above it, and equation (4.10). Equations (4.8) and (4.10) relate the intensity measured at the sample to the percent of desaturation. Solving for the intensity of the photolyzed HbS areas gives:

$$I_{oo} = \frac{I_{oc} - I_{bg}}{10^{-K*OD_{co420}}} + I_{bglsr} \tag{4.19}$$

where I_{oo} is the intensity of a pixel with the lamp on and laser on (Deoxy HbS), I_{oc} is the intensity with the lamp on and laser closed (CO HbS), I_{bg} is the background image with the lamp and laser both off, and I_{bglsr} is the image with the lamp off and laser on. K is as defined in (4.10) and is a function of the fraction of deoxygenated species and other known constants. To solve for the actual desaturation, the following values were used: I_{oc}=500, I_{bg}= I_{bglsr} =120, OD_{co420}=1.3. These were the average values measured during the experiment. Other values within reason (I_{oc}=600 in steps of 100 up to 2000) were used and they changed the calculated relation minimally, by 1-

3% which is within error. Once the actual value for I_{oo} (lamp and laser on, deoxygenated HbS intensity) is known for each fractional desaturation, the same intensity values are then modified to account for the 11% light leak. The intensities then become:

$$I_{CO} = I_{oc} - I_{bg} + f * I_{oc} \tag{4.20}$$

$$I_{DO} = I_{oo} - I_{bglsr} + f * I_{oc} \tag{4.21}$$

where I_{CO} is the CO HbS intensity with the background intensity subtracted and the fraction *f* of light leak, IDO is the intensity of the photolyzed area with the background intensity subtracted and the light leak added. The measured fraction of desaturation becomes:

$$fraction\ of\ desaturation = \frac{\log_{10}\frac{I_{CO}}{I_{DO}} * \epsilon_{CO420} + \epsilon_{CO432}}{OD_{CO420}} \tag{4.22}$$

Figure [4.15] shows the relation of the measured fractional deoxy HbS to the actual fractional deoxy HbS. The data points were fit with a second order polynomial:

$$y = 0.2656 * x^2 + 0.983 * x - 0.267 \tag{4.23}$$

and this was used to adjust the experimental desaturation percentages. The desaturation error was recalculated by averaging the 10% maximum raw desaturation values in each experiment, and finding the standard deviation, which was 4.8. This value was combined with the standard deviation from averaging the percent desaturation values by squaring the two error values, adding them and then taking the square root.

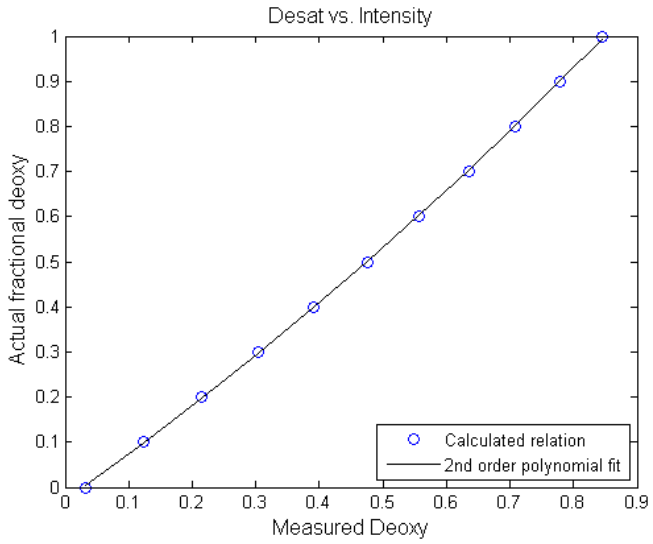

Figure [4.15]: Measured fractional deoxy HbS vs. actual fractional deoxy HbS.

Chapter 5: Analysis and theory of CO HbS partial photolysis

5.1 Results of CO HbS partial photolysis experiment: raw data

There were six different concentrations measured in the CO HbS partial photolysis experiment. Each concentration was measured at a varying percent desaturation, which was controlled via the power output of the laser and through filters. Shown in figures [5.1] to [5.6] are the percent desaturations versus time for the six different samples. The figures are designated with the power level of the laser, as opposed to the intensity. This is because the power level is a single setting, whereas the intensity varies in each spot producing the varied desaturations shown in figures [5.1] to [5.6]. The desaturation curves shown demonstrate that the samples had stable desaturation levels until polymerization occurs (polymerization is when the percent desaturation reaches 100 or above). Greater than 100% is possible due to the polymers absorbing some of the monochromator's light. In some figures, the desaturation level reaches 100% or more, but will then decrease back to a lower percent. This is due to two factors; first, due to memory limitations of the imaging capturing software only four consecutive desaturation images could be measured at a time (recall that each final desaturation image is a product of four other images). Second, because nucleation of HbS is stochastic, when the next set of desaturation images are taken, they might not have nucleated that time. Figure [5.4] with sample #4, has such a scenario with the 0.06WF (F means there was an additional filter) desaturation measurement. Due to the low level of photolysis, there was a longer delay in nucleus formation and the stochastic effects became more apparent.

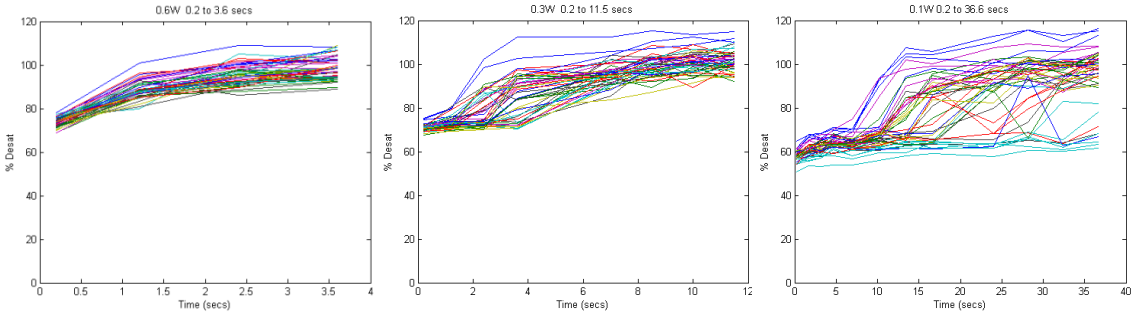

Figure [5.1]: Desaturation of sample #1: 9/30/2010 28.3 g/dl. The x-axis is time in seconds and the y-axis is percent desaturation.

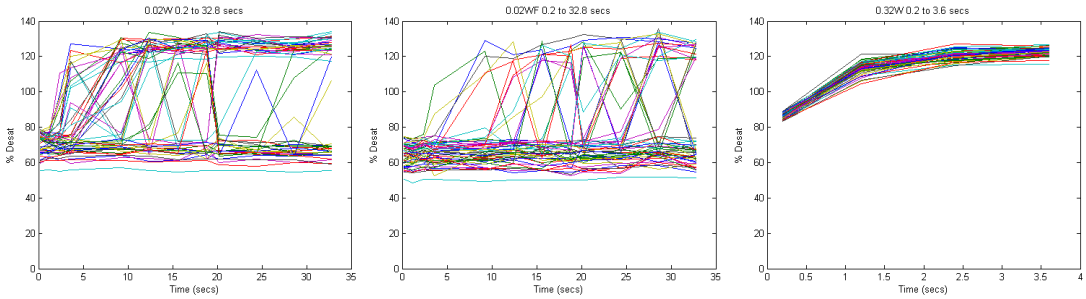

Figure [5.2]: Desaturation of sample #2: 12/22/2010.

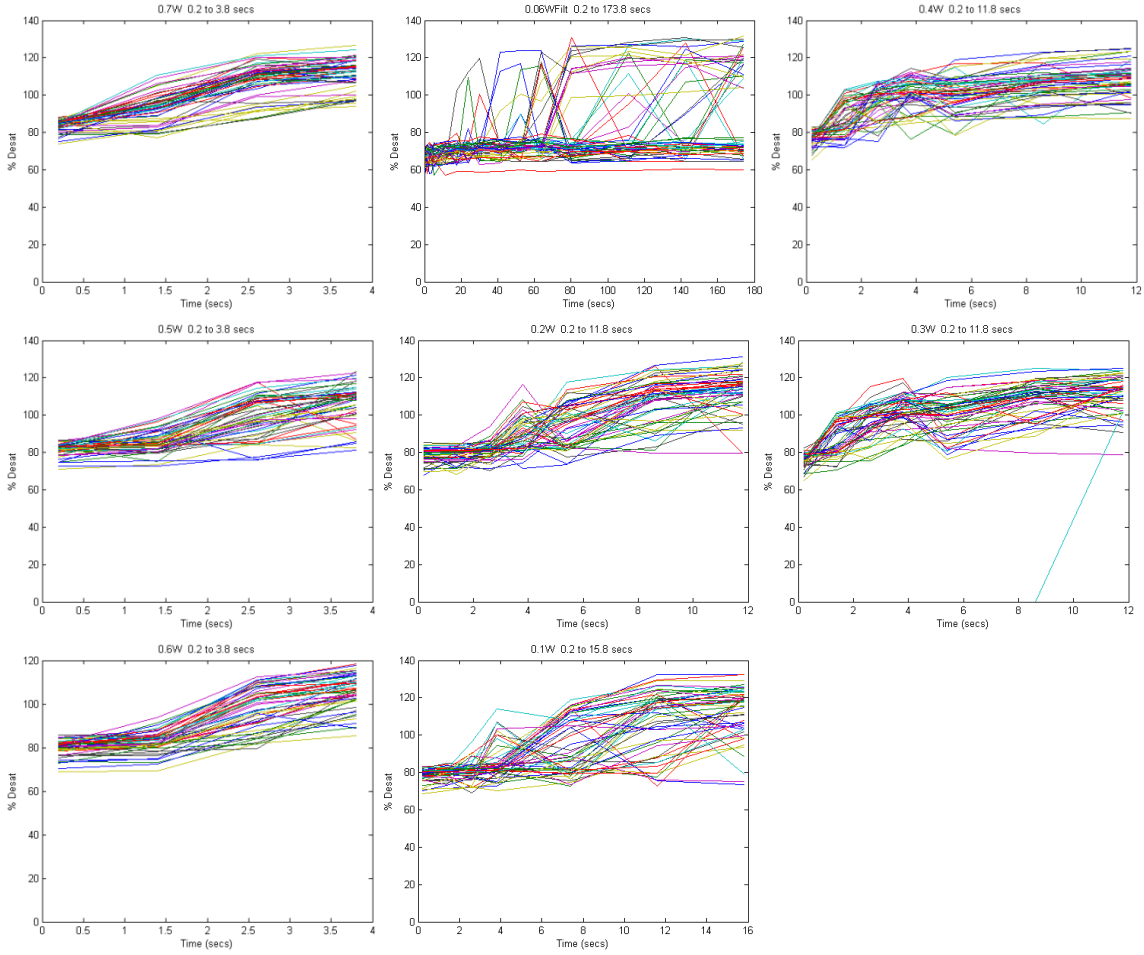

Figure [5.3]: Desaturation of sample #3 2/9/2011.

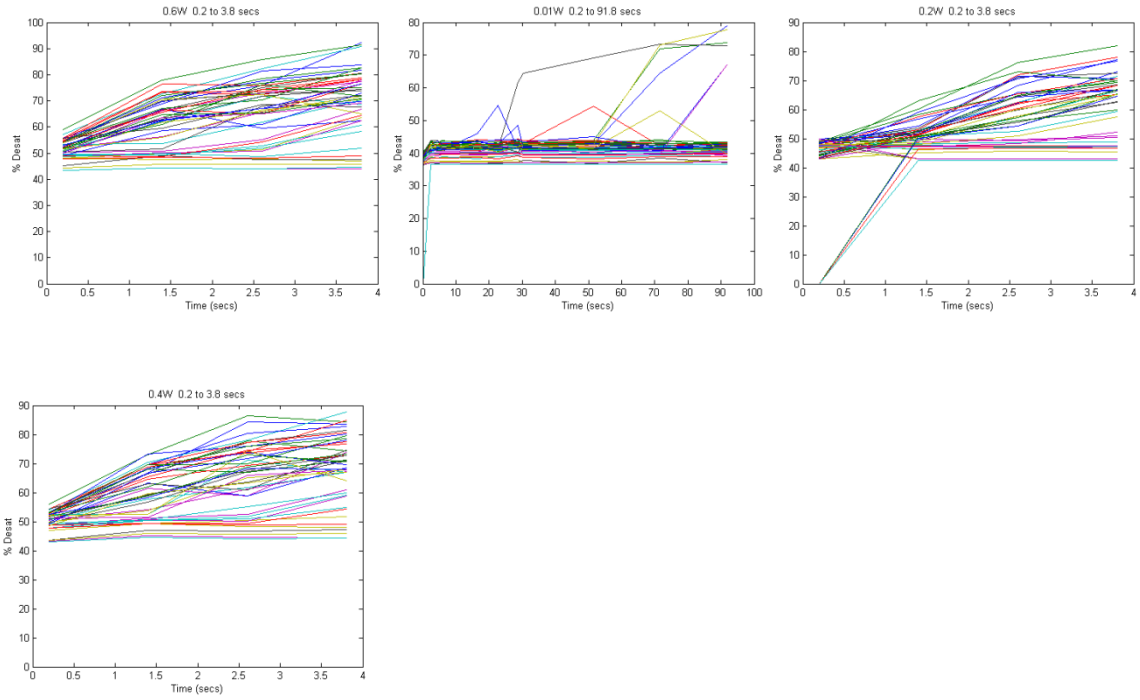

Figure [5.4]: Desaturation of sample #4 2/18/2011.

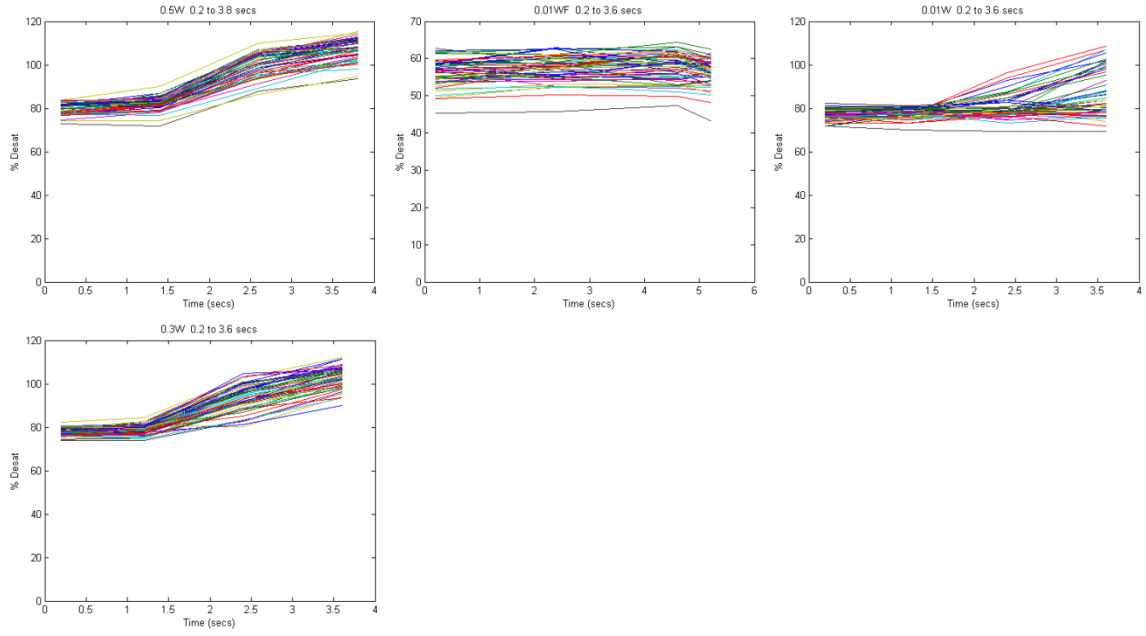

Figure [5.5]: Desaturation of sample #5: 4/29/2011.

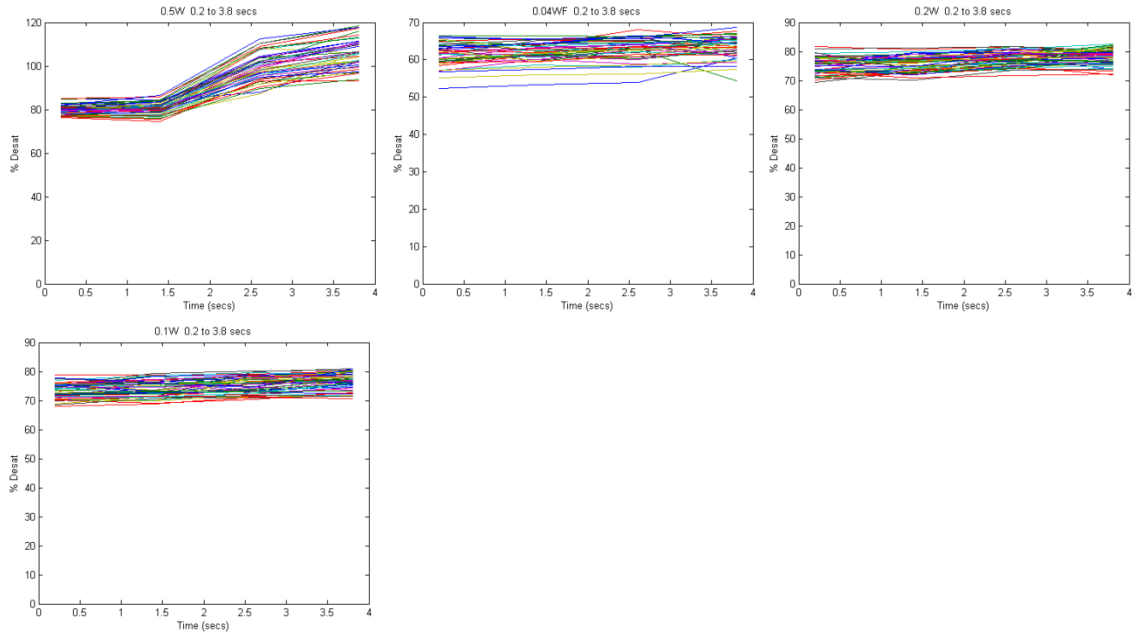

Figure [5.6]: Desaturation of sample #6 6/7/2011.

After the kinetics curves are divided into their corresponding percent desaturation they are analyzed in groups which are incremented by 5%, for example, 70-75% and 65-70%. The final value for the percent desaturation of a group of data curves is found by averaging the desaturation values in that group. The error for the percent desaturation was discussed in section 4.3.2. For easy of understanding the data, the desaturation was converted into saturation and presented as such in tables [5.1] to [5.6]. The error for log B was found by combining two different errors by taking the root of the sum of their squares. The first error in log B arose from the standard deviation of the average B values obtained from the fit to the polymer growth curves. The second source of error is the standard deviation of the different log B values which are measured in an experiment under all the same experimental conditions. The standard deviation among the measured log B values is 0.15 s^{-1}. The log f_o errors are also a

combination of two errors. First, as in the log B values, there is a standard deviation among experiments measured under all the same conditions. Such an error may be a consequence of the stochastic behavior of the system. The second source of error is a bit more complex however. Recall that log f_o is found by fitting function (2.32) to the histogram of tenth times (time it takes for a kinetics curve to reach $1/10^{th}$ its maximum) the error is the uncertainty in the fit. To find the error, a value in the histogram is varied until the chi squared value of the fit has increased by 1.[115] The new distribution is fit for log f_o again, and the difference between the new and old values gives the error. Figure [5.7] shows three different tenth time distributions. The top graph in [5.7] is a histogram of the tenth times from 135 data curves with an average desaturation value of 77.4%. The log f_o value is -7.63 mM/s. The fit of function (2.26) to the histogram is excellent, and a change in chi squared of 1 yields' a small error of 0.08 mM/s. The middle graph is a plot of tenth times from 44 curves, with an average desaturation of 81.28%. The peak of the distribution is between 3 and 5 seconds, but is not as well defined as the peak in the distribution on the top. The middle distribution has a log f_o of -7.73 mM/s and an error of 0.28 mM/s. The distribution on the bottom, has an even greater error as the shape and peak of the curve is more ambiguous. It has only 30 data curves, and a log f_o of -7.46 mM/s and error 0.47 mM/s. Although this data may appear to have a large error, it is still small when compared to the scale of log fo's in this sample set; with the values varying between -9.28 mM/s to -7.34 mM/s (63% and 86% desaturation).

[115] Bevington, P. R. and D. Keith Robinson. (2003) Data Reduction and Error Analysis for the Physical Sciences, p190.

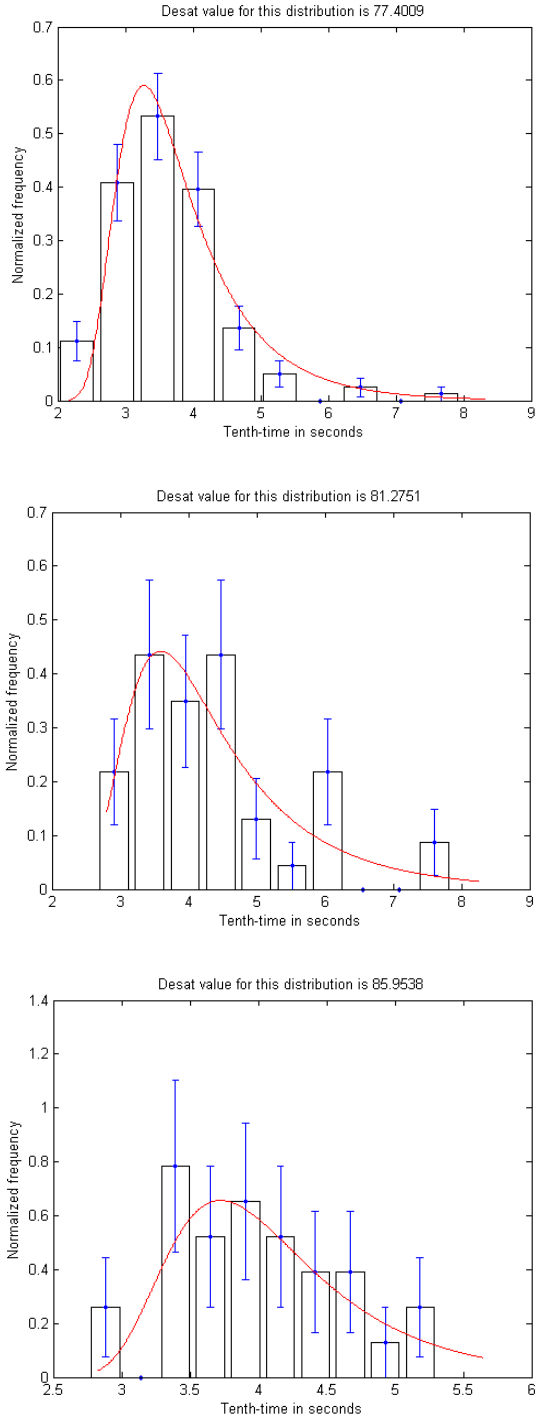

Figure [5.7]: An example of three different tenth time distributions fit for log f_o from sample 2/9/2011.

5.1.1 A note on χ^2

The chi-squared value listed in the data tables in the next section is the normalized χ^2.

χ^2 is defined as:[116]

$$\chi^2 = \sum_{j=1}^{n} \frac{[h(x_j) - NP(x_j)]^2}{\sigma_j(h)^2} \quad (5.1)$$

With N as the total number of measurements of quantity x. There are n different possible x_j and the data can be grouped into frequencies of observations, with the number in each bin as $h(x_j)$. The probability of observing x_j is $P(x_j)$ and the expected number of these observations is $N*P(x_j)$. In the observed frequencies $h(x_j)$, each measurement x_j has a standard deviation $\sigma_j(h)$ associated with it.

The normalized χ^2 is:

$$\chi_v^2 = \chi^2/v \quad (5.2)$$

where v is the number of degrees of freedom and is also equal to the number of sample frequencies minus the number of parameters calculated from the data.

The expected value of the reduced or normalized χ_v^2 is 1. Values much larger or smaller than 1 come from large deviations from the assumed distribution and can imply poor measurements, incorrect assignment of uncertainties, or incorrect choice of probability function.

[116] Bevington, P. R. and D. Keith Robinson. (2003) Data Reduction and Error Analysis for the Physical Sciences, p65-68.

For the histograms in figure [5.7] the χ_v^2 was calculated by first calculating the variance of each binned frequency as:

$$\sigma_j(h)^2 = \sqrt{\frac{h(x_j)}{N*\Delta t}} \tag{5.3}$$

next, the area of the histogram was normalized to 1, and a new function f was fit to the data, which is equivalent to the expected number of observations. The equation is then divided by j the number of bins in the histogram, minus 3 (since the function fit to the data is constrained using two variables as well as by N).

5.2 Results of CO HbS partial photolysis experiment: kinetics data

There were six CO partial photolysis experiments successfully completed. Table [5.1] to [5.6] shows the tabulated data from each experiment. The first column is the power setting of the laser. The power setting is not an indicator of the light intensity nor the photolysis level. The different power settings listed designate an experiment in which that group of data was collected together. The second column shows a specified saturation range (where saturation is 100- % desaturation) in which data curves where analyzed. Next is the adjusted saturation, which accounts for the diffracted monochromator light. The standard deviation of the saturation is a combination of the deviation from the averaged saturation values and the deviation from adjusting the values. The tenth time given in the table is the minimum measured tenth time measured in that data set. It should be noted however, that given more data, this value could become smaller. The 'data size' lists the number of photolyzed progress curves

which were analyzed to obtain the data. A large number of data should generate a better fit for log f_o, although this might not be the case if the data has a large spread (as in slow kinetics). Finally as explained in section 5.1, the log f_o error is found by changing the tenth time histogram so as to increase χ^2 by 1.

Table [5.1]: Sample #1 9/30/2010 28.8 g/dl analyzed data results.

9/30/2010 Conc=28.8 g/dl thickness=3.1um, T=25°C											
Laser power (Watts)	**Sat. range**	**Sat. avg (%)**	**Sat. adj.**	**Sat. std**	**t10min (sec)**	**log B (s^{-1})**	**log B std**	**log f_0 (mM^{-1} s^{-1})**	**log f_0 error**	χ^2_ν	**Data size**
0.6W	30-25	26.85	16.55	6.29	1.35	0.54	0.09	-6.24	0.31	2.94	150
0.6W	25-20	23.57	12.02	5.51	1.45	0.49	0.07	-6.4	0.36	2.42	68
0.3W	30-25	28.97	19.45	5.61	1.83	0.53	0.1	-7.89	0.55	3.37	75
0.3W	35-30	31.1	22.33	5.47	2.1	0.54	0.11	-7.49	0.68	0.44	29
0.1W	45-40	42.24	37.03	5.69	4.94	0.27	0.13	-8	0.64	0.17	26

Table [5.2]: Sample #2 12/22/2010 27.9 g/dl analyzed data results.

12/22/2010 Conc=27.9 g/dl Thickness =4.46um, T=25°C											
Laser power (Watts)	**Sat. range**	**Sat. avg (%)**	**Sat. adj.**	**Sat. std**	**t10min (sec)**	**log B (s^{-1})**	**log B std**	**log f_0 (mM^{-1} s^{-1})**	**log f_0 error**	χ^2_ν	**Data size**
0.32W	20-15	15.8	1.07	5.21	1.63	0.43	0.1	-6.62	0.34	2.29	40
0.32W	15-10	13.08	-2.84	5.9	1.63	0.44	0.08	-6.53	0.32	3.06	170
0.02W	30-25	26.42	15.96	5.69	5.37	0.14	0.1	-8.36	0.48	0.59	55
0.02W	25-20	22.96	11.18	5.84	3.95	0.18	0.11	-8.15	0.31	1.19	116
0.02WF	35-30	31.12	22.36	5.63	8.17	0.14	0.12	-8.66	0.74	1.49	27
0.02WF	30-25	27.388	17.29	6.47	5.18	0.25	0.11	-8.34	0.47	0.59	47

Table [5.3]: Sample #3 2/18/2011 26.64 g/dl analyzed results.

2/9/2011 Conc=26.64 g/dl Thickness=3.3um, T=25°C											
Laser power (Watts)	**Sat. range**	**Sat. avg (%)**	**Sat. adj.**	**Sat. std**	**t10min (sec)**	**log B (s^{-1})**	**log B std**	**log f_0 (mM^{-1} s^{-1})**	**log f_0 error**	χ^2_v	**Data size**
0.06WF	40-35	37.12	30.36	6.27	27.2	-0.36	0.19	-9.28	0.99	1.08	21
0.06WF	35-30	31.85	23.34	5.82	19.7	-0.29	0.17	-9.26	0.60	1.18	44
0.1W	25-20	21.83	9.60	6.3	4.45	-0.03	0.2	-7.82	0.32	0.69	122
0.1W	30-25	28.63	18.98	5.83	4.47	-0.1	0.17	-8.00	0.80	0.49	22
0.1W	20-15	18.29	4.62	5.82	4.72	-0.06	0.17	-7.78	0.35	2.19	72
0.2W	20-15	18.57	5.01	5.98	4.05	0.13	0.28	-7.93	0.31	0.37	102
0.2W	25-20	22.04	9.89	6.09	3.34	0.15	0.21	-7.76	0.32	0.33	96
0.2W	30-25	27.27	17.13	6.54	4.13	0.09	0.2	-7.37	0.38	1.09	28
0.3W	30-25	26.97	16.72	6.12	3.29	0.33	0.18	-7.6	0.49	0.32	44
0.3W	25-20	23.08	11.34	6.22	3.36	0.27	0.18	-7.58	0.30	0.77	151
0.3W	20-15	18.82	5.37	5.58	3.34	0.23	0.21	-7.42	0.82	0.67	24
0.4W	20-15	18.72	5.23	5.71	2.8	0.34	0.19	-7.73	0.41	1.21	44
0.4W	25-20	22.6	10.67	6.01	2.17	0.4	0.14	-7.63	0.31	1.62	135
0.4W	30-25	27.56	17.52	6.4	2.34	0.43	0.14	-7.76	0.62	1.53	38
0.5W	25-20	22.07	9.93	5.71	2.92	0.43	0.15	-7.19	1.54	1.29	22
0.5W	20-15	17.3	3.21	5.96	2.63	0.43	0.13	-7.36	0.32	1.04	150
0.5W	15-10	14.05	-1.44	5.07	2.83	0.37	0.16	-7.46	0.56	0.47	30
0.6W	20-15	17.93	4.11	6.13	2.68	0.37	0.14	-7.42	0.30	1.25	118
0.6W	25-20	21.79	9.54	6.26	2.61	0.42	0.14	-7.46	0.31	2.05	67
0.6W	30-25	27.09	16.88	5.98	2.79	0.42	0.11	-7.38	0.62	0.65	22
0.7W	25-20	22.24	10.17	6.38	2.5	0.47	0.2	-7.43	0.80	0.43	21
0.7W	20-15	16.6	2.21	6.18	2.4	0.42	0.14	-7.37	0.33	0.51	106
0.7W	15-10	13.92	-1.63	5.75	2.67	0.4	0.15	-7.34	0.36	0.78	64

Table [5.4]: Sample #4 2/18/2011 36.33 g/dl analyzed results.

2/18/2011 Conc=36.33 g/dl Thickness =2.8um, T=25°C											
Laser power (Watts)	**Sat. range**	**Sat. avg (%)**	**Sat. adj.**	**Sat. std**	**t10min (sec)**	**log B (s^{-1})**	**log B std**	**log f_0 ($mM^{-1} s^{-1}$)**	**log f_0 error**	**χ^2_ν**	**Data size**
0.01W	65-60	61.11	60.42	5.64	34.5	-0.16	0.16	-9.81	0.74	0.53	27
0.2W	60-55	55.96	54.23	5.31	2.58	0.4234	0.261	-7.14	2.04	2.12	29
0.2W	55-50	52.24	49.66	6.13	1.68	0.613	0.17	-7.065	0.32	2.97	161
0.4W	55-50	50.69	47.74	5.35	0.96	0.86	0.14	-7.08	0.96	1.02	22
0.4W	50-45	47.32	43.51	5.8	1.04	0.83	0.097	-6.79	0.34	1.52	97
0.6W	50-45	47.07	43.20	6.2	0.67	0.84	0.13	-7.05	0.31	1.57	134
0.6W	55-50	50.83	47.91	5.22	0.77	0.85	0.161	-7	0.79	0.36	23
0.6W	45-40	43.54	38.70	6.03	0.69	0.91	0.12	-6.76	0.44	0.39	37

Table [5.5]: Sample #5 4/29/2011 26.5 g/dl analyzed data results.

4/29/2011 Conc=26.5 g/dl thickness=3.45 um, T=25°C											
Laser power (Watts)	**Sat. range**	**Sat. avg (%)**	**Sat. adj.**	**Sat. std**	**t10min (sec)**	**log B (s^{-1})**	**log B std**	**log f_0 ($mM^{-1} s^{-1}$)**	**log f_0 error**	**χ^2_ν**	**Data size**
p01WF	45-40	41.48	36.05	5.86	18.44	-0.103	0.103	-9.33	0.44	1.74	71
0.01WF	40-35	38.12	31.67	5.28	18.56	-0.033	0.066	-9.124	0.62	0.815	38
0.01W	30-25	26.75	16.41	5.84	3.93	0.155	0.13	-8.04	0.49	1.46	57
0.01W	25-20	22.63	10.72	6.13	2.42	0.158	0.129	-7.81	0.30	3.08	266
0.01W	20-15	19.24	5.96	5.53	4.035	0.11	0.19	-7.576	1.23	2.79	36
0.1W	20-15	18.25	4.56	5.99	3.08	0.27	0.19	-7.58	0.30	1.72	213
0.1W	25-20	21.57	9.24	5.9	3.12	0.226	0.178	-7.62	0.30	1.35	184
0.3W	25-20	22.42	10.42	5.95	2.33	0.39	0.126	-7.19	0.30	0.86	111
0.5W	25-20	21.95	9.77	5.63	2.08	0.572	0.11	-6.85	0.38	0.82	29
0.5W	20-15	18.05	4.28	5.79	1.9	0.54	0.087	-7	0.51	0.65	35

Table [5.6]: Sample #6 6/7/2011 26.65 g.dl analyzed data results.

6/7/2011 Conc=26.65 g/dl Thickness=3.8 um, T=25°C											
Laser power (Watts)	**Sat. range**	**Sat. avg (%)**	**Sat. adj.**	**Sat. std**	**t10min (sec)**	**log B (s^-1)**	**log B std**	**log fo (mM^-1 s^-1)**	**log fo error**	χ_v^2	**Data size**
0.04WF	40-35	37.03	30.24	5.87	19.96	-0.07	0.067	-8.92	0.91	1.02	19
0.04WF	35-30	34.24	26.54	5.27	15.45	0.05	0.038	-8.86	0.64	1.711	34
0.04W	30-25	27.64	17.63	5.92	3.48	0.25	0.27	-7.95	0.30	0.43	169
0.1W	30-25	27.67	17.67	6.35	8.5	-0.2	0.11	-8.18	0.32	0.95	77
0.1W	25-20	23.92	12.51	5.86	6.86	-0.2	0.14	-8.22	0.33	1.37	75
0.2W	25-20	22.89	11.08	5.99	5.45	-0.026	0.11	-8.14	0.32	1.26	92
0.2W	30-25	27.19	17.02	6.22	5.55	-0.11	0.121	-8.13	0.46	0.796	48
0.5W	20-15	14.29	-1.09	6.08	1.98	0.64	0.093	-6.95	0.32	1.35	149
0.5W	20-17	18.26	4.57	5.65	1.98	0.65	0.10	-6.94	0.36	1.37	89

For the lower concentrations: 26.65 g/dl and 26.64 g/dl between 0% to 30% saturation the log f_o decreases by 0.066 mM/s and 0.046mM/s respectively per percent decrease in saturation. The log B for these two concentrations decreases by 0.022 s^{-1} and 0.018 s^{-1} for each percent decrease in saturation. For the 36.33 g/dl sample, within the range of 38% to 60% saturation, the log f_o decreases by 0.12 mM/s and the log B decreases by 0.05 s^{-1}.

It is clear from the data tables [5.1] to [5.6], that the data does not extend from 0% saturation to 90% saturation. The lower concentration samples have a range from about 0% to 40% and the highist concentration 36.33 g/dl from 38% to 60% saturation. The lower concentrations have tenth times around 1 to 2 seconds at 0% saturations. Recall that tenth time is one tenth the time it takes for the scattered light from the polymers to reach its peak intensity. The tenth times must be measured precisely because they are the values plotted in a histogram to solve for log f_o. The resolution of time measurement for kinetics on the CCD

camera is about 0.12 seconds and the shortest time that can be measured is 0.12 seconds. This means that as the concentration of HbS increases, the tenth times will decrease. For a concentration of 36.33 g/dl, the tenth times at 0% saturation will be faster than the measureing capabilities of the CCD camera. That is why the lowest saturation measured for 36.33 g/dl was 38.7%, with a tenth time of 0.69 seconds. There are limitations on how high of a fractional saturation can be measured on a low concentrated sample. The lower concentrations stop at about 37% and the longest tenth time measured was about 27 seconds. Recall that homogeneous nucleation is a stochastic event, therefore, the nucleation event which happened at around 27 seconds is only the first. The other nucleation events in such a sample would take several minutes to appear. Measuring such a sample would take several hours and would yield a small amount of data. In several hours, the sample may begin to dry and the sample may no longer produce reliable results. For these reasons, lower concentrations are difficult to measure below 38% saturation.

5.2.1 Modeling the CO HbS partial photolysis data

What is definitively measured here is the behavior of deoxy HbS polymerization in the presence of a mixed species of liganded CO HbS. In simplified terms, such an experiment can be modeled as having a polymerizing population and a non-polymerizing population. In fact, the general model for such a system has already been presented by Rotter et. al. in 2005.[117] However, the conditions presented here are unique in that the fraction of non-polymerizing HbS is related to a ligand distribution and not a mixture of HbS species, as was presented in Rotter's

[117] Rotter, Maria. Et. al. (2005). Molecular crowding limits the role of fetal hemoglobin in therapy for sickle cell disease. *Biophysical Journal.* (347). 1015-1023.

work. Modeling the ligand distribution of HbS is complicated because HbS has four ligands, and each liganded state has a probability of being in an R or T configuration (whereas the R configuration cannot polymerize, and the T-state has a probability of doing so which depends on the number of ligands which the CO HbS has), each fractional saturation of CO HbS has a unique distribution of ligands which are derived through the allosteric model described in section 2.3. In addition to this, photolyzing HbS changes its allosteric parameters in comparison to a partial pressure measurement, which must also be accounted for. The allosteric parameters used in modeling the data were: $Lo=6x10^4$, $K_R=160$ and $c=0.06$.[118] The Lo and c parameters produced the graph in figure [5.8] where the circles show the different fractional species of T which were used to fit the data at the different saturations listed in column 4 of tables [5.1] to [5.6].

[118] Ferrone, F. A. (1985). Kinetics of sickle hemoglobin polymerization I. Studies using temperature-jump and laser photolysis techniques. J. Mol. Biol. (183), 591-610.

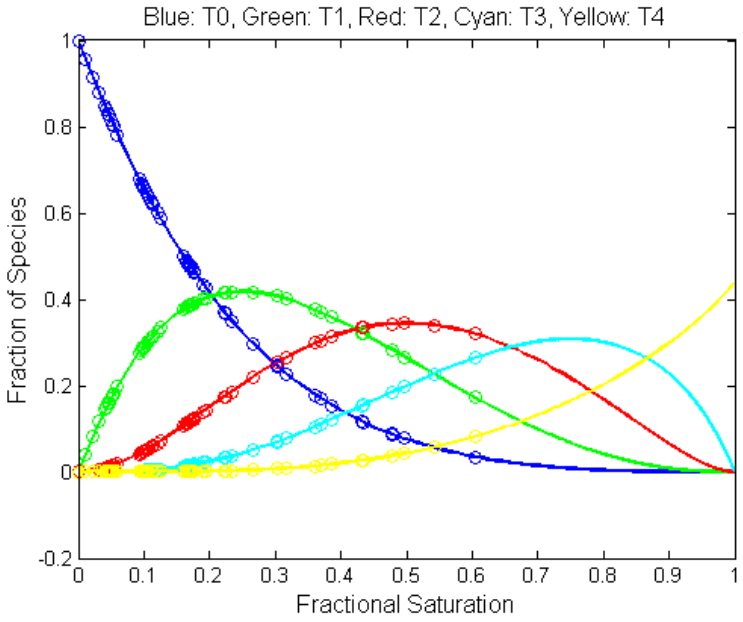

Figure [5.8]: Fraction of T0,T1, T2, T3 and T4 species versus fractional saturation for the allosteric parameters $L_o=6x10^4$, $K_R=160$, and c=0.06. Each circle is a fractional saturation at which an experiment was performed.

The species of T0, T1, T2, T3 and T4 in the CO HbS experiment have been solved through the allosteric model, using the parameters for Hb under photolysis. In chapter 3, section 3.2, it was discussed that Sunshine et. al. found oxygen had a copolymerizing probability of 0.37 for the T1 state, $(0.37)^2$ for T2, etc. To include this in the model, the number of T1, T2 etc. species would be multiplied by this factor, and the number of species left are added together to find the fraction of polymerizable species. For example, figure [5.9] shows the total number of T states (T0 +T1+T2+T3+T4) in blue plotted against fractional saturation (notice the total number of T-states decreases as fractional saturation increases, this is because the Hb is switching into the R-

state configuration). The green line in figure [5.9] shows the model for: T0+0.37*T1+ (0.37^2)*T2+ (0.37^3)*T3+ (0.37^4)*T4 with the sum as the new fraction of polymerizable species. The circles in figure [5.9] are fractional saturations at which data was collected.

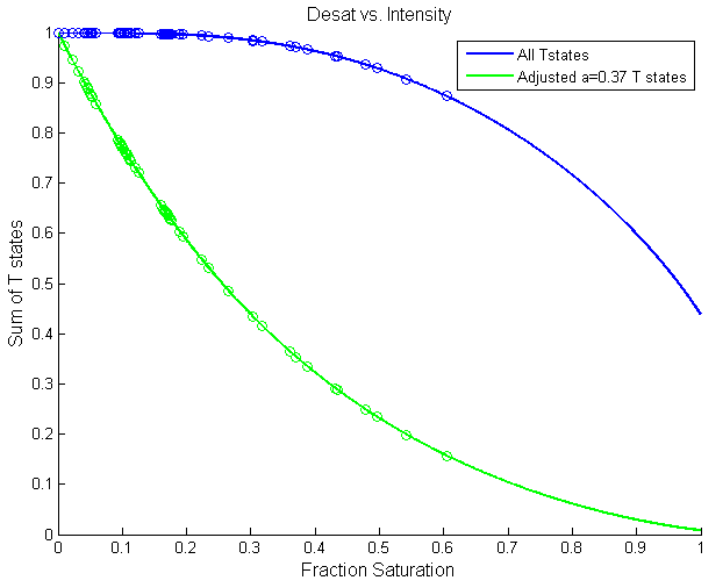

Figure [5.9]: The sum of T states for two different copolymerization models. Blue: T0 +T1+T2+T3+T4. Green: T0+0.37*T1+ (0.37^2)*T2+ (0.37^3)*T3+ (0.37^4)*T4. Circles show fractional saturations at which data was collected.

In relating the fraction of non-polymerizing species to the double nucleation theory defined in chapter 2, sections 1 and 2, it is found that there four main changes. First is the supersaturation, S (equation 2.24) which is the ratio of the activity of Hb at that concentration to the activity of the Hb at equilibrium. The super saturation becomes:

$$S = \gamma_T c_d / \gamma_s c_s \tag{5.4}$$

where c_d is the concentration of deoxy HbS (or in our case the fraction of polymerizing species), γ_s c_s are the activity and the concentration at solubility, and γ_T is the activity of the total HbS, including the non-polymerizing fraction. Since S has changed, the nucleus size will in turn be modified:

$$i^* = \frac{\xi}{\ln S} \tag{5.5}$$

therefore, becoming a larger value with the addition of a non-polymerizing species.

The elongation rate of a polymer decreases as well becoming:

$$J(c) = k_+(\gamma c_d - \gamma_s c_s) \tag{5.6}$$

where k+ is the monomer addition rate. The addition of a fractional non-polymerizing species requires a larger nucleus size, and simultaneously decreases the polymer growth rates. Contrast this to instead decreasing the concentration of the monomers, c. Doing such would decrease the activity coefficient, γ, which depends on concentration as:

$$\ln \gamma = 8\phi/(1-\phi)^2 \tag{5.7}$$

and ϕ is

$$\phi = Vc \tag{5.8}$$

where V is the volume of the Hb molecule and c is the concentration. A decrease in both γ and c would clearly have a greater impact than decreasing c alone. In comparison to just decreasing the monomer concentration, a non-polymerizing species crowds the solution, thereby slightly

counteracting the decrease in kinetics with a small increase. Such an effect is modeled effectively by the change in c and not γ in the nucleation theory.

5.3 Comparison of data to model

The CO HbS data was fit to the model proposed in chapter 2 section 2 by Sunshine et. al. The model is a two-state allosteric model which stipulates that only HbS molecules in the T-state can polymerize; polymerized HbS can still bind oxygen and have the same oxygen affinity as solution phase T-state molecules; and the binding of oxygen is not influenced by the ligation state of other HbS nearby in the polymer. From this model it was deduced that HbS in the polymer have a 0.37 probability to have a bound T1. Likewise, there is a 0.37^2 probability for T2, and so forth for T3 and T4. Letting a equal 0.37, the co-polymerization probability for T1, the fraction of polymerizable species becomes:

$$X_{frac} = T0 + a\,T1 + a^2T2 + a^3T3 + a^4T4 \qquad (5.9)$$

This model was successful in describing the gelation of HbS in the presence of oxygen, which is the polymer binding curve in the Hill plot in figure [3.5]. This model was also successful in describing the polymer growth rate, J, in an experiment on 25.5 g/dl HbS at 25.5 °C with 49% CO HbS at pH 7.35, as well as in other experiments with a pH of 6.85.[119] When this model was applied to the data collected for the nucleation rates of the CO HbS experiment, it was found to only have some correlation to the log f_o and log B of the 36.33 g/dl sample. The other lower concentrations had nucleation rates which were faster than the theory predicted (figure [5.10]). The goodness of fit χ^2 is given in table [5.7] for the sum of the points of each concentration.

[119] Aprelev, A. et. al. (2011). The growth of sickle hemoglobin polymers. Biophy. J. (101) 885-891.

The HbS used in these experiments had values of log f_o and log B for 0% saturation which were faster than the original nucleation theory predicted. The difference at 0% cannot be caused by the partial ligand populations, but it can however, be modeled in the original theory by a change in c_s, the solubility concentration. Figure [5.11] shows the data plotted with c_s modified as stated in table [5.8]. The value for the solubility concentration is usually 17.6 g/dl at 25°C. In addition to adjusted c_s, a parameter in the theory of log B is in turn slightly adjusted to compensate. The term is: ln ϕ, which was introduced in chapter 2 as the proportionality of nucleation sites per polymer. This value is increased by 3.5 in the analysis of each of the samples. Notice table [5.8] the three samples from the same preparation of HbS, B, have similar adjusted values. In fact, two of them have the same adjustment. Based on the dates these samples were made, it appears there may be some relation between the age of the HbS and the amount that c_s is adjusted.

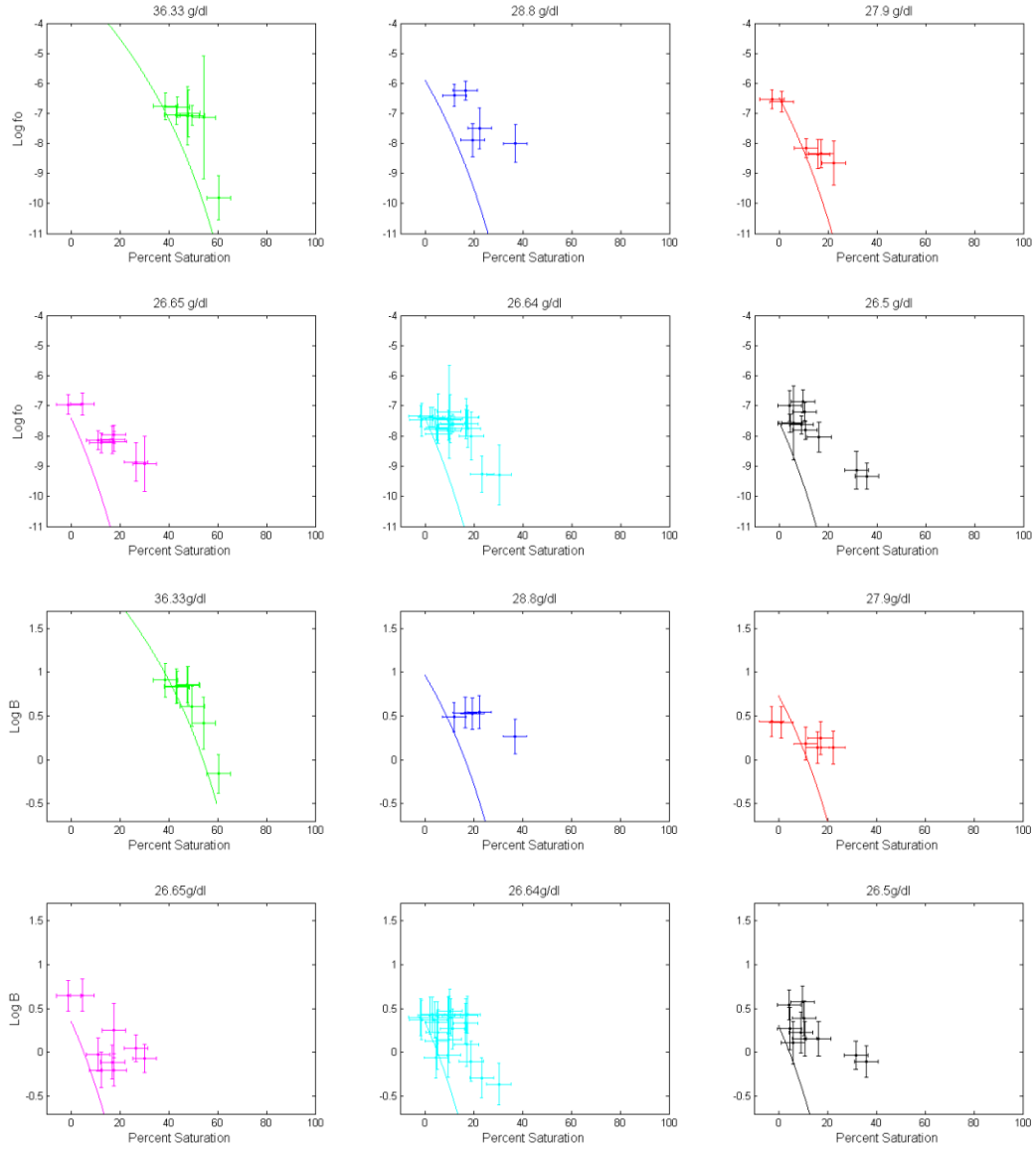

Figure [5.10]: The model of a=0.37 without adjusted c_s. Top 6 plots show log f_o data fit for the six samples with a, the copolymerization constant, with a value of 0.37. Bottom 6 plots are the log B's.

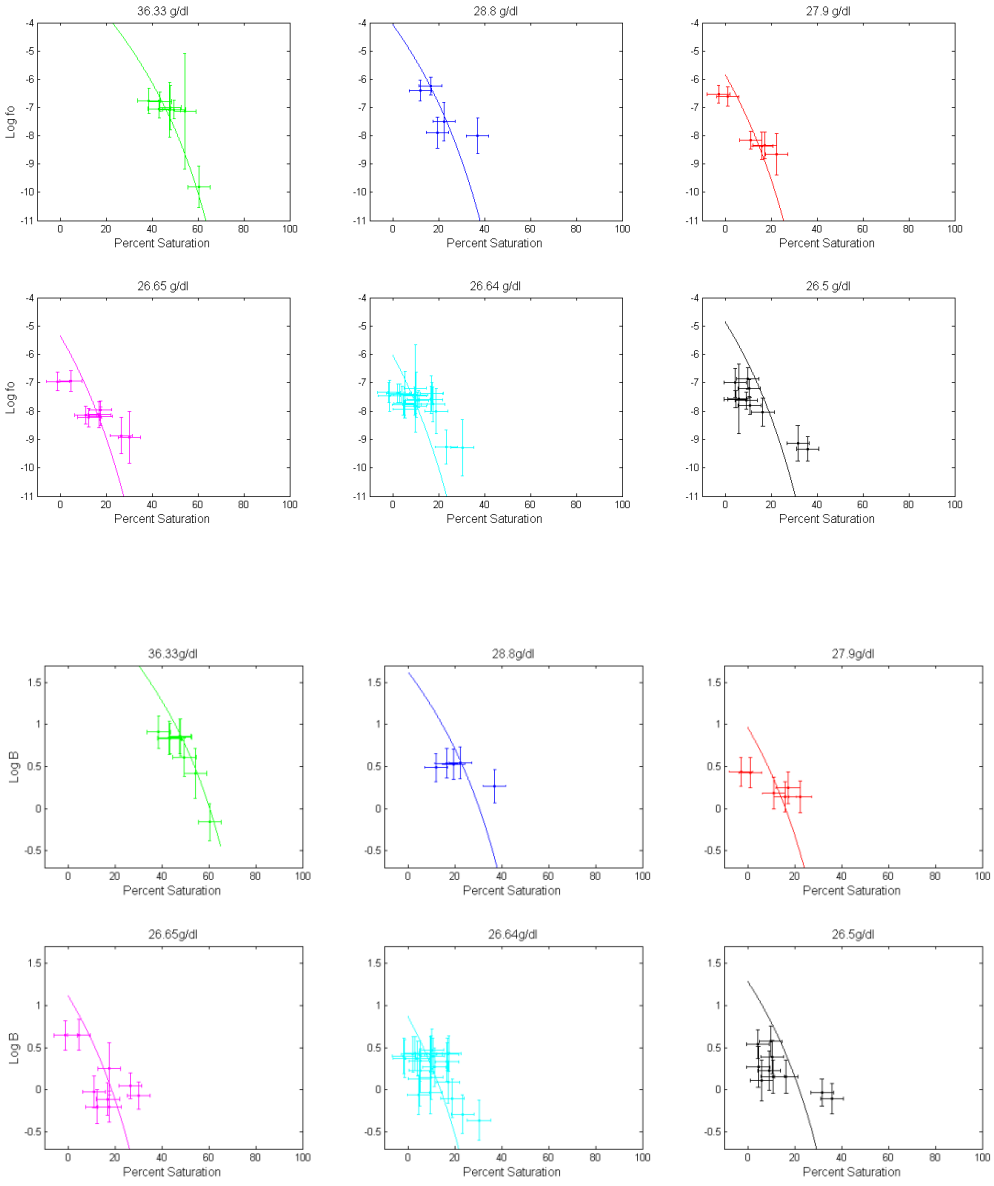

Figure [5.11]: Top 6 graphs are log f_o with modified c_s. Bottom 6 are log B with modified c_s. All data is fit for a=0.37.

Table [5.7] The χ^2 values of the CO partial data fit to theory.

χ^2 for CO Partial Experiment			
Sample	**Conc (g/dl)**	**χ^2 log fo**	**χ^2 log B**
9/30/2010	28.8	27	39
12/22/2010	27.9	16	33
2/9/2011	26.64	152	112
2/18/2011	36.33	10.7	11
4/29/2011	26.5	195	160
6/7/2011	26.65	71	103

Table [5.8] The values used for the adjustment of c_s in analyzing the kinetics data.

HbS Prep	**Date**	**Concentration (g/dl)**	**c_s modifier (g/dl)**
A	9/30/2010	28.8	-2.45
B	12/22/2010	27.9	-1.03
B	2/9/2011	26.64	-1.61
B	2/18/2011	36.33	-1.61
C	4/29/2011	26.5	-2.84
D	6/7/2011	26.65	-2.26

The oxy-CO HbS data was then plotted with the CO HbS data in a correlation plot (figure [5.12]). A correlation plot is a plot where the values measured by the experiment are plotted as the x-axis and the values predicted by the theory are plotted on the y-aixs. A perfect fit between theory and experiment would place a point on the diagonal black line in the plot. The goodness of fit χ^2 for each concentration is given in table [5.10]. The oxy-CO HbS samples also had a percentage of met HbS which was incorporated into the fraction of non-polymerizable species (the same method was used in the Sunshine et. al. oxygen experiment described in

chapter 3). The oxy-CO HbS data also had its c_s adjusted by -1.03 g/dl and ln ϕ by 3.5. The model shows a greater agreement with the faster nucleation rates in both graphs. For the lower values of log f_o and log B, the theory predicts a slower homogenous and heterogeneous nucleation rate than was actually measured. Such a result signifies that a copolymerization probability of 0.37 may be too generalized to describe all the data. The nucleus size increases as the fraction of non polymerizable species increases. It is possible that a larger nucleus could allow a more lenient arrangement of liganded monomers, thereby causing a faster kinetic rate as opposed to the slower ones predicted by the theory. However, such an observation cannot be clearly discerned from just these measurements alone. A future direction with this work would be a study of the larger size HbS nuclei in the presence of liganded HbS.

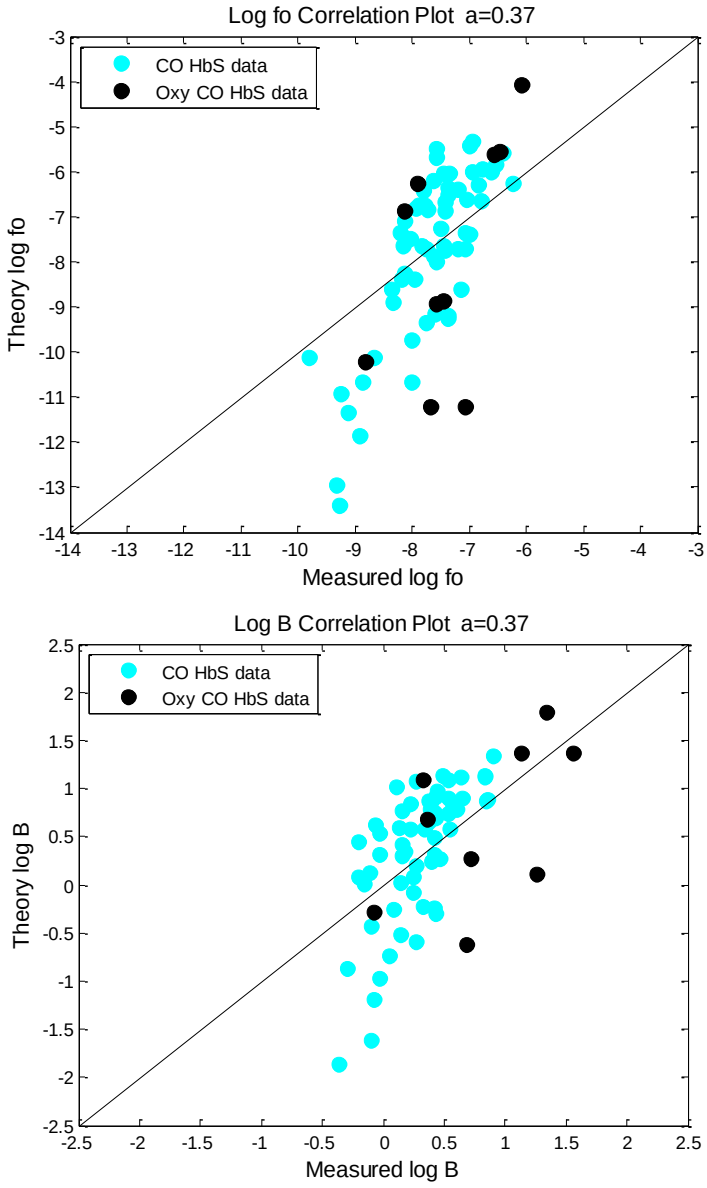

Figure [5.12]: Top: Correlation plot of CO HbS and oxy-CO HbS data for log f_o. Bottom: Correlation plot of CO HbS and oxy-CO HbS data for log B.

The data from the oxy-CO HbS experiment which is plotted in figure [5.12] is listed in table [5.9]. Std is standard deviation, and t_{10} is the minimum measured tenth time for that sample. The error for log f_o and B is the same as described for the CO HbS experiment.

Table [5.9] The data from the oxy-CO HbS experiment.

Date	Conc (g/dl)	Std Conc	% Oxy	% Met	Log f_o	Log f_o error	Log B	Std logB	t_{10} (secs)
6/7/2011	33.2	0.30	2.93	10.53	-6.08	0.38	1.34	0.19	0.29
6/8/2011	29.2	0.31	9.14	9.66	-8.13	0.30	0.36	0.21	2.69
6/9/2011	32.2	0.16	34.68	21.5	-8.82	0.45	-0.08	0.24	9.21
6/9/2011	33.85	0.21	20.98	20	-7.9	0.33	0.33	0.21	3.3
6/10/2011	34.78	0.81	22.43	16.46	-6.47	0.31	1.56	0.18	0.26
6/10/2011	32.5	0.07	43.75	17.09	-7.67	0.33	0.69	0.22	1.2
6/10/2011	32.5	0.07	43.75	17.09	-7.07	0.32	0.69	0.22	1.52
6/11/2011	31.18	0.56	22.5	22.9	-7.44	0.31	1.26	0.23	0.49
6/11/2011	35.1	1.13	19	22.7	-6.57	0.30	1.13	0.21	0.5
6/11/2011	34.5	1.24	38.1	21.64	-7.57	0.30	0.72	0.21	1.01

Table [5.10] χ^2 for partial oxygen experiment.

χ^2 for Oxygen Experiment			
Conc (g/dl)	**% Oxy**	χ^2 **log fo**	χ^2 **log B**
33.2	2.93	28.4	5.5
29.23	9.14	17.5	2.3
32.24	34.68	9.4	0.8
33.85	20.98	24.6	14
34.77	22.43	8.3	1.1
32.5	43.75	115	35.6
32.5	43.75	169	35.6
31.2	22.5	21.7	25.8
35.1	19	9.9	1.3
34.5	38.1	20.3	4.9

The homogenous nucleation data presented here can in turn be related to the delay times measured by Hofrichter, and discussed in chapter 3. Figure [5.13] shows the $\log_{10}$ of the

tenth times (in minutes) of two samples measured by Hofrichter (one at 20°C the other at 35°C). The delay time can be calculated from the theory by solving for the time at which the concentration of monomers in polymers, Δ, is one tenth of its maximum value. The equation for Δ is:

$$\Delta = \frac{A}{2}(\exp(Bt) - 1) \tag{5.10}$$

and the maximum of delta occurs when:

$$\Delta = \frac{2}{3}(c_o - c_s) \tag{5.11}$$

One tenth this will give the delay time, or also called, the tenth time:

$$\frac{\Delta}{10} = \frac{2}{30}(c_o - c_s) = \frac{A}{2}(\exp(Bt_{10}) - 1) \tag{5.12}$$

$$t_{10} = \frac{ln\left(\frac{\frac{2}{15}(c_0 - c_S)B^2}{J_o f_o} + 1\right)}{B} \tag{5.13}$$

where $B^2A = J_o f_o$. The values for J_0, f_0, and B can all be solved using the nucleation theory which is modified to account for the fraction of non-polymerizing. The fraction of non-polymerizing is calculated from the copolymerization model using a=0.37 and the allosteric parameters for CO HbS, c=0.01 and Lo=6e4.

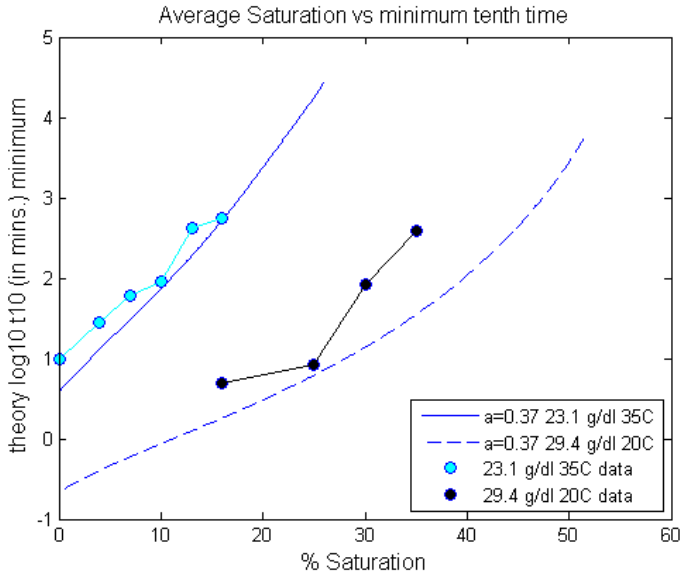

Figure [5.13]: Delay times measured by Hofrichter on gelled CO HbS samples, compared to the theory for a=0.37 copolymerization probability.

When considering the data and theory curves in figure [5.13], it is clear that at 0% saturation the theory and the data do not match. To appropriately align the theory with the 0% saturation data, the theory requires an increase in c_s of 0.64 g/dl. Such adjustments to the cs value demonstrate that there is a slight difference between the HbS used in different experiments. The cause of such inconsistencies has been considered, but the exact mechanism has not yet been identified. One theory put forth, has been that the amount of free heme in the HbS solution changes the kinetics. A free heme is the non-protein component of the HbS, and the removal of the heme will decrease the polymerization rates, while the addition will increase it.[120] When HbS becomes met HbS it may release the heme, and this heme could potentially be

[120] Uzunova, V. V. et. al. (2010). Free heme and polymerization of sickle cell hemoglobin. Bio. J. (99). 1976-1985.

removed or even concentrated through the processes of purifying HbS. Another possible explanation of the discrepancy could be the change in pH brought about through the reduction of met HbS with sodium dithionite. Differing amounts of oxygen and met HbS could cause the reaction of the solution with sodium dithionite to have slightly different final pH values. Finally, there have also been some anecdotal observations in the Ferrone research group, that fresh and older samples had slightly varying kinetics, with older samples being faster. Such differences may be due to the sodium dithionite interacting with the HbS for long periods of time, but no rigorous study of this has been done on the samples used in these experiments.

5.4 Relating the model to previous experiments

The two experiments described in chapter 3 were conducted on polymers which were already gelled. The results showed here come from a laser photolysis experiment. Laser photolysis allows the measurement of the homogenous and heterogeneous nucleation rates, whereas gelled experiments can be used to study solubility and polymer composition. Fundamentally these are very different experiments, but ideally the results should agree once the difference in allosteric conditions is accounted for. From the experiment conducted by Sunshine et. al. it was concluded that the relative affinity of the polymer for oxygen and carbon monoxide must be the same at the same temperature. The oxy-CO HbS data presented here has a large dispersion; however, it generally lies within the range of dispersion for the CO HbS data. This further demonstrates that the polymer and nucleus's tolerance for ligands is the same regardless of whether the ligand is CO or O_2.

5.5 Therapeutic implications of the data

Currently it is now possible to model the delay time for polymerization of intracellular HbS at 50% saturation. The allosteric parameters for oxy HbS are defined, and now the behavior of oxy HbS polymerization is defined. Combining these two models, it is possible to calculate the time it takes for intracellular HbS to polymerize at 50% saturation. The value of 50% is used because this is the amount of oxygen most cells will release on average during their circulation. The concentration for intracellular HbS is in the range of 29 g/dl to values as high as 35 g/dl. A 50% saturated oxy HbS solution with concentration 32 g/dl and at 37.5°C will have a delay time of about 37 seconds, and will reach solubility in about 6 minutes. A 34 g/dl solution at 37.5°C will have a delay time of 6 seconds, and will reach solubility in one minute (see figure [5.14]). These times however, are for a pH of 7.05. At the physiological pH of 7.35, these times will be slightly faster. The transit time of red blood cells through the capillary is 1 second or less.[121] According to the data in figure [5.14], one second is approximately the delay time for concentrations of 36 g/dl.

[121] Kaul, D. K. et. al. (2004). In vivo studies of sickle red blood cells. Microcirculation. (11). 153-65.

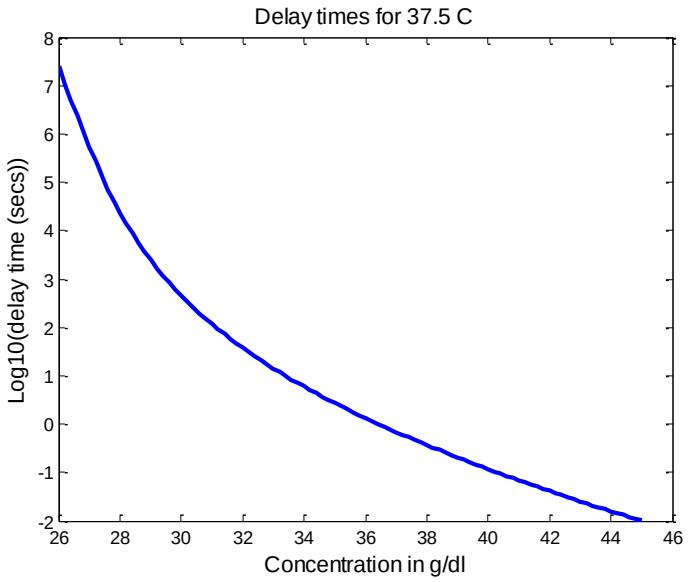

Figure [5.14]: Delay times of 50% saturated oxy HbS at 37.5°C.

Chapter 6: Summary

6.1 Review

This work was the first to measure the nucleation kinetics of partially saturated CO and oxygen HbS samples. Such an experiment was not done previously due to the complex nature of the measurement. Measuring nucleation, which is a stochastic event, requires a large amount of data to be collected. The creation of partial saturation areas requires precise control of the laser intensity, capability to measure the amount of saturation through both programs and individualized optics, and lastly, extensive analysis must be conducted to extract the correct amount of partial saturation and relate it to the nucleation kinetics. Here we have provided an experimental procedure to measure partial saturations using laser photolysis. There is also now a new method of preparing CO-oxygen samples to be used in laser photolysis experiments. This is also the first time that the allosteric model and ligand populations have been incorporated into the nucleation theory.

There are two major findings of this thesis. First, the copolymerization of liganded Hb is a reasonable approximation for describing the behavior of homogeneous and heterogeneous nucleation. Second, the nucleation rates for fractional saturation with CO and O_2 are similar, implying that the kinetic data with CO as a ligand is a good surrogate for data with the physiological ligand of O_2. The amount of noise in the data makes it difficult to definitively say whether another model would be a better fit. Now that a methodology for measuring partial CO and oxygen HbS saturations exists, perhaps future experiments can improve the precision of the measurement.

6.2 Directions of future work

These experiments show that equilibrium polymer behavior and nucleation behavior is similar (considering the error involved in the nucleation measurements), in the presence of liganded HbS. However, there are two discrepancies which warrant further study in this field. The first, is the deviation of the slower kinetics from the a=0.37 model. It appears that for larger nuclei sizes there may be a higher copolymerization probability. This is similar to stating that lower concentrations (around 26 g/dl) appear to fit better to a model with a higher co polymerization probability than 0.37 (as compared to samples at the same fractional saturation but with a higher concentration). A more extensive study on nuclei sizes of partially liganded HbS could yield information regarding a more forgiving conformation of larger nuclei with partially liganded HbS. The second discrepancy which should be further studied, is the adjustment of the c_s to appropriately describe 0% saturated HbS. Could such a discrepancy be due to the free hemes? Although there has been some study done on this issue, this question has still not been definitively answered and warrants future study.

List of References

[1] Ross, M. H. (2003). *Histology:* A Text and Atlas: With Cell and Molecular Biology. (4, Ed.) Lippincott Williams & Wilkins.

[2] Guyton, A. C. (2005). Textbook of Medical Physiology: Guyton Physiology. (11 ed.). Saunders.

[3] McCurdy, P. R., and A. S. Sherman. 1978. Irreversibly sickled cells and red cell survival in sickle cell anemia: a study with both DF32P and 51Cr. *Am. J. Med.* 64:253-258.

[4] Hogg, J. C. Et. al. (1994) Erthrocyte and polymorphonuclear cell transit time and concentration in the human pulmonary capillaries. J. Appl. Physiol. 1795-1800.

[5] http://www.nlm.nih.gov/medlineplus/ency/article/003648.htm. Accessed March 2011.

[6] Bunn, H. F. et al. (1986). Hemoglobin Molecular, Genetic and Clinical Aspects. John Dyson. Saunders Co. Chap. 1 p. 2.

[7] Hoppe, F. (1862). Über das Verhalten des Blutfarbstoffes im Spectrum des Sonnenlichtes. *Virchows Arch. Path. Anat. Physiol. 23*:446.

[8] Stokes, G. G. (1864). On the reduction and oxidation of the colouring matter of the blood. *Proc. R. Soc. Lond.* 13:355.

[9]Ada ir, G. S. (1925). A critical study of the direct method of measuring the osmotic pressure of hemoglobin. *Proc. R Soc*. 108A:627.

[10] Pauling, L. and C.D. Corynell. (1936). The oxygen equilibrium of hemoglobin and its structural interpretation. *Proc. Natl. Acad. Sci.* 22:210.

[11] http://nobelprize.org/nobel_prizes/chemistry/laureates/1962/perutz-bio.html. Accessed April 2011.

[12] IUPAC-IUB Commission on Biochemical Nomenclature (1970). Abbreviations and symbols for the description of the conformation of polypeptide chains. *Journal of Biological Chemistry* 245: 6489–6497.

[13] Finelstein. A. V. and O. B. Ptitsyn. (2002). Protein physics: A course of Lectures. *Academic Press*.75-76

[14] Bunn, H. F. et al. (1986). Hemoglobin Molecular, Genetic and Clinical Aspects. John Dyson. Saunders Co. p. 13.

[15] Bunn, H. F. et al. (1986). Hemoglobin Molecular, Genetic and Clinical Aspects. John Dyson. Saunders Co. p. 29.

[16] Bunn, H. F. et al. (1986). Hemoglobin Molecular, Genetic and Clinical Aspects. John Dyson. Saunders Co. p. 25.

[17] Bunn, H. F. et al. (1986). Hemoglobin Molecular, Genetic and Clinical Aspects. John Dyson. Saunders Co. p. 22.

[18] Bunn, H. F. et al. (1986). Hemoglobin Molecular, Genetic and Clinical Aspects. John Dyson. Saunders Co. p. 33-34.

[19] Shulman, R.G., J. J. Hopfield. S. Ogawa. (1975). Allosteric Interpretation of Hemoglobin Properties. *Quarterly Review of Biophysics*. 8:325-420.

[20] Shulman, R.G., J. J. Hopfield. S. Ogawa. (1975). Allosteric Interpretation of Hemoglobin Properties. *Quarterly Review of Biophysics*. 8:325-420, p. 5.

[21] Bunn, H. F. et al. (1986). Hemoglobin Molecular, Genetic and Clinical Aspects. John Dyson. Saunders Co. p. 69.

[22] Bunn, H. F. et al. (1986). Hemoglobin Molecular, Genetic and Clinical Aspects. John Dyson. Saunders Co. p. 70.

[23] Mendis K. B. et. al. (2001). The neglected burden of Plasmodium vivax malaria. *Am. J. Trop. Med. Hyg.* 64:97–106.

[24] Bodmer, W.F. et. al. (1976). Genetics, Evolution and Man. San Francisco, W. H. Freeman, p. 307.

[25] Power, H. W. (1975). A model of how the sickle cell gene produces malaria resistance. *J. Theor. Biol.* 50:121.

[26] Chen, Q. et. al. (2000). Molecular aspects of severe malaria. *Clin. Microbiol. Rev.* 13 (3): 439–50.

[27] Luzzato, L. et. al. (1970). Increased sickling of parasitized erythrocytes is mechanism of resistance against malaria in the sickle trait. *Lancet* 1:319.

[28] Kwiatkowski D. P.(2005). How malaria has affected the human genome and what human genetics can teach us about malaria. *Am J Hum Genet.* 77: 171–92.

[29] Konotey_Ahulu, F. I. (1910). The sickle cell diseases: clinical manifestations including the "sickle crises." *Arch. Intern. Med.* 6:517.

[30] Herrick, J. B. (1910). Peculiar elongated and sickle-shaped red blood corpuscles in a case of severe anemia. *Arch. Intern. Med.* 6:517.

[31] Emmel, V. E. (1917). A study of the erythrocytes in a case of severe anemia with elongated and sickle-shaped red blood cell corpuscles. *Arch. Intern. Med.* 20:586.

[32] Murphy, R. C. et. al. (1944). Sickle cell disease. I. Observations on behavior of erythrocytes in sickle cell disease. *Arch. Intern. Med*. 74:28.

[33] Pauling, L. et. al. (1949). Sickle cell anemia: A molecular disease. *Science* 110:543.

[34] Gill, S. J. et. al. (1979). Oxygen binding to sickle cell hemoglobin. *J. of Mol. Bio*. 130(2) 175-189.

[35] Bookchin, R. M., and R. L. Nagel. (1973). Molecular interactions of sickling hemoglobins. In Abramson, H., Bertles, J. F., and Wethers, D. L. (eds.): Sickle Cell Disease. St Louis. *C. V. Mosby Co.,* p. 140.

[36] Hemoglobin, p. 456.

[37] Hofrichter, J. et. al. (1973). Structure of hemoglobin S fibers: Optical determination of the molecular orientation in sickled erythrocytes. *Proc. Natl. Acad. Sci.* 70:3604.

[38] Eaton, W. A., and J. Hofrichter. (1981). Polarized absorption and linear dichroism spectroscopy of hemoglobin. *Methods Enzymol.* 76:175.

[39] Singer, K., and L. Singer. (1953). The gelling phenomenon of sickle cell hemoglobin: Its biological and diagnostic significance. *Blood* 8:1008.

[40] Bertles, J. F., R. Rabinowitz, and J. Dobler. (1970). Hemoglobin interaction: Modification of solid phase composition in the sickling phenomenon. *Science* 169:375.

[41] Briehl, R. W. and S. Ewert. (1974). Gelation of sickle hemoglobin. II. Methemoglobin. *J Mol. Biol.* 89:759.

[42] Briehl, R. W. and J. M. Salhany. (1975). Gelation of sickle hemoglobin. III. Nitrosyl hemoglobin. *J Mol. Biol.* 96:733.

[43] Gupta, R. K. (1976). Nuclear relaxation and gelation study of the interaction of organophosphates with human normal and sickle oxyhemoglobins. In vitro gelation of sickle oxyhemoglobin in the presence of iosital hexaphosphate. *J Biol. Chem.* 25:6815.

[44] Hofrichter, J. (1979). Ligand binding and the gelation of sickle cell hemoglobin. *J Mol. Biol.* 128: 335.

[45] Sunshine, H. R., J. Hofrichter, F. A. Ferrone, W. A. Eaton. (1982). Oxygen binding by sickle cell hemoglobin polymers. *J Mol. Biol*. 158:251.

[46] Hofrichter, J. (1979). Ligand binding and the gelation of sickle cell hemoglobin. *J Mol. Biol.* 128: 335.

[47] Chung, L. L. and B. Magdoff-Fairchild. (1978). Extent of polymerization in partially liganded sickle hemoglobin. *Arch. Biochem. Biophys*. 189:535.

[48] Christakis, J. et. al. (1977). Mechanism of inhibition of hemoglobin S polymerization by cyanate. *J Lab. Clin. Med*. 89:992.

[49] Solomon O. A. and K. Ohene-Frempong. (2007). Beyond National Borders: A Global Perspective on Advances inSickle Cell Disease Research and Management, and New Challenges in The Genome Era. [book auth.] B Pace. Renaissance of Sickle Cell Disease Research in the Genome Era. pp. 333-345.

[50] Platt O. S. et. al. (1994). Mortality in sickle cell disease. Life expectancy and risk factors for early death. *N. Engl. J. Med.* 330 (23): 1639–44.

[51] Hoppe, C. (2005). Defining stroke risk in children with sickle cell anaemia. *J. of the British Society for Haematology.* 128:751-766.

[52] http://sickle.bwh.harvard.edu/scdmanage.html. Accessed April 2011.

[53] Powars, D. et. al. (1978). The Natural History of Stroke in Sickle Cell Disease. *Am J Med*. 65:461-471.

[54] Powars, D. et. al. (1978). The Natural History of Stroke in Sickle Cell Disease. *Am J Med*. 65:461-471.

[55] Balkaran, B. et. al. (1992). Stroke in a Cohort of Pateints with Homozygous Sickle Cell Disease. *J. of Pediatrics*. 120:360-366.

[56] Adams R. J. et. al. (1998). Stroke Prevention in Sickle Cell Anemia. *Control Clin. Trials.* 19:110-129.

[57] Steen, R. G. et. al. (2003). Brain Imaging in Pediatric Patients with Sickle Cell Disease. *Radiology.* 228:216-225.

[58] Dowling, M. M. et. al. (2010). Brief report acute silent cerebral infarction in children with sickle cell anemia. *Pediatric Blood & Cancer*. 54:461-464.

[59] Steen R. G. et. al. (1999). Subtlebrain abnormalities in children with sickle cell disease: relationship to blood hematocrit. *Ann. Neurol*. 45:279-286.

[60] Walters, M.C. et. al. (1996). Bone marrow transplantation for sickle cell disease. *New Eng. J. of Med.* 335(6):369-376.

[61] Walters, M. C. et. al. (2001). Stable mixed hematopoietic chimerism after bone marrow transplantation for sickle cell anemia. *Biol. Blood Marrow Transplant*. 7(12):665-673.

[62] Clarice, D. R. et. al. (1995). Management and therapy of sickle cell disease. *NIH publication.* Third ed. 59-67.

[63] Yhaya, A. H. et. al. (2011). 203 Donation or infection: retrospective assessment of transfusion transmissible HIV among sickle cell anemia patients. Journal of Acquired Immune Deficiency Syndromes. 56:86.

[64] Zimmerman, S. A. et. al. (2004). Sustained long-term hematologic efficacy of hydroxyurea at maximum tolerated does in children with sickle cell disease. *Blood*. 103: 2039-2045.

[65] Steinberg, M. H. et. at. (1997). Fetal hemoglobin in sickle cell anemia: determinants of response to hydroxyurea. *Blood.* 89:1078-1088.

[66] Gray, A. et. al. (1991). Patterns of mortality in sickle cell disease in the United Kingdom. *J Clin Pathol*. 44:459-463.

[67] Gladwin, M. T. et. al. (2011). Nitric oxide for inhalation in the acute treatment of sickle cell pain crisis. *J of the Amer Med. Ass.* 305(9):893-902.

[68] Platt, O.S. et. al. (1994). Mortality in sickle cell disease. Life expectancy and risk factors for early death. *N Engl J Med*. 330(23):1639-44.

[69] Gupta, A. K. et. al. (1991). Effects of alpha-thalassemia and sickle polymerization tendency on the urine-concentrating defect of individuals with sickle cell trait. *J Clin Invest.* 88(6):1963-1968.

[70] Thogmartin, J. R. et. al.: (2011). Sickle cell trait associated deaths: a case series with a review of the literature. *Journal of Forensic Sciences.*

[71] Tsaras, G. et. al. (2009). Complications associated with sickle cell trait: a brief narrative overview. *The American Journal of Medicine.* 507-512.

[72] Key, N. S. and V. K. Derebail. Sickle-cell trait: novel clinical significance. *American Society of Hemato*logy. 418-422.

[73] Eaton, W. A. and J. Hofrichter. (1990). Sickle cell hemoglobin polymerization. *In Advances in Protein Chemistry.* 40:63-262.

[74] Roufberg, A. and F. A. Ferrone. (2000). A model for the sickle hemoglobin fiber using both mutation sites. *Protein Science.* 9:1031-1034.

[75] Hofrichter, J. (1979). Ligand binding and the gelation of sickle cell hemoglobin. *J. Mol. Biol.* 128:335.

[76] Sunshine, H. R., J. Hofrichter, F. A. Ferrone, W. A. Eaton. (1982). Oxygen binding by sickle cell hemoglobin polymers. *J. Mol. Biol.* 158:251.

[77] Rotter, Maria. Et. al. (2005). Molecular crowding limits the role of fetal hemoglobin in therapy for sickle cell disease. *Biophysical Journal.* (347). 1015-1023.

[78] Rotter, Maria. Et. al. (2011). Nucleation of Sickle Hemoglobin Mixed with Hemoglobin A: Experimental and Theoretical Studies of Hybrid-Forming Mixtures. *Biophysical Journal.* (101) 2790-2797.

[79] Ferrone, F. A. (1985). Kinetics of sickle hemoglobin polymerization II. A double nucleation mechanism. *J. Mol. Biol.* 183:611-631.

[80] Aprelev, A. et. al. (2007). Metastable polymerization of sickle hemoglobin in droplets. *J. Mol. Biol.* 369:1170-1174

[81] Ferrone, F.A. (1999). Protein aggregation kinetics. *Methods of Enzymology.* 309:259.

[82] Ferrone, F. A., Hofrichter, J., Eaton, W. A. (1985). Kinetics of Sickle Hemoglobin Polymerization, II. A double nucleation mechanism. *J. Mol. Biol.* 183:611-631.

[83] Rotter, M. A., Suzanna, K., Briehl, R. W., Ferrone, F.A. (2005). Heterogeneous nucleation in sickle hemoglobin: experimental validation of a structural mechanism. *Bio. J.* 89:2677-2684.

[84] Steinberg, M. H. Forget, B. G., Higgs, D. R., Nagel, R. L. (2001). Disorders of hemoglobin: genetics, pathophysiology, and clinical management. Ferrone, F. A., Nagel, R. L.: Polymer structure and polymerization of deoxyhemoglobin S. Cambridge University Press. Chapter 23. 577-610.

[85] Ferrone, F. A. et al. (2002). Heterogeneous nucleation and crowding in sickle hemoglobin: An analytic approach. *Bio. J.* 82:399-406.

[86] Bishop, M. F., Ferrone, F. A.: Kinetics of nucleation-controlled polymerization. A perturbation treatment for use with a secondary pathway. Biophysical Journal. 1984. 46(5) 631-644.

[87] Ferrone, F. A. (1985). Kinetics of sickle hemoglobin polymerization II. A double nucleation mechanism. *J. Mol. Biol.* 183:611-631.

[88] Ferrone, F. A., Hofrichter, J., Eaton, W. A.:(1985). Kinetics of Sickle Hemoglobin Polymerization, II. A double nucleation mechanism. *J. Mol.* 183:611-631.

[89] Hofrichter, J. (1986). Kinetics of sickle hemoglobin polymerization: III. Nucleation rates determined from stochastic fluctuations in polymerization progress curves. *J. Mol. Biol.* 189:553-571.

[90] Aprelev, A. et al. (2005). The effects of erythrocyte membranes on the nucleation of sickle hemoglobin. *Bio. J*. 88:2815-2822.

[91] Szabo, A. (1988). Fluctuations in the polymerization of sickle hemoglobin: A simple analytic model. *J. of Mol. Biol.* 199:539-542.

[92] Wyman, J., Gill, S. (1990). Binding and Linkage: Functional Chemistry of Biological Macromolecules. University Science Books.

[93] Hofrichter, J. Ligand binding and the gelation of sickle cell hemoglobin. J. Mol. Biol. 1979. 128, 335-369.

[94] Hofrichter, J. Ross, P. D., Eaton, W. A.: Kinetics and mechanism of deoxyhemoglobin S gelation: A new approach to understanding sickle cell disease. PNAS. 1974. 71(12) 4864-4868.

[95] Eaton, W. A., Hofrichter, J., Ross, P. D., et al. Comparison of sickle cell hemoglobin gelation kinetics measured by NMR and optical methods. *Biochem. Biophys. Res. Commun*, 69 (1976), pp. 538–547.

[96] Eaton, W. A., Hofrichter, J., Ross, P.D.: Delay time of gelation: a possible determinant of clinical severity in sickle cell disease. Blood. 1976. 47, 621-627.

[97] Bookchin, R. M., Balazs, T., Landau, L. C.: Determinants of red cell sickling. Effects of varying pH and of increasing intracellular hemoglobin concentration by osmotic shrinkage. J. of Lab. And Clin. Med. 1976. 87(4): 597-616.

[98] May, A., Huehns, E. R., The concentration dependence of the osxygen affinity of haemoglobin S. Brit. J. of Haem. 1975. 30(3) 317-335.

[99] Hofrichter, J. Ross, P. D., Eaton, W. A. Supersaturation in sickle cell hemoglobin solutions. Proc. Natl. Acad. Sci. 1976. 73 (9) 3035-3039.

[100] Sunshine, H. R., Hofrichter, J., Ferrone, F.A., Eaton, W. A.: Oxygen Binding by Sickle Cell Hemoglobin Polymers. J. Mol. Biol. 1982. 158. 251-273.

[101] Becklake, M. R., Griffiths, S. B. et. al.: Oxygen dissociation curves in sickle cell anemia and in subjects with the sickle cell trait. J. Clin. Invest.. 1955. May; 34(5): 751-755.

[102] Mizukami, H. et. al. Hysteresis-like behavior of oxygen association-dissociation equilibrium curves of sickle cells determined by a new method. Exp. Biol. Med. 1977. 154(2) 304-309.

[103] Huehns, M. A.: The mechanism of the low oxygen affinity of red cells in sickle cell disease. Hamatologie und Bluttransfusion. 1972. 10: 279-283.

[104] Gill, S.J. et al. Oxygen binding to sickle cell hemoglobin. J. of Mol. Biol. 1979. 130 (2) 175-189.

[105] Aprelev, a., Weng, W., Zakharov, M., Rotter, M., Yosmanovich, D., Kwong, S., Briehl, R., Ferrone, F. A.: Metastable polymerization of sickle hemoglobin in droplets. J. of Mol. Biol. 2007. 369(5) 1170-1174.

[106] Rotter, M., A. Aprelev, K. Adachi, F. A. Ferrone. (2005). Molecular crowding limits the role of fetal hemoglobin in therapy for sickle cell disease. *J Mol. Biol*. 347(5):1015-23.

[107] Rotter, M. A. et. al. (2005). Heterogeneous nucleation in sickle hemoglobin: experimental validation of a structural mechanism. *Biophysical Journal.* 89(4):2677-84.

[108] Singer, K., and L. Singer. (1953). The gelling phenomenon of sickle cell hemoglobin: Its biological and diagnostic significance. *Blood* 8:1008.

[109] Galkin, Oleg. Et. al. (2007). The kinetics of nucleation and growth of sickle cell hemoglobin fibers. J. of Mol. Biol. 365. (425-439).

[110] Cao, Zhiqi. Et. al. (2002), a 50^{th} order reaction predicted and observed for sickle hemoglobin nucleation. J. Mol. Biol. (256) 219-222.

[111] Van Assendelft, O.W. et. al. (1970). Extinction coeffients for use in equations for the spectrophotometris analysis of haemoglobin mixtures. Analytical Biochemistry. (69) 43-48.

[112] Ferrone, F. A. (1985). Kinetics of sickle hemoglobin polymerization I. Studies using temperature-jump and laser photolysis techniques. J. Mol. Biol. (183), 591-610.

[113] Parkhurst, L. J. (1979). Hemoglobin and myoglobin ligand kinetics. Annu. Rev. Phys. Chem. (30) 503-546.

[114] Longmuir, I. S. et. al. (1952). The diffusion coefficients of carbon monoxide and nitrogen in haemoglobin solutions. J. Physiol. (118) 264-275.

[115] Bevington, P. R. and D. Keith Robinson. (2003) Data Reduction and Error Analysis for the Physical Sciences, p190.

[116] Bevington, P. R. and D. Keith Robinson. (2003) Data Reduction and Error Analysis for the Physical Sciences, p65-68.

[117] Rotter, Maria. Et. al. (2005). Molecular crowding limits the role of fetal hemoglobin in therapy for sickle cell disease. (347). 1015-1023.

[118] Ferrone, F. A. (1985). Kinetics of sickle hemoglobin polymerization I. Studies using temperature-jump and laser photolysis techniques. J. Mol. Biol. (183), 591-610.

[119] Aprelev, A. et. al. (2011). The growth of sickle hemoglobin polymers. Biophy. J. (101) 885-891.

[120] Uzunova, V. V. et. al. (2010). Free heme and polymerization of sickle cell hemoglobin. Bio. J. (99). 1976-1985.

[121] Kaul, D. K. et. al. (2004). In vivo studies of sickle red blood cells. Microcirculation. (11). 153-65.

Vita

Donna Anne Yosmanovich
Queens, New York
October 13, 1983

2012 Doctor of Philosophy, Physics, Drexel University
2007 Master of Science, Physics, Drexel University
2005 Bachelors of Science, Physics, Fordham University

Publications

2011 Maria Rotter, Donna Yosmanovich, Robin W. Briehl, Suzanna Kwong, Frank A. Ferrone. Nucleation of Sickle Hemoglobin Mixed with Hemoglobin A: Experimental and Theoretical Studies of Hybrid-Forming Mixtures. Biophysical Journal. Volume 101, Issue 11, pages 2790-2797.

2007 Alexey Aprelev, Weijun Weng, Mikhail Zakharov, Maria Rotter, Donna Yosmanovich, Suzanna Kwong, Robin W. Briehl, Frank A. Ferrone. Metastable Polymerization of Sickle Hemoglobin in Droplets. Journal of Molecular Biology. Volume 369, Issue 5, pages 1170-1174.

Awards

Graduate Student Service Award: In recognition of leadership and dedicated service to the graduate student body, Drexel Physics Department, 2010.
Best Graduate Student Poster Presentation, Biological Sciences, Drexel Research Day 1st place 2009 & 2nd place 2011.
Robert E. Davis Travel Award: From the Association for Women In Science 2009.
Drexel Physics Department Travel Award: to represent Drexel at the Canadian American Mexican physics graduate conference, 2007.
Drexel Research Graduate Student Travel Award, to attend biophysical society meetings, 2007, 2009 & 2011.
Matteo Ricci Fellowship: scholarship to conduct research in Russia and at Fordham 2004-2005.
Clare Booth Luce Scholarship: competitive fully paid scholarship awarded to undergraduate women studying physics, 2003-2005.

Current Employment

Janssen Pharmaceuticals, a Family of Johnson & Johnson Company, Spring House PA, pre-clinical small animal imaging / biostatistics.